

KAUNAS UNIVERSITY OF TECHNOLOGY

NERINGA ŠEPERIENĖ

**THE DEVELOPMENT OF POLYMER GELS
AND COMPOSITES WITH THE ENHANCED
SENSITIVITY TO LOW-DOSE IRRADIATION**

Doctoral Dissertation
Technological Sciences, Materials Engineering (08T)

2018, Kaunas

This doctoral dissertation was prepared at Kaunas University of Technology, Faculty of Mathematics and Natural Sciences, Department of Physics during the period of 2013–2017. The studies were supported by Research Council of Lithuania.

Scientific Supervisor:

Prof. Dr. Diana ADLIENĖ (Kaunas University of Technology, Technological Sciences, Materials engineering–08T).

Doctoral dissertation has been published in:
<http://ktu.edu>

Editor:

Brigita Brasienė (Publishing house “Technologija”)

© N. Šeperienė, 2018

ISBN 978-609-02-1487-9

The bibliographic information about the publication is available in the National Bibliographic Data Bank (NBDB) of the Martynas Mažvydas National Library of Lithuania.

KAUNAS TECHNOLOGIJOS UNIVERSITETAS

NERINGA ŠEPERIENĖ

PADIDINTU JAUTRUMU MAŽŲ DOZIŲ
APŠVITAI PASIŽYMINČIŲ POLIMERINIŲ
GELIŲ IR KOMPOZITŲ KŪRIMAS

Daktaro Disertacija
Technologijos mokslai, medžiagų inžinerija (08T)

2018, Kaunas

Disertacija rengta 2013-2017 metais Kauno technologijos universiteto Matematikos ir gamtos mokslų fakultete Fizikos katedroje. Mokslinius tyrimus rėmė Lietuvos mokslo taryba.

Mokslinė vadovė:

Prof. dr. Diana ADLIENĖ (Kauno technologijos universitetas, Technologijos mokslai, medžiagų inžinerija – 08T)

Interneto svetainės, kurioje skelbiama disertacija, adresas:
<http://ktu.edu>

Redagavo:

Brigita Brasienė (leidykla “Technologija”)

© N. Šeperienė, 2018

ISBN 978-609-02-1487-9

Leidinio bibliografinė informacija pateikiama Lietuvos nacionalinės Martyno Mažvydo bibliotekos Nacionalinės bibliografijos duomenų banke (NBDB).

ACKNOWLEDGEMENTS

The author of the dissertation would like to express her gratitude to scientific supervisor Prof. Dr. Diana Adlienė for her support and patience during all doctoral studies and preparation of the dissertation.

The author would like to thank medical physicists Dr. Jurgita Laurikaitienė and Dr. Marius Laurikaitis from the Hospital of Oncology of Lithuanian University of Health Sciences for advising in radiation physics.

Moreover, the author of the dissertation would like to acknowledge enterprise MB “Šeši partneriai” for providing analytical instrumentation for the analysis of the experimental samples.

CONTENTS

LIST OF FIGURES	8
LIST OF TABLES	13
LIST OF ABBREVIATIONS AND SYMBOLS	14
1. INTRODUCTION.....	17
1.1 Objective of the doctoral dissertation	18
1.2 Tasks of the doctoral dissertation	18
1.3 Scientific novelty and practical value.....	18
1.4 Object and methodology.....	19
1.5 Author’s contribution	20
1.6 Approbation of the research results	20
1.7 Structure of the doctoral dissertation.....	20
2. LITERATURE REVIEW.....	21
2.1 Development of polymer dose gels	21
2.2 Structure of polymer gels	25
2.3 Polymer gels for dose measurements	31
2.4 Factors that are affecting polymer dose gel stability and sensitivity	35
2.5 Methods for the evaluation of polymer dose gels.....	42
2.6 Application of polymer gels in medicine and industry.....	45
3. INSTRUMENTS AND METHODS.....	49
3.1 Fabrication and evaluation of polymer gels.....	49
3.1.1 Fabrication of dose gels	50
3.1.2 Irradiation of experimental gels.....	52
3.1.2.1 Photon irradiation of experimental gels.....	53
3.1.2.2 Particle irradiation of experimental gels.....	55
3.2 Irradiation dose measurements	58
3.3 Analysis of experimental gels.....	59
3.3.1 UV-VIS spectrometry	59
3.3.2 Raman spectroscopy	60

3.3.3 Laboratory-made photo-scanner and scanning method	61
3.4 Preparation and evaluation of nanostructured polymer composites	66
3.4.1 Preparation of polymer nanocomposites	66
3.4.2 Irradiation of composites	68
3.4.3 Experimental evaluation of composites	69
4. RESULTS AND DISCUSSION	71
4.1 Evaluation of dose gels	71
4.1.1 Influence of gel composition on the sensitivity of dose gels that were irradiated by different beams	71
4.1.2 Influence of nMAG gel components' concentrations on the sensitivity of gel	89
4.1.3 Investigations of nMAG gel polymerization processes by using Raman spectroscopy	102
4.2 Application of photo-scanning method for the evaluation of spatial distribution of polymerized derivatives in the irradiated gels	112
4.2.1 Scenario no. 1: Partially irradiated dose gel volume	113
4.2.2 Scenario no. 2: Two differently irradiated parts of dose gel volume	116
4.2.3 Scenario no. 3: Irradiated dose gel volume with no boundary restrictions	118
4.3 Evaluation of polymeric nanocomposites as filler materials for transparent radiation protection screens	121
4.3.1 Differently composed polymeric $(\text{NH}_4)_6\text{H}_2\text{W}_{12}\text{O}_{40}\text{xH}_2\text{O}$ composites ...	121
4.3.2 Polymeric composites containing different concentrations of $(\text{NH}_4)_6\text{H}_2\text{W}_{12}\text{O}_{40}\text{xH}_2\text{O}$	124
5. CONCLUSIONS	128
LIST OF REFERENCES	129
LIST OF PUBLICATIONS	137
Annex 1	141

LIST OF FIGURES

Fig. 1. The microscopic structure of non-irradiated polymer gel.....	26
Fig. 2. Different types of network bond. A) Ideal macromolecular network, B) real networks with multifunctional bonds, C) physical molecular entanglements, D) unreacted functionalities with partial entanglements, E) chain loops [35]	28
Fig. 3. Cross-linking of hydrogel. Red points are presenting not connected bonds [31]	29
Fig. 4. Different types of polymer swelling [37]	30
Fig. 5. A) The “spurs” formed after irradiation of high-energy ionizing radiation, B) the appearance of polymerization propagation to non-irradiated gel volume. The 1 cm long part of the sample is irradiated by 15 MeV energy photons [39]	32
Fig. 6. Formation of molecular products and free radicals	33
Fig. 7. Free radical polymerization mechanism in polymer gel dosimeters [32]	35
Fig. 8. Consumption of A) acrylamide and B) bis-acrylamide in irradiated PAG dosimeters with different initial bisacrylamide fractions: A) 50% C, B) 70% C	36
Fig. 9. A) Dose R_2 plots for the PAG polymer gel dosimeter, B) MAG polymer gel dosimeter that are irradiated at various temperatures [42]	38
Fig. 10. A) Biomolecular termination consumes two polymeric radicals, nMAG case; B) chain transfer reactions consume one polymeric radical, nPAG case [2]	39
Fig. 11. Dose rate influence on PAGAT dose gel response at different dose rates [52]	39
Fig. 12. X-ray CT dose response of PAGAT gels that are containing different concentrations of THPC	41
Fig. 13. A typical scheme of the optical CT scanner [17]	43
Fig. 14. A) pure materials, B) swollen gelatin, C) mixed and heated gel solution, D) prepared gel samples	52
Fig. 15. The irradiation sources and their energies	53
Fig. 16. The typical labelling of polymer gel samples	53
Fig. 17. Schematic outline of gel-filled cuvettes that were prepared for the irradiation with the indicated location of ionization chamber that was used as a reference dosimeter	54
Fig. 18. A) Varian Clinac DMX linear accelerator that was prepared for samples irradiation, B) gel samples that were covered by PMMA sheets and prepared for irradiation	54
Fig. 19. The experimental setup for gel irradiation by using the teletherapy unit with ^{60}Co source. A) Samples that were prepared for irradiation, B) full setup for irradiation with PMMA bolus on top	55
Fig. 20. The neutron generator spectrum at the irradiation position	57
Fig. 21. Energy distribution in the experimental channels of Pu(Be) neutron unit	57
Fig. 22. A) Ionization chamber PTW Freiburg, B) electrometer UNIDOSE E (PTW),	59

C) thermometer-barometer DELTA OHM HD2114B.0	59
Fig. 23. The experimental setup for the measurement of optical characteristics of irradiated dose gels	60
Fig. 24. Renishaw inVia Raman spectrometer	61
Fig. 25. Photo-scanning system for the evaluation of the transmitted light intensity in cuvette based samples	62
Fig. 26. The view of scanning chamber with a sample holder.....	63
Fig. 27. First reference measurements to test system parameters	63
Fig. 28. Characterization of dose response scanning profile	64
Fig. 29. Photograph of the irradiated dose gel cuvette with indicated zones: 1 the cap, 2 area of possible oxygen infusion, 3 area for effective measurements, 4 the bottom of cuvette.....	64
Fig. 30. Dose profile curves.....	65
Fig. 31. Dose calibration curve of the photo-scanner	65
Fig. 32. The response curve to identify gels' absorbed dose	66
Fig. 33. Three neck flask for gel composition preparation [100]	67
Fig. 34. AMWO-P composites. From the left: AMWO-DW (water and PAA only), AMWO-P15, AMWO-P30, AMWO-P50, AMWO-P60, AMWO-P70 [101]	68
Fig. 35. Experimental setup for the estimation of lead equivalency of composites.....	69
Fig. 36. UV-VIS intensity spectra of prepared VIPET, nMAG, and nPAG dose gels	72
Fig. 37. The typical UV-VIS spectra of VIPET dose gel that is irradiated by 15 MeV photons	74
Fig. 38. The typical UV-VIS spectra of nPAG dose gel that is irradiated by 15 MeV photons	74
Fig. 39. The typical UV-VIS spectra of nMAG dose gel that is irradiated by 15 MeV photons	75
Fig. 40. Dose versus intensity (sensitivity) curves for nMAG, nPAG, and VIPET gels that were irradiated to 15 MeV X-ray and read out at the selected wavelength of 650 nm	76
Fig. 41. The dose response of polymer gel dosimeter (linear part) [109].....	76
Fig. 42. The typical UV-VIS absorption spectra of VIPET dose gel that is irradiated by gamma photons from ^{60}Co source.....	78
Fig. 43. The typical UV-VIS absorption spectra of nPAG dose gel that is irradiated by gamma photons from ^{60}Co source.....	78
Fig. 44. Dose versus intensity (sensitivity) curves for nMAG, nPAG, and VIPET gels that are irradiated with ^{60}Co source. Intensity values at 650 nm wavelength	79
Fig. 45. The UV-VIS spectra of nMAG dose gel that is irradiated by 6 MeV energy electrons	80

Fig. 46. The UV-VIS spectra of nMAG dose gel that is irradiated by 16 MeV energy electrons	80
Fig. 47. The comparison of 6 MeV and 16 MeV energy electron irradiated nMAG gel, registered intensity at 650 nm	81
Fig. 48. The UV-VIS spectra of VIPET dose gel that is irradiated by 230 MeV energy	82
Fig. 49. The UV-VIS spectra of nPAG dose gel that is irradiated by 230 MeV energy protons	83
Fig. 50. The segment of the UV-VIS spectra of nMAG dose gel that is irradiated by 230 MeV energy protons	83
Fig. 51. The dose versus intensity (sensitivity) curves for 230 MeV proton irradiated nMAG, nPAG, and VIPET gels that are red out at 650 nm	84
Fig. 52. UV-VIS absorption spectra of neutron irradiated VIPET gels	85
Fig. 53. UV-VIS registered intensity spectra of neutron irradiated nPAG gels	86
Fig. 54. The UV-VIS spectra of nMAG dose gel that is irradiated with neutrons	87
Fig. 55. The comparison of dose sensitivity of nMAG dose gel to different irradiation beams	88
Fig. 56. Methacrylic acid concentration dependent nMAG gel sensitivity curves. Registered intensity values were red out at the wavelength of 650 nm	90
Fig. 57. Scanned dose response profiles of nMAG gels that are containing 8 % of MAA and irradiated to different doses.....	91
Fig. 58. Scanner dose response in the irradiated nMAG gels that are containing 8 % of MAA	91
Fig. 59. R2 dose response for nMAG (2 % MAA (filled), 4 % MAA (open), 6 % MAA (insert, filled), 8 % MAA (insert, open)) that is irradiated to the absorbed doses up to 10 Gy [114].....	92
Fig. 60. Dose-dependent registered intensity values of the irradiated nMAG dose gels that are containing various THPC concentrations (registered at $\lambda=650$ nm)	94
Fig. 61. Scanned dose response profiles of nMAG gels that are containing 15 mM of oxygen scavenger and irradiated to different low doses	95
Fig. 62. Intensity to dose response in the irradiated nMAG gels that are containing 15 mM of oxygen scavenger.....	95
Fig. 63. Dose-dependent UV-VIS light intensity values of irradiated nMAG dose gels that are containing various gelatin concentrations	97
Fig. 64. Dose-dependent intensity response profiles along the cuvettes that are filled with the irradiated nMAG gels that are containing 6 % w/w of gelatin (scanned by using $\lambda=650$ nm laser wavelength)	98
Fig. 65. Dose response that is registered at the same scanning position for nMAG gels that are containing 6 % of gelatin and irradiated to different low doses	98

Fig. 66. Amino acid arginine in gelatin [49].....	99
Fig. 67. THPC and arginine structure [49]	99
Fig. 68. A) polymer units, B) gelatin that is cross-linked to THPC structures [49]	100
Fig. 69. Dose response of reference nMAG gel that is investigated by the UV-VIS spectroscopy and photo-scanning methods.....	100
Fig. 70. Dose response of advanced nMAG gel that is investigated by the UV-VIS spectroscopy and photo-scanning methods.....	101
Fig. 71. Raman spectra of pure methacrylic acid	103
Fig. 72. A) Raman spectra of reference nMAG dose gel, B) Raman spectra of advanced nMAG dose gel.....	103
Fig. 73. Variations of FWHM with irradiation dose of nMAG gels within the area between 1200 cm^{-1} and 2400 cm^{-1}	105
Fig. 74. Raman spectra of 4 Gy irradiated nMAG gel with fitted Gauss function	106
Fig. 75. A) Raman spectra fragments with indicated specific peaks of reference and B) advanced nMAG dose gels in the range of 790 $1/$ –830 $1/\text{cm}$	107
Fig. 76. A) Raman spectra fragments with indicated specific peaks of reference and B) advanced nMAG dose gels in the range of 1350 $1/$ –1440 $1/\text{cm}$	107
Fig. 77. Monomer consumption (corresponding peak at 808 cm^{-1}) and polymer formation (corresponding peaks at 1411–1414 cm^{-1}) tendencies in the irradiated advanced nMAG gels	108
Fig. 78. A) Raman spectra fragments with indicated specific peaks of reference and B) advanced nMAG dose gels in the range of 1600 $1/$ –1750 $1/\text{cm}$	109
Fig. 79. Raman spectra fragments with indicated specific peaks of reference (A) and advanced (B) nMAG dose gels in the range of 2900 $1/$ –2980 $1/\text{cm}$	110
Fig. 80. Segmented Raman spectra of polyacrylamide dose gel [118].....	110
Fig. 81. Analysis of Raman peak intensity at 2940 cm^{-1}	111
Fig. 82. Trend of variation A) 1451 cm^{-1} , B) 801 cm^{-1} [71]	111
Fig. 83. Irradiation geometry of the advanced nMAG dose gel samples (scenario no.1)....	113
Fig. 84. Some advanced nMAG dose gel samples after the irradiation to different doses ..	114
Fig. 85. Scanned dose response profiles of the advanced nMAG dose gels that are irradiated according to scenario no. 1 with indicated 1 cm thick irradiation zone	114
Fig. 86. The increase of penumbra due to the irradiation dose	115
Fig. 87. The irradiation scheme of container that is filled with gel (left) presented the profile of scanner gel that is irradiated by 5, 10, 15 Gy doses [59]	115
Fig. 88. Irradiation geometry of the advanced nMAG dose gel samples (scenario no. 2)...	116

Fig. 89. Photograph of some advanced nMAG dose gel samples after the irradiation, according to scenario no. 2	117
Fig. 90. Scanned dose response profiles of the advanced nMAG dose gels that are irradiated according to scenario no. 2 with indicated 1 cm thick irradiation zone	117
Fig. 91. A) 5 Gy, B) 4 Gy irradiated gel samples with no polymerization spread restrictions along the cuvette	118
Fig. 92. The polymerization spread profiles of 5 and 4 Gy doses.....	119
Fig. 93. “Spurs” along the incident path and the representative secondary path. Z_{p1} and Z_{s1} are the average distances between the spurs	120
Fig. 94. The “spur” interaction model [28].....	120
Fig. 95. Comparison of optical transparency spectra of composites that are containing polyacrylamide before and after the irradiation	123
Fig. 96. Comparison of optical transparency spectra of composites that are containing gelatin before and after the irradiation	123
Fig. 97. X-ray attenuation properties in AMWO -PX composites that contain various concentrations of $(\text{NH}_4)_6\text{H}_2\text{W}_{12}\text{O}_{40} \times \text{H}_2\text{O}$: coherent scattering, photo effect, Compton scattering, and total attenuation. A) AMWO-P50, B) AMWO-P60, C) AMWO-P70, D) Lead	125
Fig. 98. The comparison of various AMWO polymer gel composites’ attenuation parameters	125

LIST OF TABLES

Table 1. Polymer gel constituents	49
Table 2. The chemical constituents of the investigated polymer gels	52
Table 3. The neutron related parameters in the experimental channels of Pu(Be) unit.....	57
Table 4. λ_{\max} and FWHM of VIPET, nMAG, and nPAG gels that are irradiated by 15 MeV photons	74
Table 5. λ_{\max} and FWHM of VIPET, nMAG, and nPAG gels that are irradiated by ^{60}Co source.....	77
Table 6. Spectral parameters of nMAG dose gel that is irradiated by electrons	81
Table 7. Spectral parameters of nMAG, nPAG, and VIPET dose gels that are irradiated by high-energy protons	84
Table 8. Spectra parameters of nMAG dose gel that are irradiated by the neutron medical source.....	87
Table 9. Concentrations of nMAG gel components	89
Table 10. The Gaussian function fitting parameters of total peak from 1200 cm^{-1} to 2400 cm^{-1} which shows the amount of polymer that was formed for reference and developed nMAG gel.....	104
Table 11. Lead equivalent of $(\text{NH}_4)_6\text{H}_2\text{W}_{12}\text{O}_{40}\text{xH}_2\text{O}$ containing polymeric composites that are produced by using different thickeners	122
Table 12. Attenuating properties of AMWO-PX composites	126

LIST OF ABBREVIATIONS AND SYMBOLS

1 D	one dimensional
2 D	two dimensional
3 D	three dimensional
%C	relative fraction of cross-linker
%T	total monomer concentration
^{60}Co	Cobalt 60
λ_{max}	wavelength where the intensity peak is at its maximum
AA	ascorbic acid
AAc	acrylic acid
AAm	acrylamide
Arg	amino acid arginine
BANANA	acrylamide, <i>N,N'</i> -methylene- <i>bis</i> -acrylamide, agarose dose gel
BANG	<i>N,N'</i> -methylene- <i>bis</i> -acrylamide, acrylamide, gelatin dose gel
BIS	<i>N,N'</i> -methylene- <i>bis</i> -acrylamide
CAGR	compound annual growth rate
CCD	charge-coupled device
CT	computed tomography
EGDA	ethylene glycol diacrylate
FA	flip angle
FT	Fourier transform
FTMC	Center for Physical Sciences and Technology
Gy	gray
HEMA	2-hydroxyethyl methacrylate
HQ	hydroquinone

HU	Hounsfield units
IAEA	International Atomic Energy Agency
IMAT	intensity modulated arc therapy
IMRT	intensity modulated radiotherapy
I/O	input/output
ITA	itaconic acid
LET	linear energy transfer
LMG	leucomalachite green
MAA	methacrylic acid
MAG	methacrylic acid based polymer dose gel
MAGAT	methacrylic acid and gelatin based dose gel
MAGIC	methacrylic acid based, metallo-organic complex dose gel
MAGICA	methacrylic acid based, ascorbic acid, agarose dose gel
MAH	maleic anhydride
MERUS	multi-echo reflection ultrasound spectroscopy
MMA	methyl methacrylate
mPEGMA	methoxy poly(ethylene glycol monoacrylate) dose gel
MRI	magnetic resonance imaging
MU	monitory units
NHMA	<i>N</i> -(hydroxymethyl) acrylamide) dose gel
NIPAM	<i>N</i> -isopropyl acrylamide based gelatin dose gel
nMAG	nomoxic methacrylic acid based dose gel
NMR	nuclear magnetic relaxometry
nPAG	nomroxic acrylamide based dose gel
NVP	<i>N</i> -vinyl-2-pyrrolidone
OCT	optical computed tomography
PAG	hypoxic acrylamide based dose gel

PAGAT	normoxic acrylamide based, hydroquinone dose gel
PAN/PMMA	poly(acrylonitrile- <i>co</i> -methyl methacrylate- <i>co</i> -styrene)
PEG	poly(ethylene glycol)
PEGMA	poly(ethylene glycol monoacrylate) dose gel
PGD	polymer gel dosimeter
PHEMA	poly(hydroxyethyl methacrylate) dose gel
PMMA	poly(methyl methacrylate)
PNHMAG	poly(hydroxymethyl) acrylamide based dose gel
PNVP	poly(<i>N</i> -vinyl-2- pyrrolidone)
PVA	poly(vinyl alcohol)
QA	quality assurance
R2	relaxation rate
RF	radio frequency
SME	small and medium-sized enterprise
SOBP	spread of Bragg peak
SR	stereotactic radiosurgery
SSD	surface to source distance
TBO	Toluidine Blue O
THP	tetrakis-hydroxymethyl phosphonium
THPC	tetrakis-hydroxymethyl phosphonium chloride
THPS	tetrakis-hydroxymethyl phosphoniumdisulfate
TOF	time-of-flight
TS	transmission signal
UV-VIS	ultraviolet and visible light spectra
VIPAR	<i>N</i> -vinyl pyrrolidone based argon treated dose gel
VIPE	<i>N</i> -vinylpyrrolidone
VIPET	<i>N</i> -vinylpyrrolidone based nomoxic dose gel

1. INTRODUCTION

Polymer structures, which could change its chemical, physical, and mechanical properties after interaction with high-energy photons or particles, are known as radiation-sensitive materials. Highly radiation-sensitive structures are hydrogels, which are made of monomer, oxygen scavenger, gelatin, radiation sensitizers, and high amount of water [1]. When ionizing radiation is applied, the polymerization process triggers, and the amount of polymerized material is a function of absorbed radiation dose [2]. It is known that radiation induces water radiolysis, and cross-linked structure of gel starts to form. The type of formed radiolytic products depends on the primary particle energy and irradiation type. When higher doses are applied, the net structure becomes thicker. The density of the cross-linked network is a potential property that is enabling evaluation of polymerized structures. It was investigated that high ionizing radiation doses (>50 Gy) initiate nano and macro sized clusters, i.e., “spurs”, which may diffuse or migrate [1, 2] in gels volume. However, chemical and physical reactions that are appearing when low-dose (<10 Gy) irradiation is applied are not well defined.

Since radiation-induced polymerization is responsible for the optical density and molecular bond variations, the evaluation of polymer structures might be performed by using different methods. UV-VIS spectrometry is known as non-destructive and as a well-developed method to investigate changes in gel transmittance and absorbance properties in ultraviolet and visible light range. In order to investigate the molecular bond formation, when low doses are applied to hydrogels, Raman spectra are used. However, in order to evaluate the diffusion of polymerized pieces and formed clusters, it is necessary to develop and adopt photo scanner, which would be able to evaluate changes with no less than 0.5–0.2 mm accuracy.

Polymer composites, which contain heavy metal nano particles, are known as well attenuating ionizing radiation. Attenuation properties highly depend on the polymer structure and composition. When constructing the composition of these polymers, it can be applied as radiation protection screens for medical and industry purposes. The best ionizing radiation attenuation properties have lead-containing structures, but lead has been restricted due to its high toxicity. EC Directive 2011/65/EU, RoHS II, which restricts the application of lead as well in medical devices, stresses the awareness. Moreover, lead particles that are mixed into protective screens composition bring to visible light opaque screens, which cannot be used where visual light transparency is needed. Lead-free and visible light transparent material could be created from the polymer composites.

The research presented in this dissertation was focused on the investigations of dose sensitivity of polymer composites irradiated to low doses up to 10 Gy. The performed investigations were addressed to two objectives: development of dose gels with enhanced sensitivity to low-dose irradiation for 3D dosimetry in radiotherapy and development of lead-free optically transparent polymer composites as a filler material in the radiation protection screens.

1.1 Objective of the doctoral dissertation

The objective of this dissertation was the development of polymer gels and composites with the enhanced sensitivity to low-dose irradiation that are applicable for radiation dosimetry or radiation protection purposes in the medical field.

1.2 Tasks of the doctoral dissertation

Specific aims of the study included the following:

1. Preparation of reference normoxic gels, their irradiation by high-energy photons and various particle beams, and assessment of optical characteristic changes due to low-dose induced polymerization processes in the irradiated dose gels.
2. Development of advanced polymerized dose gels that are sensitive to varying composition of low-dose photon irradiation and concentrations of gel constituents.
3. Development of photo-scanning method and instrumentation for dose gel read out.
4. Development of lead-free transparent polymeric composites with effective X-ray radiation shielding properties.

1.3 Scientific novelty and practical value

1. The developed nMAG dose gels possess enhanced sensitivity (0.45 a.u.) for the dose registration in the low-dose region of 0–5 Gy. Radiation-induced changes of gel optical properties can be assessed with a dose resolution of at least 0.3 Gy.
2. The developed photo-scanning method and constructed dose read out instrumentation introduce a new technical solution for the dose evaluation and verification in radiotherapy by using dose gels.
3. The experience that has been obtained developing photo-scanning method was used when constructing prototype of catheter-based gel dosimetry system BrachyDOSE, which is aimed for dose measurement and verification in high dose rate brachytherapy. For the commercialization of the proposed dosimetry system, SME “Šeši partneriai“ was established and got financial support from the EU structural funds in the frame of the Horizon 2020 project for SMEs, Phase-1 for the feasibility study related to the commercialization of the product. The author of this dissertation is the main project manager in the company.
4. The developed lead-free polymer composite was used as filler for the radiation protection screen. A new prototype of the radiation protection screen

was tested in the clinical environment and protected under the LT patent No. B6292. “Radiation protecting material composition, screen for radiation protection and method of making the same”. The author of this dissertation is one of the patent co-authors.

1.4 Object and methodology

The object of this dissertation is radiation-sensitive dose gels that are irradiated to low doses and their evaluation by using optical methods. The investigation included newly developed photo-scanning method and its instrumentation.

Various monomers (methacrylic acid, acrylamide, and N-vinylpyrrolidone) based polymer gels were manufactured in the atmospheric conditions. Gel samples were irradiated with 15 MeV X-rays (medical linear accelerator Varian Clinac), gamma rays (teletherapy unit ROKUS M with ^{60}Co source), protons (proton accelerator IBA PROTEOS C230), electrons (medical linear accelerator Varian Clinac 2100C/D), and neutrons up to 10 Gy doses. Optical properties of the irradiated gels were investigated by using UV-VIS spectrometer Ocean Optics USB 4000. Newly constructed photo-scanner was used for the dose profile evaluation in polymerized gel samples.

The dose sensitivity of polymer gels was assessed by using their optical characteristics. Various gel compositions were manufactured and tested in order to achieve their best sensitivity to low-dose photon and particle irradiation. The nMAG dose gels that are made of special composition indicated the highest sensitivity among all the investigated samples and were chosen for further investigations. In order to assess the polymerization processes on irradiation, the nMAG samples were analyzed by Raman spectrometry and polymer formation, and monomer consumption rates were estimated.

Newly constructed photo-scanner was used for spatial resolution assessment of nMAG gel samples. The segments of gel-filled cuvette were irradiated to different doses, and the cuvette and longitudinal scanning of the cuvette was performed in order to find polymerization proliferation in irradiated gel and gel's spatial resolution due to different absorbed doses. The spatial resolution of the applied laboratory-made photo-scanner was 0.20 mm.

Different tungsten salts were investigated as possible ingredients of polymer composite that provides X-ray attenuation, which complies with radiation protection requirements. Composites were irradiated in X-ray therapy unit GULMAY D3225 up to 10 Gy doses. Some samples were repeatedly irradiated by 50 Gy dose for checking their attenuation properties, structural stability, and transparency to visible light after high dose load. Composite that was containing ammonium metatungstate exhibited the best X-ray attenuation features (lead equivalent ≥ 0.5 mmPb) and transparency to visible light (87 %) and was chosen as prototype composite for the fabrication of lead-free transparent radiation protection screen.

1.5 Author's contribution

Most of the experimental work was carried out at Kaunas University of Technology, Faculty of Mathematics and Natural Sciences, Department of Physics, Institute of Materials Science, and premises of MB "Šeši partneriai". Proton irradiation of the samples was performed in OncoRay Clinic in Dresden, Germany. Electron and photon irradiation of samples was performed in Lithuanian University of Health Sciences, Kaunas Clinics, and Hospital of Oncology. Neutron irradiation of samples was performed in the Center for Physical Sciences and Technology (FTMC) in Vilnius.

The author of the doctoral dissertation has prepared all the investigated samples and analyzed their optical properties after the irradiation to different types of particles and photons. The author has constructed the photo-scanner and adopted for the evaluation of gel-filled cuvettes. The investigation of polymer composites for radiation shielding was performed in collaboration with other co-authors of the presented papers and LT patent.

The feasibility study of possible polymer gel applications and commercialization was performed by author with the support of Lithuanian startup company MB "Šeši partneriai". The short study is presented in Annex 1.

1.6 Approbation of the research results

The main results of this work were presented in 6 scientific publications included in Clarivate Analytics database; 3 articles were published in journals with impact factor, and 3 articles were published in conference proceedings, having CPCI status.

The results of this work were presented at 9 international and 1 national conferences.

1 LT patent is partly based on the results of this work.

1.7 Structure of the doctoral dissertation

The doctoral dissertation consists of five chapters. The first chapter includes introduction, objectives and tasks of the dissertation, object and methodology, author's contribution, and results approbation. Literature review, including newest polymer dose gel investigation results, is presented in the second chapter. The third chapter includes instruments and methods, which were used for polymer gel analysis. Essential results and their discussion are presented in chapter four. The last chapter presents the conclusions of the dissertation. The list of references (128 entries), the list of scientific publications on the topic of the doctoral dissertation, and participated conferences are presented at the end of the document. The total size of the dissertation is 146 pages, containing 98 figures and 12 tables.

2. LITERATURE REVIEW

2.1 Development of polymer dose gels

Polymer gel dosimeters are the chemical detectors, which are sensitive to ionizing radiation in a specific energy range. Polymer gel dosimetry is based on the radiation-induced polymerization of monomers that are infused in a gelatin matrix. After irradiation, free radicals are created in water. They induce polymerization to the irradiated region. The number of free radicals, and thus the polymer yield, increases as a function of absorbed dose [3].

These detectors are capable to record the radiation dose distribution in three dimensions (3D). Furthermore, gels are radiologically near soft-tissue equivalent material with properties that may be modified, depending on their application. 3D gel dosimetry has a specific advantages when compared with other often used one dimensional (1D) dosimeters, such as ion chambers, or two dimensional (2D) dosimeters, such as radiochromic films [1,4]. Polymer gel dosimeters have a high potential for everyday dosimetry applications in radiotherapy where the steep dose gradients exist, such as brachytherapy (BT), intensity-modulated radiation therapy (IMRT), stereotactic radiosurgery (SR). Moreover, it has been found that gel dosimeters have specific application in modern cancer treatment methods, such as the proton and neutron therapies [1, 3].

The development of chemical dosimeter started in 1927, when Fricke and Morse have developed chemical dosimeter with various gelling agents such as gelatin, agarose, dextran, and poly(vinyl alcohol) (PVA). It was the first suggestion for using the chemical dosimeter for radiation sensing. However, the ion diffusion in gel volume was a significant problem, and Fricke-type gel dosimeters, which are basically made of ferrous ammonium sulfate, did not retain a spatially stable dose distribution due to Fe^{2+} ion diffusion within the irradiated dosimeters [5].

First, polymer gels that are suitable for radiation dosimetry were introduced as early as the 1950s. The difficulties of use and complexity of dose evaluation in gel dosimeter significantly delayed its use for medical dosimetry purposes. Radiation-sensitive gels that are containing chloral hydrate, which is diffused throughout an agar gel, were investigated in 1957. Depth doses, using spectrophotometry and pH probe measurements for irradiated gel investigation, was used. The situation has changed when in 1980s, the magnetic resonance imaging (MRI) technology was presented to display information of dose in three dimensions. The magnetic resonance analysis became the first method to evaluate dose in polymer gels [6].

Later, gels were introduced as radiation detectors when ionizing radiation was used to produce color changes in gels that were containing dyes, such as methylene blue. In 1984, the ferrous sulfate dosimeter was developed for the radiation dosimetry purposes. Nuclear magnetic relaxometry (NMR) and MRI were employed for the evaluation of gel dosimeter [7].

Polymer systems for the use of radiation dosimetry were proposed in 1954. The effects of ionizing radiation on PMMA poly(methyl methacrylate) were discussed [8]. After this study, the era of polymers for dose detection has started. In 1961, polyacrylamide was first used as gamma dosimeter, and the polymerizing liquids as possible irradiation detectors were investigated. Nineteen ninety-two was the year when *N,N'*-methylene-bis-acrylamide (BIS), often used cross-linking agent, was investigated by the MRI. The results showed that the relaxation rates increase due to the absorbed dose. At the same time, a new type of polymer gel dosimeter (BANANA) which was made of acrylamide (AAM), BIS monomers, and nitrous oxide, infused in an aqueous agarose matrix, was introduced. The studies showed that BANANA dosimeter has a relatively stable post-irradiation dose distribution and does not suffer from ion migration as Fricke type dosimeter [1].

Agarose was changed to gelatin, and BANG dosimeter, consisting of BIS, AAM, nitrogen, and aqueous gelatin, was introduced. The polymerization was caused by the cross-linking of neighboring monomer chains that are initiated by the free radicals resulting from the water radiolysis. Later, the BANG formulation was patented, and now, it is commercially available through the MGS Research Inc. as BANG [9]. Since that time, the variety of different compositions and formulations of polymer gel dosimeters have been presented. Anoxic gel dosimeter, which is made of acrylamide and gelatin (PAG), became the object of radiation-induced polymerization studies that focused on the clinical applications of gel dosimetry by using MRI analysis [10]. The investigations on the accuracy of anthropomorphic polymer dose gel phantom for the verification of conformal radiotherapy treatments were carried out. The results showed that the temperature during the irradiation and oxygen inhibition has a significant impact on the dosimeter accuracy and stability. The clinical aspects of polymer gel dosimetry in conformal therapy, brachytherapy, IMRT, IMAT (intensity modulated arc therapy), and proton therapy, low-energy X-ray therapy, stereotactic radiosurgery, boron capture neutron therapy that is using MRI were investigated as well [3, 11–14].

The optical-CT and ultrasound methods that are used for the readout of PAG polymer gel dosimeters was introduced later. These new sample evaluation techniques had the advantages of lower price, easier experimental performance, and better resolution [14]. In 2003, the Raman spectroscopy technique for the evaluation of electron depth dose distribution in the irradiated PAG dosimeter was introduced [15].

It is well known that acrylamide is toxic; therefore, there was a need to find another composition of dose gel. A few less toxic formulations of dose gels were introduced. Toxic acrylamide has been replaced with less harmful monomers: *N*-isopropylacrylamide (NIPAM), diacetone acrylamide, and *N*-vinylformamide, in these gels. It has been shown that optical CT evaluation of these dose gels is more advantageous as compared to MRI [16].

The appearance of the free radicals in dose gel, due to the water radiolysis reactions in the presence of the atmospheric oxygen, required the manufacturing of dose gels in an oxygen-free environment, for example, in a glove box with inert gas such as nitrogen or argon. New type of dose gel, which was made of methacrylic acid

(MAGIC), where the oxygen from the atmosphere was bonded in a metallo-organic complex, was introduced. This resolved the problem of oxygen inhibition and enabled the manufacturing of polymer gels in oxygen environment [17]. The principle behind removing the problem of oxygen in the MAGIC gel is in the use of oxygen scavenger such as ascorbic acid [18]. It has been found that other antioxidants may be as well used for the manufacturing of normoxic gels: tetrakis hydroxymethyl phosphonium chloride (THPC), tetrakis-hydroxymethyl phosphonium disulfate (THPS), or hydroquinone (HQ). The dose gels that contain antioxidants are called normoxic dose gels and can be produced under normal atmospheric conditions, avoiding the undesirable damage to the dosimetric properties of gels.

The investigations of dose gel content and polymerization processes in it revealed that the reactions between THPC and polymer radicals reduce the polymerization rates and dose sensitivity, and THPC helps to improve temporal and spatial stability of the polyacrylamide gel dosimeters [19]. This knowledge led to the adaption of iodine doped normoxic gel as a low-dose 3D dosimeter for the diagnostic radiology. The effect of the iodine doping was applied as well for the enhancement of the dose sensitivity in *N*-isopropylacrylamide based (NIPAM) and MAGAT dose gels [20].

The authors [21] introduced a highly sensitive to radiation dose gel with Toluidine Blue O (TBO) for dose range from 1 to 150 Gy evaluation in gamma rays. The spectrum of the prepared dyed gel samples changes after the application of gamma irradiation and fading of the blue gel color is present when the radiation dose is increasing. It has been shown that these gels are suitable for monitoring various radiation processing applications and relative dose distribution verification in clinical applications. A new polymeric gel that is based on the itaconic acid (ITA) and *N,N'*-methylene bisacrylamide, which recorded low oxygen infusion in the gel volume, was studied as possible candidate for the X-ray dosimetric purposes [22].

Recently, several research groups have started searching for alternatives to toxic polymer gels. The leucomalachite green (LMG) dosimeters exhibit good radiation properties and were found to be stable and less temperature-sensitive than the polymer gel dosimeters [23]. The clinical use of the LMG dosimeter was validated for the IMRT treatment of the pituitary gland carcinoma. A good agreement between measured dose distribution and calculated dose distribution was found by giving clinical confidence to carry out the treatment on the patient. Moreover, the new gels scanning and evaluation methods is under investigation. The new type dosimeter was developed in order to control Tyndall (Mie) scattering that is appearing during the optical scanning. The imaging distortions cause severe uncertainties in the extracted dose distribution. This has encouraged research for the new 3D dosimeters where the light is only absorbed at specific wavelengths [23].

Another low toxicity polymer gel that is based on *N*-hydroxymethyl acrylamide (NHMA) showed very promising results in terms of dose evaluation by using NMR spin-spin relaxation rate up to 20 Gy. No significant dose rate and radiation energy dependence was observed in PNHMAG polymer gel dosimeters. This type of polymer gel formulation was adopted for the Quality Assurance (QA) in radiation therapy [24].

Further studies of polymer gels dosimeter application in medicine were focused on the pretreatment verification in clinical radiation therapy. It has been shown that the pass rate map can be used to evaluate the dose temporal readability of polymer gel dosimeters (PGDs) and the NIPAM PGD can be used as well for the clinical pretreatment verifications [25].

The main challenge for the ionizing radiation that is used in cancer treatment is to destroy DNA strands, thus preventing the ability of cancer cells to divide [26]. Electron and proton beams, in rare cases, high-energy photons may introduce cell damages directly interacting with DNA strands, but in most cases, reactive radicals are produced during the atomic interactions that destroy DNA structure. Particle beams are defined as low linear-energy-transfer (low-LET) radiation, where the whole energy is deposited to the target along the short particle range. The neutral neutrons are defined by high linear energy transfer (high-LET) radiation; thus, the primary damage of DNA due to the nuclear interactions is dominating. If a tumor cell is damaged by low LET radiation, it has a good chance to repair itself and continue to grow. With high LET radiation, the chance for the damaged tumor cell to repair itself is very small [26].

Proton therapy is one of the cancer treatment methods that is using high-energy protons. Proton has relatively large mass and little lateral side scatter in the tissue. The beam does not broaden much and stays focused on the irradiation target. All protons of the given energy have a certain penetration range. Very few protons penetrate beyond that distance. Furthermore, the dose delivered to the target is maximized only over the last few millimeters of the particle's range: this maximum is called the Bragg peak. Due to this very specific interaction of protons with matter, it is highly important to evaluate the delivered dose to the target correctly. Since dose gels are nearly tissue equivalent, they might be used for dose verification during the proton irradiation. There are only very few studies related to the dose gel evaluation after the proton irradiation [1, 27]. The studies of proton beam induced changes in the irradiated polymer gels revealed that the characteristics of polymerized dose gels are dependent on the linear energy transfer (LET) and radiobiological effect (RBE). Monte Carlo simulations of clinical proton beam-line under a range of beam conditions were compared with MRI analysis of the irradiated polymer gel BANG-1. The gel investigation results were found to underestimate the height of the full energy Bragg peak that is relative to the simulation by the order of 30 %, due to the increased LET in this region [28]. The dose response of MAGAT gel detector at different depth positions from the beam entrance for a single field Bragg peak irradiation scheme was investigated. It showed that MAGAT type polymer gel is effective enough for the fundamental reproducibility tests of 3D treatment-planning system, such as monitor unit verification and standard isodose verification by using a single field proton beam [27].

The use of polymer gel dosimeters for quality assurance purposes in the neutron beam applications was investigated [29]. The aim of the study was to find the optimal

composition of the MAGAT polymer gel, which will be suitable to sense the thermal neutron, fast neutron, and gamma ray components in the irradiation field that is used for boron neutron capture therapy.

The polymer dose gels development and application for medical dosimetry purposes is a significant step towards higher quality and more accurate dosimetry. During the years of polymer gels development, 1D dosimeters were improved to 3D systems for treatment planning quality assurance. The ability of monomers based gels to attenuate the ionizing radiation makes gels suitable for the dose sensing as well as radiation protection. These properties are essential for the radiation shielding screens and personal radiation protection equipment.

2.2 Structure of polymer gels

Polymer gels are known as cross-linked bulk polymeric structures. They contain either covalent bonds that are produced by the simple reaction of one or more comonomers, association bonds such as hydrogen bonds, or strong van der Waals interactions between chains, crystallites bringing together two or more macromolecular chains or physical cross-links from entanglements. The complexity of the possible bonding after the irradiation leads to its specific characteristics. The network structure, gelation point, swelling mechanism, inhomogeneity, adhesion properties, and gel mechanics are known as the most important features for all types of polymer gels [30–33]. The structure of non-irradiated dose gel can be determined from the basic calculations taking into account the amount of gelatin and monomers. When radiation is applied, the network of 3D polymer chains grows. Meanwhile, the renaturing of collagen leads to the network bonds formation. The collagen unit (tropocollagen) is a rod shape structure made of three polypeptide and amino acids, such as proline, hydroxyproline, and glycine chains. The rod length is approximately 280 nm. The chains are twisted into a left-handed helix and all three wrapped into a super-right-handed helix [1]. The microscopic structure of non-irradiated polymer gel that is based on the stoichiometric calculations is presented in Fig. 1.

The initial composition of polymer gels is described by the total weight fraction $\%T$ of monomers and relative weight fraction $\%C$ of cross-linker to total monomer amount. These may be expressed as Eq. 2.1 and Eq. 2.2 [30]:

$$\%T = 100 \frac{m_{a+b}}{m_{sol}} \%, \quad (2.1)$$

$$\%C = 100 \frac{m_b}{m_{a+b}} \%, \quad (2.2)$$

where m_{a+b} (g) is a total mas of monomer and cross-linker; m_b , (g) is a mass of cross-linker; m_{sol} (g) is a total mass of solution.

The distance between polymer chains is random, but according to the other researchers [1], cubic topology could be considered, and the size of vacant spaces in

gelatin network was found to be in order from 7 nm to 12 nm. The size of the monomers is in the order of a few ångstroms. For AAm, it is 0.4–0.3 nm, for BIS, 1–0.3 nm. The average intermolecular distance of monomers in the non-irradiated dose gel can be calculated from the molecular weight and the molecular weight fraction [1]. For (6%T, 50%C) PAG, the average intermolecular distance is 2.0 nm for the AAm monomers and 2.5 nm for the BIS cross-linker. The average molecular distance between the water molecules is in the order of 0.39 nm. Taking into account that the distance between the structure made of gelatin molecules (see Fig. 1) is large compared to the sizes of monomer and water molecules, it can be concluded that this gelatin structure may not interfere the migration of monomer and cross-linker molecules [1].

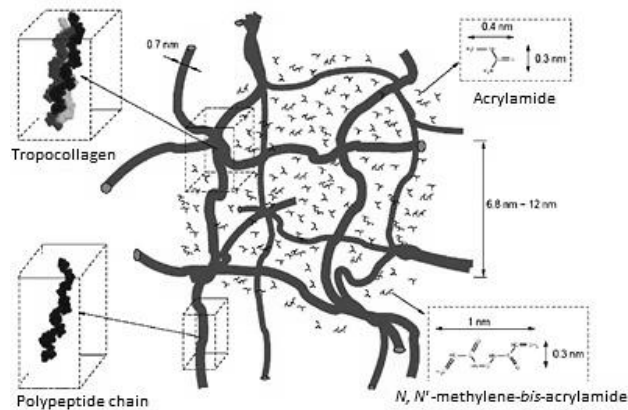


Fig. 1. The microscopic structure of non-irradiated polymer gel [1]

When radiation is applied, different polymer bonds are created in the gel. When PAG gel has high amounts of cross-linking agents, polyacrylamide network can be seen as microgel particles embedded in the gelatin hydrogel. Moreover, the size of the formed microgel is different due to the applied dose. As a result, the polymer chain density in the irradiated PAG dosimeters is not uniform. The studies showed the formation of high and low gel density domains [1].

Gelation rate studies demonstrated that the gelation occurs in the first minutes after quenching the sol-gel at temperatures below 35 °C [1, 34]. After 1 hour, it becomes slower. This chemical instability causes the changes in dose response and sensitivity to the radiation curves. Using FT Raman spectroscopy, it was shown that the anti-oxidant (e.g. THPC) might cross-link gelatin macromolecules. Moreover, it was stated that the irreversible gel change, when broken chemical bonds due to the polymerization could not be rebuilt, might have an effect on the polymerization kinetics [1, 34].

Polymer networks are commonly classified as “physical” and “chemical”. While chemical networks consist of chains that are interconnected by the permanent covalent bonds, physical networks are obtained by non-covalent interactions between the chains. Typical examples of these non-covalent interactions are helical, glassy, or

nanocrystalline chain associations; these cross-links are strong, and the physical gels that are obtained from them usually resemble the behavior of covalently bonded networks [35].

The network of the whole polymer gel volume is defined by the method of preparation, ionic charge, and physical structure features. Taking into account the physical structural features of the polymer system, gels are classified as amorphous hydrogels, semi-crystalline hydrogels, hydrogen-bonded or complex structures. According to their preparation method, the polymer gels are classified as homopolymer hydrogels, copolymer hydrogels, multipolymer hydrogels, and interpenetrating polymeric hydrogels. Based on their ionic charges, hydrogels may be classified as neutral hydrogels, anionic hydrogels, cationic hydrogels, or ampholytic hydrogels [36].

Homopolymer hydrogels are cross-linked networks of one type of hydrophilic monomers; whereas, the copolymer hydrogels are produced by cross-linking of two comonomers, at least one of which must be hydrophilic to render them swellable. Multipolymer hydrogels are produced from three or more comonomers that are reacting together. Finally, hydrogen bonds and complex structures may be responsible for the three-dimensional structure formation. The structural evaluation of the hydrogels reveals that the ideal networks are only rarely observed. Fig. 2A shows an ideal macromolecular cross-link (hydrogel), indicating tetrafunctional (bonded at four sites) cross-links (bonds) that are produced by the covalent bonds. However, in real networks, it is possible to encounter multifunctional cross-linking points (Fig. 2B) or physical molecular entanglements (Fig. 2C) that are playing the role of semi-permanent bonds. Hydrogels with molecular defects like unreacted functionalities with partial entanglements (Fig. 2D) and chain loops (Fig. 2E) are always possible [35]. Neither of these effects contributes to the mechanical or physical properties of the polymer network. The terms “cross-link,” “bond,” or “tie-point” (an open circle symbol in Fig. 2D) indicate the interconnection points of several chains. These bonds may be carbon atoms, but they are usually small chemical bridges with molecular weights that are much smaller than those of the cross-linked polymer chains. In other situations, a bond may be an association of macromolecular chains caused by van der Waals forces. Finally, the network structure may include effective bonds that either can be simple physical entanglements of permanent or semi-permanent nature or ordered chains forming crystallites. Thus, the bonds should never be considered as points without volume, which is the usual assumption made when developing structural models for the analysis of the cross-linked structure of hydrogels. Instead, they have a finite size and contribute to the deformational distribution during the biomedical applications [35].



Fig. 2. Different types of network bond. A) Ideal macromolecular network, B) real networks with multifunctional bonds, C) physical molecular entanglements, D) unreacted functionalities with partial entanglements, E) chain loops [35]

Cross-linking. Polymer networks and gels consist of three-dimensional, percolated assemblies of cross-linked macromolecules. They are versatile materials for various applications, including those as super absorbers. Cross-linking point is a chemical bond, atom, or a group of atoms that connects two adjacent chains of atoms in a large molecule such as a polymer and other protein [37]. Adding cross-links between the polymer chains affect the physical properties of the polymer, depending on the type of cross-links, the amount of cross-linked points per unit gel volume (mol/cm^3), and presence and absence of crystallinity [31]. Cross-linking results in elasticity, in some cases, the decrease in viscosity, insolubility of the polymer, increased glass temperature (T_g) and increased strength and toughness, transformation of thermoplasts into thermosets. Non-biodegradable synthetic hydrogels can be prepared from the copolymerization of various vinylated monomers or macromers, such as 2-hydroxyethyl methacrylate (HEMA), 2-hydroxypropyl methacrylate (HPMA), acrylamide (AAm), acrylic acid (AAc), *N*-isopropylacrylamide (NIPAM), and methoxyl poly(ethylene glycol) (PEG) monoacrylate (mPEGMA or PEGMA) with cross-linkers, such as *N,N'*-methylenebis(acrylamide) (BIS), ethylene glycol diacrylate (EGDA), and PEG diacrylate (PEGDA) [31].

The cross-linking proceeds when a bond links one polymer chain to another after the environmental impact, such as ionizing radiation. The bonds may be covalent or ionic. The schematic view of cross-linked molecules is presented in Fig. 3. Cross-linking usually refers to the use of cross-links to promote a difference in the polymers' physical properties, and the cross-linking density (cross-linked points per unit gel volume) directly affects the mechanical properties of the gel. Polymers with low cross-link density are viscoelastic.

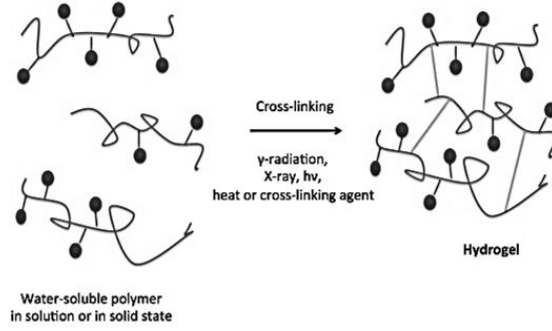


Fig. 3. Cross-linking of hydrogel. Points are presenting not connected bonds [31]

Chemical cross-linking is a highly versatile method to improve the mechanical properties of gels. However, cross-linking agents are often toxic compounds and not environmentally friendly. They give unwanted reactions with the bioactive substances that are present in the hydrogel matrix [31].

The molecular weight of the chains between cross-links, M_c , describes the basic structure of the hydrogel. This parameter defines the average molecular length between two cross-linking points (Eq. 2.3) [38].

$$\frac{l}{M_c} = \frac{2}{M_c} - \frac{\frac{v}{V_1} [\ln(1-2v_{2,s}) + v_{2,s} + \chi_1 v_{2,s}^2]}{(v_{2,s}^{\frac{1}{3}} - \frac{v_{2,s}}{2})} \quad (2.3)$$

An additional parameter of importance in structural analysis of hydrogels is the cross-linking density, ρ_x , which is defined by Eq. 2.4.

$$\rho_x = \frac{l}{vM_c} \quad (2.4)$$

In these equations, v is a specific volume of the polymer, and M_c is the molecular weight of the monomer [38].

The model to characterize the density change as a function of the amount of the formed polymer was developed. The intrinsic density change that occurs when monomer is polymerized is calculated by using the formulation Eq. 2.5 [38]:

$$\Delta\rho_{gel} = \%T_{0Gy} (1-f_m) \Delta\rho_{polymer}, \quad (2.5)$$

where $\Delta\rho_{gel}$ is the gel density change; $\%T_{0Gy}$ is the total monomer fraction in un-irradiated gel; f_m is the fraction of monomer remaining at a given dose (Gy), and $\Delta\rho_{polymer}$ is the intrinsic gel density change per unit dose.

The major advantage of the chemical cross-linking is that it can be customized and designed to satisfy specific needs.

Hydrogel swelling. The physical behavior of hydrogels is dependent on their equilibrium and dynamic swelling behavior in water. Since preparation, they must be brought in contact with water to yield the final, swollen network structure. The Flory-

Huggins theory is used to describe the equilibrium degree of cross-linked polymers, taking into account that the degree to which a polymer network swelled was governed by the elastic retroactive forces of the polymer chains and the thermodynamic compatibility of the polymer and the solvent molecules.

Thermodynamic swelling contribution is counterbalanced by the retractive elastic contribution of the cross-linked structure. The volume degree of swelling, Q , can be determined from Eq. 2.6 [38].

$$v_{2,s} = \frac{\text{volume of polymer}}{\text{volume of swollen gel}} = \frac{V_p}{V_{gel}} = \frac{1}{Q} \quad (2.6)$$

In terms of the free energy of the system, the total free energy change upon swelling is (Eq. 2.7) [38]:

$$\Delta G = \Delta G_{elastic} + \Delta G_{mix}, \quad (2.7)$$

where, $\Delta G_{elastic}$ (J) is the energy contribution due to the elastic retractive forces, and ΔG_{mix} (J) represents the thermodynamic compatibility of the polymer and the swelling agent (water).

Basically, highly swollen hydrogels include those of cellulose derivatives, poly(vinyl alcohol), poly(*N*-vinyl-2-pyrrolidone) (PNVP), and poly(ethylene glycol), among others. Moderate and poor swollen hydrogels are those of poly(hydroxyethyl methacrylate) (HEMA) and many of its derivatives. In general, the basic hydrophilic monomer can be copolymerized with other more or less hydrophilic monomers to achieve desired swelling properties. Swelling influences the solute diffusion coefficient through hydrogels, the surface properties, and surface mobility, the optical and mechanical properties [38]. Different types of polymer gel swelling due to the polymer volume fraction in the gel are represented in Fig. 4.

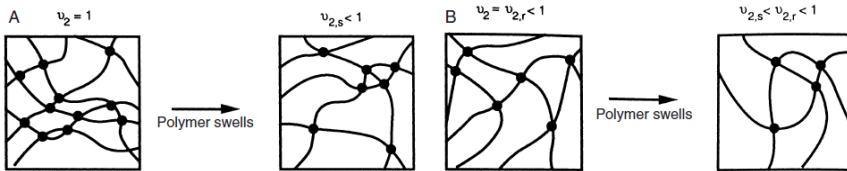


Fig. 4. Different types of polymer swelling [37]

Inhomogeneity. Spatial gel inhomogeneity is a feature of non-ideal polymer gels. In contrast to ideal gels with a homogeneous distribution of cross-links, some dose gels exhibit an inhomogeneous cross-link density distribution, known as the spatial gel inhomogeneity. In polymer dose gel case, it may happen when the irradiation field is not uniform, the dose is fractionated, and other causes. The spatial inhomogeneity dramatically changes the optical properties and mechanical strength of hydrogels [33].

The researchers [33] have used light scattering, small angle neutron scattering, and small angle X-ray scattering to evaluate the spatial inhomogeneity. The gel inhomogeneity may appear as different scattering intensities from the gel and semi dilute solution of the same polymer at the same concentration. The scattering intensity from gels is always larger than that from the polymer solution.

Network imperfections produce the regions that are more or less rich in cross-links, and then, the spatial inhomogeneity increases with the gel cross-link density. However, the inhomogeneity decreases with the ionization degree of gels due to the effects of the mobile counter ions, electrostatic repulsion, and the Donnan potential. The initial monomer concentration that is used in the gel preparation significantly affect the scattering intensity [33].

2.3 Polymer gels for dose measurements

Polymer gel dosimetry is a promising technique, especially in clinical field, to measure the absorbed dose and verify spatial dose distributions that are delivered by the ionizing radiation sources. Gel dosimetry involves a few steps: first, the radiation-sensitive gel, basically made of gelatin, monomer, water, and polymerization sensitizers, is fabricated and poured into an appropriate container and left to set. Second, the prepared gel in the vial is irradiated to a certain dose by using any medical radiation technique in order to initiate polymerization. Due to cross-linking, polymerization processes, and probable sensitivity to ultraviolet and visible light, gels are usually left in the dark for 8–12 hours after the irradiation. Then, the irradiated gels are scanned by using dedicated techniques, and the acquired data is subsequently analyzed [1].

Typical recipes for dose gels are: monomers, gelatin, water, and small amounts of other agents such as oxygen scavengers and dose sensitizers. The most common polymer dose gels are produced of acrylic acid (AAc), methacrylic acid (MAA), acrylamide (AAm), and *N*-isopropyl acrylamide (NIPAM). Plenty of chemical ingredients, such as ascorbic acid, copper sulfate, and the sequence of initiated water radiolysis reactions between monomers and oxygen scavengers, co-monomers, and sensitizers makes polymerization possible [22].

Radiation-induced processes. Chemical reactions that are induced by the irradiation are highly dependent on the particles' type and energy, irradiation dose rate, and chemical ingredients of gels. Some dose gels constituents are environmental temperature and irradiation angle depended. In this section, basic chemical reaction and polymerization mechanisms will be discussed.

A polymer gel dosimeter is based on distilled, deionized water. The percentage content of water varies from 80 to 97 %. Upon irradiation, water molecules are dissociated into several highly reactive radicals and ions. The radiolytic products turn into clusters, and other species forms in the first femtoseconds after the irradiation [1]. The cluster size and the types of species are highly dependent on the type of irradiation and the energy of the primary particles. In the case of X-rays, gamma rays, and electrons, the radiolytic products appear in clusters that are called 'spurs' (see Fig.

5A). Clusters of radicals may diffuse in non-irradiated gels' volume. Therefore, the polymerization may propagate to non-irradiated gel and cause an increase in the optical density (Fig. 5B) [39].

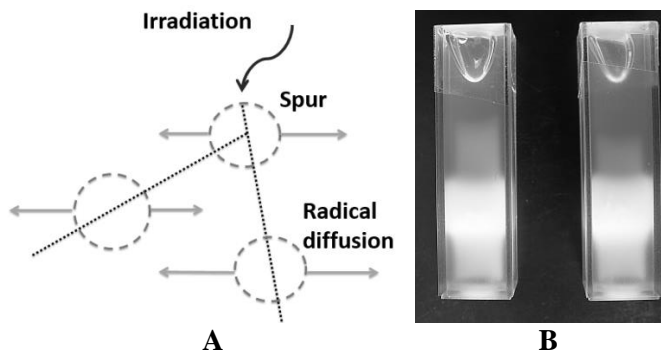


Fig. 5. A) The “spurs” formed after irradiation of high-energy ionizing radiation, B) the appearance of polymerization propagation to non-irradiated gel volume. The 1 cm long part of the sample is irradiated by 15 MeV energy photons [39]

These events, which are pre-thermal, occur in a time period of about 10^{-15} s. It has been found that the location of the radiolytic products spreads within 1 nm when 6 MeV photons are applied. The radius of diffusing radiolytic products starts to grow continuously. The local thermal equilibrium in the recombination of reactive particles is reached after $\sim 10^{-11}$ s [1]. The typical intermolecular distance of the monomers in polymer gels is ten times higher than the displacement of particles from the point of creation. As the molecular diffusion coefficient of water in the hydrogel is only 15 % lower than in the pure water, it can be expected that the diffusion coefficient of the radiolytic products of water is in the same order of magnitude. The radiolytic products of water may react subsequently with the monomers [1].

Polymerization is a key factor for polymer gel dosimeters, since the amount of polymer is directly related to the absorbed dose. Radiation-induced polymerization proceeds by a chain addition mechanism. As it was already mentioned, high energy radiation interacts with organic matter by various physical and chemical mechanisms resulting in the formation of short-lived excited species and other chemical entities such as thermalized electrons and neutral or ionic free radicals, exhibiting longer lifetimes that allow them to undergo bimolecular reactions with various molecular compounds by the translational diffusion [40]. The *in-situ* generation of such longer-lived reactive species can be exploited to initiate the chain polymerization mechanism. The resulting process is called radiation-initiated polymerization [40].

It is known that ionizing radiation acts indirectly to form nano and micro scale structures in dose gel volume. The network formation starts with the continuous reactions of radiolytic products such as H_2 , H_2O_2 , e^-_{aq} , $H\cdot$, $OH\cdot$. Ionizing radiation produces abundant secondary electrons that rapidly slow down (thermalize) to energies below 7.4 eV, the threshold to produce electronic transitions in liquid water [32]. The water radiolysis process is presented in Fig. 6.

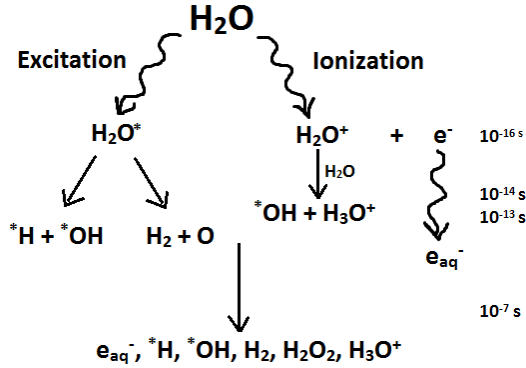


Fig. 6. Formation of molecular products and free radicals [41]

Free radicals can react with carbon-carbon double bond of the vinyl group of monomer molecules. It is essential to form the cross, i.e., the linked network structure of the polymer dose gel, because cross-linked polymer chains are insoluble in water, and they precipitate to form microgels.

The basic chemical reactions and polymerization mechanism that occur in polymer dose gels are as follows [1, 2, 32]:

1. Generation of different types of free radicals by radiolysis of water;
2. Propagation that results in the formation of polymer and the release of heat;
3. Primary cyclization reaction that consumes the remaining vinyl groups;
4. Cross-linking reaction when the net structure is formed;
5. Chain transfer to monomer;
6. Termination of chain;
7. Chain transfer to gelatin;
8. Propagation of gelatin-centered radicals;
9. Termination with primary radicals.

In summary, the decomposition of reactive intermediates R^\bullet can be written as a simplified reaction of which the dissociation rate (k_d) is proportional to the absorbed dose (Eq. 2.8) [32]:



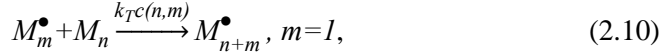
where R^\bullet is the reactive intermediate, radical; k_d is dissociation rate.

The radicals initiate the polymerization of monomers by reacting monomer. The initiation step can be written as follows (Eq. 2.9) [32]:



where M is monomer; M_1^\bullet is initiated monomer radical; k_i is initiation rate.

The general case in which a polymer radical with n monomer units reacts with a monomer or a dead polymer chain containing m monomer units is shown in Eq. 2.10 [32]:



where M_m^\bullet is monomer radical with m monomer units; M_n is monomer with n monomer units; k_{TC} is termination rate; M_{n+m}^\bullet is monomer radical with $n+m$ reactive units.

The termination of the polymerization reaction occurs by the reaction of two radicals by either combination or disproportionation (Eq. 2.11, Eq. 2.12) [32]:



There, M_n^\bullet is a monomer radical with n monomer units; k_{Td} is the disproportionation rate.

Primary radicals generated by the water radiolysis can as well react with growing polymer chains to induce the termination (Eq. 2.13) [32]:



Moreover, primary radicals can react with pendant vinyl groups on dead polymer chains to initiate additional polymerization reactions (Eq. 2.14):



In addition to termination reactions, the growing polymer radical may as well terminate by transfer of the radical group to the other molecules. Most likely, the polymerization mechanism for free radicals is presented in Fig. 7 [32].

a) Generation of primary radicals by radiolysis	$H_2O + \text{Radiation} \rightarrow H_2, H_2O_2, e_{aq}^-, H^*, OH^*$
b) Propagation with monomer	
c) Propagation with crosslinker	
d) Primary cyclization	
e) Crosslinking	
f) Chain transfer to monomer	
g) Termination	
h) Chain transfer to gelatin	
i) Propagation of gelatin-centred radicals	$G\bullet + \text{=} \rightarrow G\text{-}$
j) Termination with primary radicals	

Fig. 7. Free radical polymerization mechanism in polymer gel dosimeters [32]

Typical chain transfer constants $C_M = k_{trans}/k_p$ of radicals are in order from 10^{-3} to 10^{-4} . When cross-linker molecules such as BIS are consumed via propagation reactions, one vinyl group on the cross-linker polymerizes, and the other group becomes a pendant vinyl group along the polymer chain, which is available for the later propagation reactions, which lead to the formation of cross-links [43]. The polymeric gelatin radicals that are formed are too slow to propagate with an additional monomer; thus, the increasing gelatin concentration results in the polymerization extent reduction. The reaction coefficients of the hydrated electron, e_{aq}^- , and the hydroxyl-radical with gelatin are respectively $6.4 \times 10^{10} \text{ l mol}^{-1} \text{ s}^{-1}$ and $9.1 \times 10^{10} \text{ l mol}^{-1} \text{ s}^{-1}$ [32, 42–44].

2.4 Factors that are affecting polymer dose gel stability and sensitivity

The polymer dose gels may be affected by the environmental conditions and their constituents. In the following section, the main factors which affect the dose gel stability and dose sensitivity are discussed. The most important factors that have an impact on the properties of gel are as follows: type and concentration of the cross-linker and concentrations of monomer and gelatin, environmental and inner gel temperature, presence of oxygen scavengers, and dose rate. The influence of direct ultraviolet, visible, and infrared light should be taken into consideration as well.

Cross-linker and monomer concentrations. The typical monomer and cross-linker concentration vary from 3 to 9 % in dose gels, since these are hydrogels, and the main component is water (80–95 %). The increase of BIS and monomer concentrations is limited by their solubility in water and gel's crystallization, which happens when the gel is stored. It was reported that BIS is hard to dissolve at the

concentration above 3 % by weight [45]. If the monomer is a strong acid, it can affect the gelatin within the time of storage; thus, the gel may lose its shape [45].

It was found that the increase of %C (relative fraction of cross-linker) in nPAG, PAG, and 2-hydroxy ethyl acrylate type gels while maintaining constant %T (total monomer concentration) results in the increased dose sensitivity. Increasing %T (in the range from 0 to 8%T), while keeping %C constant, results in the increased dose sensitivity for PAG and nPAG dosimeters. Sensitivity is calculated as the slope of R_2 (spin-spin relaxation in MRI) versus dose curve. Better sensitivity at higher (>15 Gy) doses was explained by the fact that after the BIS dissolution and consumption in polymerization reaction, the precipitated BIS dissolves and is involved in polymerization. Due to the increased monomer concentration, polymerization rate may increase. It was reported that the point at which dose sensitivity starts to decrease is almost at the room temperature solubility limit of BIS [2, 32].

The increase of dose sensitivity was observed when the %T was increased from 2 to 6 %, but no significant sensitivity changes were observed when %T was increased to 8 %. The dose sensitivity changes below 6 % of %T were attributed to the BIS precipitation during the gel preparation and subsequent dissolution induced by the BIS consumption. Less monomer is consumed per radical generated at higher doses because of the decreased (consumed) concentrations of both monomers [2, 32]. The consumption of acrylamide and the BIS in the irradiated PAG dosimeters with different initial BIS fractions are presented in Fig. 8.

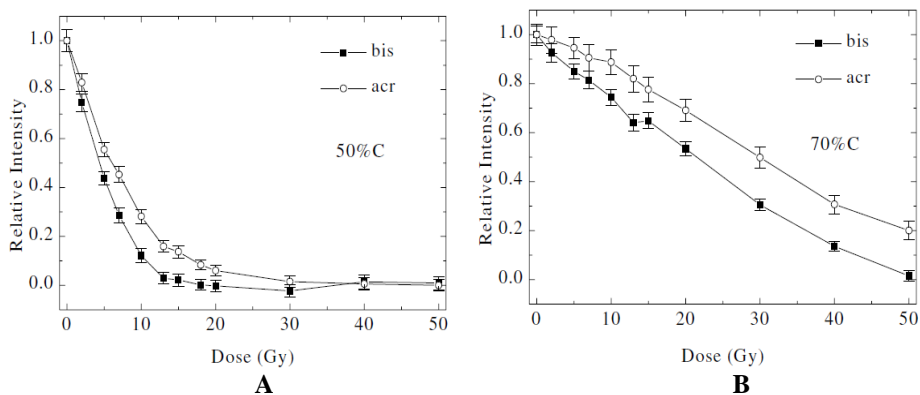


Fig. 8. Consumption of A) acrylamide and B) bis-acrylamide in irradiated PAG dosimeters with different initial bisacrylamide fractions: A) 50% C, B) 70% C [45]

PAG gels which contained low BIS concentrations (<10 %) and were irradiated to moderate doses (5–13 Gy) appeared to form white grains ~48 h post irradiation. This phenomenon is not seen when doses higher than 13 Gy are applied. Raman spectra analysis showed that the grains have the structure of polyacrylamide with no monomer or cross-linker remains. It is concluded that monomer and cross-linker forms tightly knotted polymer network [45].

Temperature. Temperature plays an important role during the gel manufacturing and irradiation. The heating of the mixture to 40–50 °C is needed in order to get gelatin well dissolved and mixed. However, it is recommended to keep the mixture temperature below 55 °C to avoid pre-polymerization reactions. In order to get samples that are well settled and solidified, it was recommended to keep temperature lower than 15 °C [46, 47].

Due to the exothermic reactions during the irradiation, the temperature in polyacrylamide based gels increase and may have an impact on the polymerization reactions and could cause inaccuracy in the dosimeter calibration [2]. The temperature has higher impact on the polymerization propagation rate than on the termination of polymerization in nMAG gels. It is needed to keep the gel temperature constant during the irradiation and evaluation processes to avoid changes in measurement results and let the gel sample to equilibrate [46, 47].

The reaction kinetics is influenced by the temperature at which the reaction takes place. Most reaction rate constants obey the Arrhenius relation [48]:

$$k=Ae^{\frac{E_a}{RT}}, \quad (2.15)$$

where E_a is the activation energy for the reaction (J); T is the absolute temperature (K); R is the universal gas constant (J·mol⁻¹·K⁻¹); A is the pre-exponential factor.

It was reported that the lifetime of the hydrophobic interaction as well as the structure of the associations, such as the quantity of the inter- and intra-chain cross-linking, changed due to the temperature changes. The decrease in the lifetime was evidently demonstrated with the increase in temperature between 25–55 °C; the viscosity at the gel point decreased [48].

The rapid rise of temperature was seen due to the exothermic radiation-induced polymerization. Higher radiation doses cause the increase of temperature in dose gel [46, 49]. The increase of temperature after the ionizing irradiation exposure is called “overshoot”. This phenomenon shows that after applying lower dose (5–10 Gy) irradiation, the unreacted radicals continue to cause the polymerization of gel. There are more unreacted radicals when low doses are applied rather in case of high doses (>10 Gy) [49].

The experiments showed that the room temperature when gel is manufactured and later irradiated has an impact on the polymerized gel dose response. Some examples of common dose gels response to different doses due to temperature variations are presented in Fig. 9.

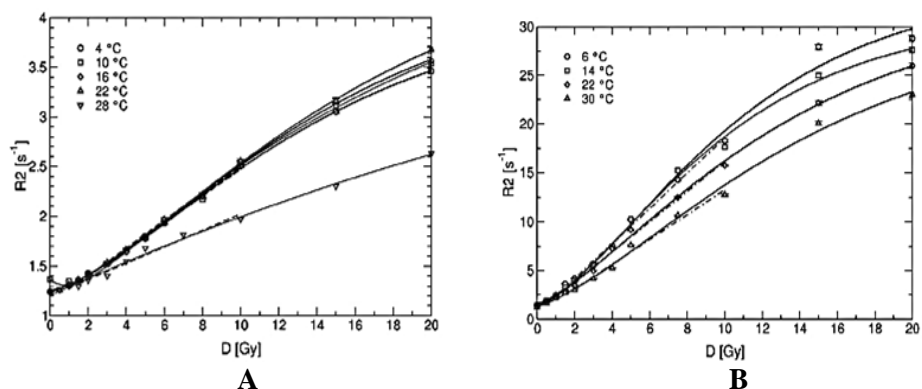


Fig. 9. A) Dose R_2 plots for the PAG polymer gel dosimeter, B) MAG polymer gel dosimeter that are irradiated at various temperatures [42]

A higher sensitivity to the irradiation temperature was found in a normoxic methacrylic acid based dosimeter gels (MAG polymer gel dosimeter). In the case of the MAG polymer gel dosimeter, no gel-sol transition was observed at 30 °C [42].

Dose Rate. The dose rate is one of the most important parameters of ionizing radiation, and it shows the quantity of radiation that is absorbed per unit time. It was shown that the dose rate dependence in nPAG dose gels is less significant as compared to the nMAG gels [1]. This may be a result of competing radiation-induced chemical reactions. nMAG systems contain two radicals that participate in the bimolecular termination. The rate of termination reaction highly depends on the concentration of polymeric radicals. In the case of methacrylic acid, free radical consumption reaction predominates due to the fact that production of the higher radical concentrations at higher dose rates results in much faster radical consumption. The dose sensitivity of MAGICA polymer gel, which was irradiated by the electron beam, was dependent on the electron energy, but no significant dependence on the dose rate was stated [50].

In the case of nPAG dose gel, the dose rate dependence is small because the radical consumption reactions involve only one growing polymer radical (see Fig. 10). Gelatin plays an important role in polymer and radical consuming reactions in nPAG, because a strong dependence of polymerization rate on gelatin concentration was observed for the nPAG type dosimeters. Moreover, the contribution of oxygen scavenger in the free radical consuming reaction must be taken into account [2, 51].

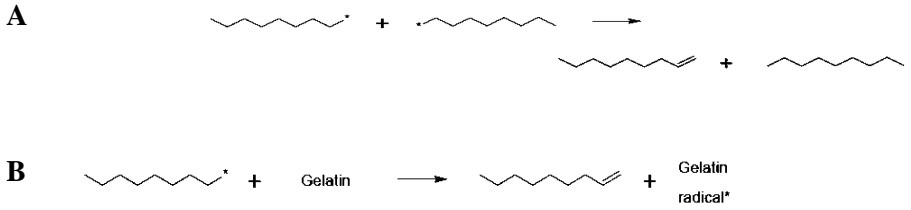


Fig. 10. A) Biomolecular termination consumes two polymeric radicals, nMAG case; B) chain transfer reactions consume one polymeric radical, nPAG case [2]

Only very small dose rate dependence of PAGAT gel sensitivity was reported [52]. The results of dose evaluation of 15 MeV X-ray photon beam (medical linear accelerator) irradiated PAGAT gel dosimeter by using X-ray CT scanner showed the small trend of polymer gel sensitivity dependence on the dose rate in the range of 0.5–5 Gy/min. However, it was stated that this dose rate dependence was clinically insignificant [52, 53]. The same conclusions were made after the dose sensitivity investigation of PAGAT dose gel in the broad range of dose rates from 2 to 288 Gy/h. Other researchers [54] found that for the samples that were irradiated by ¹³⁷Cs brachytherapy source by low-dose rate (8 Gy/h), the response of the PAGAT gel is linear for doses from 2 to 30 Gy. High dose rate (from 48 to 288 Gy/h) does not affect PAGAT gel response to dose. At dose rates, which are < 2 Gy/h, significant reduction of gel response was recorded [54].

Different situation of dose rate effect was seen when PAGAT polymer gel was irradiated by 15 MeV photons at low and moderate doses from 0 to 30 Gy. The CT scanner was used to find out dose response curves due to 0.5 Gy/min to 5 Gy/min dose rates [52]. Fig. 11 presents dose response curves of PAGAT polymer gel dosimeters irradiated with 15 MeV X-ray beam at different dose rate.

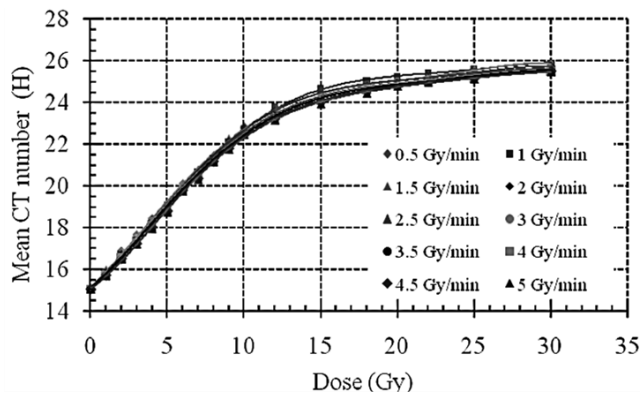


Fig. 11. Dose rate influence on PAGAT dose gel response at different dose rates [52]

Dose rate dependence of PAGAT gel dosimeters was examined by comparing the dose response determined at 2 Gy/min. The dose response curves obtained at 0.5 Gy/min and 5 Gy/min were almost identical to the ones obtained at 2 Gy/min [52].

Oxygen scavenging. Oxygen (O_2) penetration into the gel-filled container impedes the polymerization of gels and contaminates the resultant dose response. Moreover, it can inhibit free radical copolymerization reactions in polymer gel dosimeters, reducing the gel dosimeters' ability to measure the dose. In order to prevent oxygen contamination, the oxygen scavenger can be added to the gel solution in various concentrations. The introduction of oxygen scavengers, such as THPC, ascorbic acid (AA), and hydroquinone (HQ), resolve the "oxygen" problem and allow the manufacturing of normoxic dose gels under normal environmental conditions [55]. Very small amounts of free radical scavenger hydroquinone may be added to the normoxic polymer gels that are containing THPC to prevent the pre-irradiation polymerization, since it is known that HQ reduces the polymerization rate over the whole duration of the polymerization process [19].

Moreover, nitrogen and argon gases are used in the glow boxes for the reduction of the oxygen inhibition during the gel manufacturing processes. Hermetical sealing of the gel-filled containers help to reduce the oxygen infusion into the samples [19].

The investigation of oxygen-affected zones on the samples that were performed by using MRI was introduced by many researchers [56]. It was shown that after the irradiation, the infiltrated oxygen results in an inhibition region within the first centimeter from the top of the gel. Furthermore, the first 1–2 mm from the top of the gel were dehydrated [56].

The reactions that are involving THPC and other oxygen scavengers have not been incorporated into the fundamental mathematical models yet; thus, the experimental data were investigated. THPC was found to be the most reactive antioxidant [57]. THPC, which was left after the reactions with O_2 , was able to react with other constituents in polymer gel, thereby affecting the dose response of the dosimeters and temporal stability of the dose gel. The changes in the gelatin matrix were reported when comparing 100 mM THPC concentration to 0 mM. However, no gel density variations were observed due to the scavengers' concentration [57]. The results of Raman spectroscopy were used for the assessment of the THPC concentration influence on the acrylamide and *bis*-acrylamide. It was found that THPC was reacting with acrylamide and *bis*-acrylamide in non-irradiated PAGAT gels; however, no significant changes in the structure of monomers were observed [57].

The model related to the oxygen reactions in PAG dose gels was extended when the oxygen inhibition reactions were included as well. The extended model enabled the prediction of prolongation of the inhibition periods and contamination levels in the PAG dosimeters [19].

The prepared nPAG dose gels, containing of 6%T, 50%C with varying THPC concentrations, were evaluated by using X-ray CT. Significantly lower dose

sensitivities of the nPAG dosimeters as compared to the anoxic PAG were observed (i.e., 0.32 H Gy^{-1} for nPAG containing 5 mM THPC compared to 0.83 H Gy^{-1} for anoxic PAG) were presented after the measurements with the CT scanner. The authors suggested that this difference in dose sensitivities may be due to the reduction in monomer mobility caused by the more cross-linked gelatin molecules [19].

The experiments with different THPC concentration in PAGAT gels showed low-dose response in the dose range from 1 to 20 Gy for the gels containing 2 mM THPC. It was found that the O_2 inhibition occurred above 10 Gy for the gels containing 3 mM THPC and above ~ 2 Gy for the gels containing 4 mM THPC. The inhibition of oxygen radical scavenging was not observed for the PAGAT gels containing more than ~ 4.5 mM of THPC, as it is shown in Fig. 12 [57].

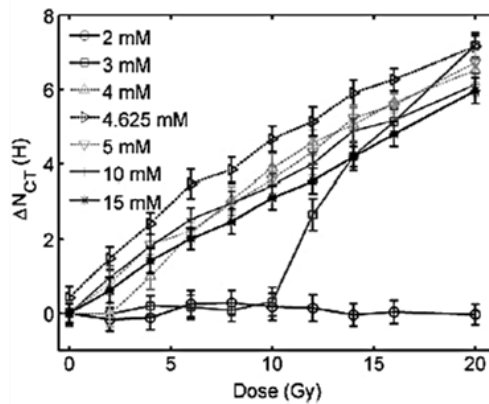


Fig. 12. X-ray CT dose response of PAGAT gels that are containing different concentrations of THPC [57]

It was concluded that the optimal THPC amount was equal to 4.625 mM. When the amount of THPC is above 5mM, THPC reacts with gelatin, thus increasing the coagulation and cross-linking of gelatin and inhibiting monomer migration [57]. Due to this, gels with high amounts of THPC (10–20 mM), exhibiting the highest O_2 consumption rates, were not considered as suitable for dosimetry purposes; THPC as oxygen scavenger was as well used in not gelatin based Fricke detectors, radiation sensitivity of which depends on the oxygen concentration. It was found that the oxygen contamination in Fricke type detectors can cause severe problems, even when THPC is used as a scavenger [58].

Some controversial results were obtained when investigating gels with MRI. It was found that 5 mM of THPC is enough to get the highest sensitivity for a 5 Gy irradiated PAGAT gel samples [59]. The experiments with methacrylic acid showed that for gels consisting of 9 % methacrylic acid, 8 % gelatin and minimal hydroquinone concentrations (~ 0.01 mM), the best MRI response was achieved when 10 mM of THPC was used. Another researchers team provided MRI results indicating

that methacrylic acid based dose gels containing 2 mM THPC record the maximum sensitivity without any evidence of O₂ contamination [59].

2.5 Methods for the evaluation of polymer dose gels

The linear dose response and a constant sensitivity irrespective of energy and dose rate are the most important parameters in polymer gel dosimetry. Radiation related information that is accumulated in irradiated dose gel can be read out by using different imaging techniques. These are based on the specific physical and chemical changes that take place in the irradiated polymer gels. The most well-known and mostly explored imaging techniques for the evaluation of irradiated polymer gels are MRI, Optical-CT, and X-ray CT [1]. The evaluation of the dose, which was accumulated in the irradiated polymer gel, is a technical challenge in some gels due to their thermal instability, sensibility to a visible light, or difficulty to control migration of polymerized species into the gel's volume. The spatial resolution and dose sensitivity are the main parameters that must be assessed in order to record the suitability of the gels to be used for the dosimetric applications.

Magnetic resonance imaging. MRI is most commonly used technique of dose gel evaluation. It is based on the nuclear magnetic resonance (NMR) phenomenon, which is present when atomic nuclei absorb and emit radio frequency energy when placed in an external magnetic field. The ability to differentiate between tissues or materials in MRI is mainly based on various NMR relaxation times exhibited by the water protons in materials. After being excited by the radio frequency (RF) pulses, the proton spins return to their initial conditions at different rate. This phenomenon is called relaxation [3].

The mobility of water molecules in dosimeter is affected by the radiation-induced polymerization. The movement of water molecules, which are attached to the polymers, is restricted, and these molecules are slow in motion. Using the MRI method, one can detect the difference between the motion of polymer restricted and free water molecules measuring their relaxation rates. Spin-lattice relaxation rate R_1 and spin-spin relaxation rate R_2 are affected due to the radiation-induced polymerization in dose gel. Usually, R_2 , the relaxation rate, is used to determine the absorbed dose.

It is to point out, that the MRI based evaluation of dose distribution within a polymerized gel volume is possible because the extension of the polymer network is related to the absorbed dose [49].

The imaging parameters such as echo time (TE), repetition time (TR), and flip angle (FA) have a large influence on the contrast in the diagnostic MR images. The most commonly used MR contrast related parameter in polymer gel dosimetry is the spin-spin relaxation rate R_2 .

Transverse relaxation rate, R_2 (1/ms), is determined as follows (Eq. 2.16) [49]:

$$R_2 = \frac{1}{T_2} = \frac{\ln(S_1/S_2)}{TE_2 - TE_1}, \quad (2.16)$$

where T_2 is the transverse relaxation time (s), and S_1 and S_2 are the signal intensities (a.u.) at TE_1 and TE_2 , respectively [49].

The collection of clinically used T_2 weighted images are used to calculate R_2 maps [1]. Despite the wide applicability of MRI for dose gel evaluations, it is limited by temperature dependence in some dose gels and high equipment related gel processing price [60, 61].

Optical-scanning. The majority of polymer gels becomes increasingly opaque upon the irradiation due to the increasing number of radiation created polymer micro structures and related density. This feature enables the application of optical equipment for the absorbed dose evaluation [1].

A few different optical scanner types have been presented during the last decade. The optical CT scanner is one of them. It consisted of a laser light source and photo-detector, which was collecting transmitted information that was obtained from the laser beam, which was passing through the rotating gel sample at the fixed position [62]. The whole gel volume was evaluated by reading out scanned information from the rotated sample at different fixed detector locations (projections). Another optical scanner was based on the cone beam shaped diffuse light source, which illuminated the gel phantom, and the transmission images were acquired by using a CCD camera [63]. Commonly used scanner generates parallel incident light and has a large plano-convex lens that is installed. The second plano-convex lens is used to focus the light beam onto a CCD camera when the light passes through the gel sample. A typical scheme of the optical CT scanner is presented in Fig. 13 [17].

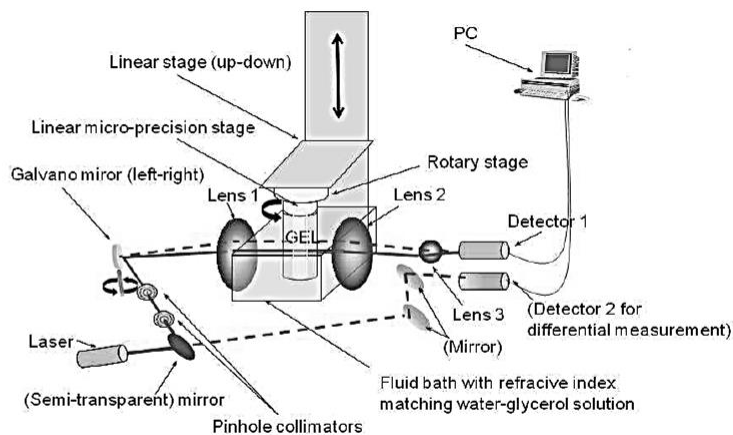


Fig. 13. A typical scheme of the optical CT scanner [17]

Light scattering was defined as a primary mechanism responsible for the optical contrast, since the absence of absorption bands in the turbidity spectra of gels irradiated to different doses was observed. It was found that the refractive index of the irradiated gels was increasing with the increasing dose. Light scatter and light refraction are the potential sources of artifacts in the optical-CT dosimetry.

The Beer's law relates the measured signal intensity I to the signal in the absence of the sample I_0 by the formulation (Eq. 2.17):

$$I=I_0\exp[-\int_{ray-path}\mu(s)ds], \quad (2.17)$$

where μ (m^{-1}) is a quantity known as the optical attenuation coefficient, and s (m) is a distance along the selected ray path through the sample. Under appropriate circumstances, the changes in μ are proportional to the absorbed dose or can be related to the dose by calibration [17].

If projections are obtained with the sample that is positioned in a range of rotation angles (typical of the order of several hundred), the mathematical procedure of filtered back-projection may be used to reconstruct 3D images of attenuation coefficient, μ , and appropriate calibration dose.

Optical-CT could provide low cost and attractive alternative to the MRI scanning of the polymer gels [1].

The exploration of advanced optical scanning technique led to the new investigations of the polymerization reaction duration in the irradiated gels. Dose response, uniformity/linearity, the evaluation of tissue equivalency of specific gel, the reproducibility of features in the manufactured gel dosimeters were investigated. However, it should be noticed that light reflection, refraction, and scattering may cause inaccurate dose reconstruction, and it is still a challenge for the engineers [64–66]. Moreover, it should be reminded that MRI based dose gel evaluation retains unique abilities that are enabling the imaging of arbitrarily shaped dose gels within the opaque or inhomogeneous phantoms [66].

UV-VIS spectroscopy. Ultraviolet-visible (UV-VIS) light spectroscopy refers to absorption, transmittance, or reflectance spectroscopy in the ultraviolet-visible spectral region. UV-VIS is in most cases used in the analytical chemistry for the quantitative determination of different analytes, such as transition metal ions, highly conjugated organic compounds, and biological macromolecules [67]. For a polymer gel investigation, UV-VIS spectroscopy is used to find out the hydrogel transmittance or absorbance spectra changes due to the absorbed dose. Usually, the wavelength range from 300 to 800 nm is investigated. The authors [68] report this investigation method as accurate and reliable for the investigation of hydrogels irradiated ^{60}Co medical source up to 12 Gy and 6 MeV energy linear accelerator source up to 10 Gy. The maximum absorbance (intensity) peaks that are measured for gels are reported to be placed in the range of 300–500 nm. The recorded absorption reaches from 0.5 to 3.2 a.u for the investigated silver nitrate doped HEMAG (2-hydroxyethyl methacrylate monomer) and PAGAT [68, 69].

Raman spectroscopy. Raman spectroscopy is a vibrational nondestructive spectroscopic technique. It provides information on molecular vibrations and crystal structures. Usually, a laser is used to irradiate sample, and scattered light is detected as Raman spectra by using a CCD camera. The characteristic fingerprinting pattern in the Raman spectra makes it possible to identify substances, including polymorphs,

and evaluate local crystallinity, orientation, and stress. The recorded spectra give information about the molecular structure of complex mixtures and solutions [70].

Therefore, the method is useful to study the radiation-induced changes in the polymer gels. The correlation of monomers' vibrational bonds before and after the radiation was recorded by the authors [71–73]. Moreover, Raman spectroscopy was used to investigate the dose distribution with spatial resolution near 1 μm , the changes of gels' chemical structure, monomer consumption, and polymer formation rates for NIPAM [74, 75], PAGAT, PHEMAG, VIPET, and other hydrogels [71, 76]. The tendency to increase the Raman peak intensity was recorded for the bonds that are representing the polymer formation and the decrees of intensity for the peaks that are representing the amount of monomer. The peaks broadening and shifts due to the absorbed doses were reported in papers as well [77]. FT-Raman spectroscopy was reported as a tool to investigate cross-linking density changes during the copolymerization of PAG. Moreover, it was considered as a quantitative method for measuring absorbed radiation dose in the radiation dosimetry [78].

2.6 Application of polymer gels in medicine and industry

Due to the electrical and mechanical properties and tissue equivalency, the polymerized dose gels became highly applicable. From microelectronics to dose measurements in radiotherapy, from pharmacy to industry, these gels are used for a variety of applications. The numerous choices for polymeric formulations allow to design and manufacture chemical and physical cross-linked hydrogels that are having macromolecular structures of the desired swelling and mechanical characteristics.

Summing up, the applications of polymer gels in the scientific areas include tissue engineering, transplantation, microencapsulation, controlled drug delivery, wound dressing, bio-sensing, dosimetry of radiotherapy, food industry, micro and nano patterning.

Biomedical applications. The most widely used hydrogel is cross-linked poly(hydroxyethyl methacrylate) (PHEMA) gel. Moreover, acrylamides, *N*-vinyl-2-pyrrolidone (NVP), methacrylic acid (MAA), methyl methacrylate (MMA), and maleic anhydride (MAH) have been proven as useful monomers to form polymer hydrogels for the biomedical applications [79].

Some polymer gels are inert to normal biological processes, show resistance to degradation, are permeable to metabolites, are not absorbed by the body, biocompatible, could be sterilized by gas or heat, and can be prepared in a variety of shapes and forms [80]. The main properties of such gels depend on the method of their preparation, polymer volume fraction, and degree of cross-linking, temperature, and swelling agent. The swelling, mechanical and biomedical characteristics of PHEMA gels as well as their diffusivity have been widely studied. Due to their biocompatibility and possible hydrophilicity, they can impart desirable release characteristics to controlled and sustained release formulations. These gels as well represent blood-compatible biomaterial. Nonionic hydrogels for blood contact applications have been

prepared from poly(vinyl alcohol), polyacrylamides, PNVP, PHEMA, and poly(ethylene oxide) [81]. Due to high oxygen permeability, the mechanical stability, and favorable refractive index of polymer gels, they are used as a material to manufacture contact lenses. Other potential applications of hydrogels include bio adhesives, wound-healing, artificial tendon materials, artificial skin, vocal cord replacement materials, maxillofacial, artificial kidney membranes, and articular cartilage [79–81].

Pharmaceuticals. Polymer gels became very popular for pharmaceutical applications recently. They are used for drug absorption and delivering. It is known that poly(vinyl alcohol) systems, theophylline, polyHEMA-*co*-MAA, and their copolymers are mainly used for the pharmaceutical purposes. Hydrogel systems represent matrices with incorporated drugs that are swollen to equilibrium. Basically, the system that is prepared by incorporating drug into a hydrophilic, glassy polymer can be swollen when brought in contact with the biological fluids. If the polymer is cross-linked or it is of sufficiently high molecular weight, the equilibrium state is a water-swollen gel. The equilibrium water content of such hydrogels can vary from 30 to 90 % [82]. The swelling process proceeds towards the equilibrium at a rate determined by the water activity in the system and the structure of the polymer. If the dry hydrogel contains a water-soluble drug, the drug is essentially immobile in the glassy matrix, but it begins to diffuse out as the polymer swells in the water. Thus, drug release depends on two simultaneous rate processes: water penetration into the device and drug diffusion outward through the swollen gel. The continued swelling of the matrix causes the drug to diffuse increasingly easy [82, 83].

Electronics. Nowadays, the gel polymer electrolytes are mainly used for the manufacturing of lithium ion battery. The gel polymer electrolyte is using polymer as a matrix to fix solvents. It was shown that polymer gels have the higher stability than liquid electrolyte. Moreover, they provide an alternative solution to safer lithium ion battery [84]. In the last decade, many gel polymer electrolytes have been developed based on the homopolymer or copolymer, including vinylidene fluoride-hexafluoropylene, poly(vinylidene fluoride), poly(methyl methacrylate), poly(ethylene oxide), poly(acrylonitrile-methyl methacrylate), polyacrylonitrile, poly(acrylonitrile-*co*-methyl methacrylate-*co*-styrene). It is as well known that the electrospun PAN/PMMA membrane was identified as being suitable for the application in safe, reliable, and long-lasting lithium batteries [84].

Another field where polymer gels play a significant role is the ensuring of proton conductivity in semi-solid electrolytes of electrochemical capacitors, micro super capacitors, flexible solid-state supercapacitors, and dye-sensitized solar cells [85–87]. Proton conducting systems are very promising as solid ionic conductors because of their superior ionic conductivities. Polymer gels help to solve many cases related to corrosion, packing, leakage, and self-discharge issues. The key issue for the application of proton conducting systems is to maintain high ionic conductivity as well as a good contact at the electrolyte-electrode interface. Electrical double layer

capacitors, where high surface area carbons are used as active materials, were created recently. Polymer gel membranes are used as electrolytes or separators in various applications such as photosynthesis, fuel cells, sensors, supercapacitors, or electrochromic devices [88].

Radiation protection equipment. Polymeric nanocomposites as materials for the radiation attenuation are mainly used as radiation protection equipment for personnel. The majority of protective screens that are used in clinics contain lead, which is highly toxic. Recent EC Directive 2011/65/EU, RoHS II, restricts the application of lead in medical devices (exception: shielding constructions against ionizing radiation), stresses the awareness that in the future, lead shall be fully replaced by other materials (EC Directive 2011/65/EU). Cu, W, Bi, Mo, or lanthanides nanoparticles that are embedded into the polymer matrix can be used for the fabrication of radiation protection screens [89].

Different methods are used for synthesis and stabilization of metal/oxide particles; electrochemical synthesis is one of them. Due to the electrochemical behavior of tungsten (W) and molybdenum (Mo) in electrolytes, it is impossible to synthesize pure W and Mo particles; however, it is possible to deposit electrochemically W and Mo alloys with Fe group metals: Fe, Co, and Ni, where concentrations of W may vary from 10 to 60 % and Mo from 5 to 55 % [90]. According to the modelling results of Haber and Froyer [91], the embedding of these particles into the polymer matrix shall lead to the creation of effective radioprotective nanocomposites, which X-ray attenuation properties depend on the concentration and compatibility of nanoparticles [90–92].

After reviewing the analyzed literature, it could be mentioned that polymer dose gels and polymeric composites for medical purposes have been developed for more than 20 years. Various polymer gels made of acrylamide, *N*-vinylpyrrolidone, acrylic acid were proposed for the radiation dose evaluation for the high doses irradiation. The basic radiolysis and polymerization mechanism was proposed, and the most important gels properties were discussed in the chapters.

Earlier, the radiation protection and dosimetry were focused on the high doses (>20 Gy) measurement and control. Nowadays, the biologically harmful effects were proven when low doses (0.1–10 Gy) were applied during the cancer treatment procedures. For the patient dosimetry, basically, one-dimensional dosimeters (TLD, OSL) were used, which could measure the dose in the limited area, i.e., point. Nonetheless, there is a need to visualize a dose in 3 D and find out the exact dose distribution at all the irradiated volume, which could be done by a polymer gel dosimeter. However, there was no suggested polymer gel, which could be sensitive enough to measure the irradiated dose in the low-dose range from 0.5 to 10 Gy. In order to solve this problem, the development of polymer gel, which could be sensitive to low-dose irradiation for medical radiation sources such as (linear accelerator, Co⁶⁰) photons, protons, electrons, and neutrons, was aimed. In order to achieve this goal, the normoxic polymer gels were prepared and irradiated by different medical sources,

and in order to perform accurate polymer gel sample evaluation, a new photo-scanning method was developed.

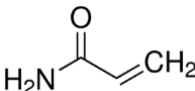
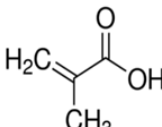
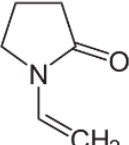
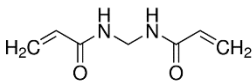
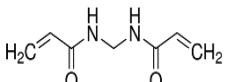
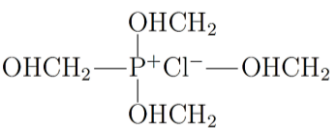
Medical doctors suffer from scattered and secondary low-dose radiation during the diagnostics and therapy procedures such as angiography. Some visible light opaque, lead rich protective equipment was suggested to protect medical personnel. However, transparency is needed to perform the surgery precisely. Therefore, highly toxic lead was restricted to use in medicine by EC Directive 2011/65/EU. In order to solve this problem and adopt knowledge from the polymer gels development, it was aimed to develop polymeric lead-free protective screen by keeping high radiation attenuation coefficient.

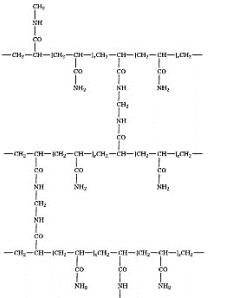
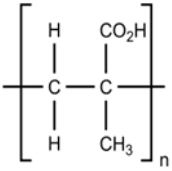
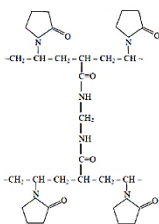
3. INSTRUMENTS AND METHODS

3.1 Fabrication and evaluation of polymer gels

Typical recipes for dose gels include water, gelatin, specific monomer(s), small amounts of radiation sensitizers, and other agents are presented in subsection 3.1.1. Three different types of normoxic dose gels: nPAG, nMAG, and VIPET, were chosen for the investigation. The configuration of acrylamide, methacrylic acid, and *N*-vinylpyrrolidone molecules and its polymeric derivatives are presented in Table 1.

Table 1. Polymer gel constituents

Gel constituents	nPAG	nMAG	VIPET
	Highly purified water ($\geq 99\%$ HPLC grade water, Sigma-Aldrich)		
	Gelatine from porcine skin (A type, 300 Bloom, Sigma-Aldrich)		
Monomer	Acrylamide (AAM), $\geq 99\%$, Sigma-Aldrich 	Methacrylic acid (MAA), 99%, Sigma-Aldrich 	<i>N</i> -vinylpyrrolidone (VIPE), $\geq 99\%$ Sigma-Aldrich 
Cross-linker	<i>N,N</i> -methylene-bis-acrylamide (BIS), 99%, Sigma-Aldrich 	—	<i>N,N</i> -methylene-bis-acrylamide (BIS), 99%, Sigma-Aldrich 
Oxygen scavenger	hydroxymethyl phosphonium chloride (THPC), 80% in H ₂ O, Sigma-Aldrich 		

Final product (polymerized dose gel)	Acrylamide-based cross-linked polymer	Poly (methacrylic acid)	<i>N</i> -vinylpyrrolidone- based cross-linked polymer
			

The proportion of a particular gel ingredients within a mixture, as measured by weight (w/w %), was calculated by following the provided recommendations [92]. The total monomer concentration %*T* was calculated by using equation (Eq. 3.1):

$$\%T = \frac{\text{mass of monomer in g} + \text{mass of cross-linker in g}}{\text{total volume in ml}} \times 100\%. \quad (3.1)$$

The weight percentage of cross-linker %*C* was calculated by using equation (Eq. 3.2):

$$\%C = \frac{\text{mass of cross-linker in g}}{\text{mass of cross-linker in g} + \text{mass of monomer in g}} \times 100\%. \quad (3.2)$$

It is to assume that %*C* is not the concentration of cross-linker in the solution; it is the ratio of cross-linker to the total monomer/cross-linker concentration.

The mass of the material that is required for the preparation of solution of known volume and concentration, and concentration of the solution that is resulting from a known mass of compound in a specific volume was calculated by formulation (Eq. 3.3) [92]:

$$\text{Mass in g} = \text{concentration} \left(\frac{\text{mol}}{\text{l}} \right) \times \text{volume (l)} \times \text{molecular weight} \left(\frac{\text{g}}{\text{mol}} \right). \quad (3.3)$$

3.1.1 Fabrication of dose gels

The typical nPAG polymer gels were prepared as follows: gelatin from porcine skin (5 w/w %, Sigma-Aldrich) was dissolved separately from the monomers in half-amount of the total water volume (89 w/w %). The solution was heated up to 40 °C and stirred (magnetic stirrer Heidolph MR 3001 K) until the solution became clear. Then, acrylamide (3 w/w%, Sigma-Aldrich) and *N,N*-methylene-*bis*-acrylamide (3 w/w %, Sigma-Aldrich) were added one by one to the solution. The solution was

mixed and cooled down to 38 °C. An antioxidant (tetrakis-hydroxymethyl phosphonium chloride THPC, 10 mmol/l, Sigma-Aldrich) was added simultaneously, and the solution was stirred for next 5 minutes. The prepared nPAG dose gel was poured into the standard disposable PMMA cuvettes (Brand 2.5 ml makro), tightly closed, and stored at a fairly low temperature (5 °C) in a dark place for 24 h to set [93].

The typical nMAG gel that consisted of 8 % of gelatin from porcine skin was dissolved in 86 w/w % of distilled water of high purity (HPLC grade water). When the gelatin was fully inflated by the water, a flask with a gel was heated up to 35 °C while stirring. After the gelatin was fully dissolved, 5 % of methacrylic acid (MAA) was added, followed by the addition of 2 mM of tetrakis-hydroxymethyl phosphonium chloride (THPC). The mixture was heated up to 45 °C under the continuous stirring. Then, the heating was stopped, and the prepared gel was left to cool down and settle. The whole process was conducted in a fume hood under the atmospheric conditions without using any oxygen purging devices. In order to minimize the possible oxidation, the prepared gel was filled up to the top of the vial into the standard PMMA cuvettes, which were immediately sealed. The cuvettes were kept at room temperature at least for 8 hours and then stored in cool and dark place until irradiation [71].

The normoxic VIPET polymer gels were composed of 7 w/w% of gelatin, 4 w/w% *N*-vinylpyrrolidone (VIPE), 4% w/w% *N,N*-methylene-*bis*-acrylamide (BIS), 10 mM of tetrakis (hydroxymethyl) phosphonium chloride (THPC), and 89 w/w% of distilled water. The manufacturing procedure was performed in normal atmospheric conditions in a fume hood as follows: the gelatin was added to the distilled water at room temperature (25 °C) and allowed to dissolve for 20 minutes. The solution was heated to 45 °C. Once the temperature was stabilized, and the solution was clear, the BIS was added. Heating was achieved through a hot-plate and stirring unit. When the solution became transparent, about 15 min later, the mixture was cooled down to approximately 35 °C, and VIPE was added. When the constituents were completely dissolved after about 5 min, THPC was added to the solution. Heating and stirring was switched off after 5 minutes, and the solution was left to settle. VIPET gel was poured into the standard PMMA cuvettes [94]. The prepared gel samples were left to settle for 5–10 min and then tightly closed and left for 24 hours in dark and cool place. Fig. 14 shows the standard preparation process of dose gel. The full chemical composition of the prepared polymer gels is given in Table 2.

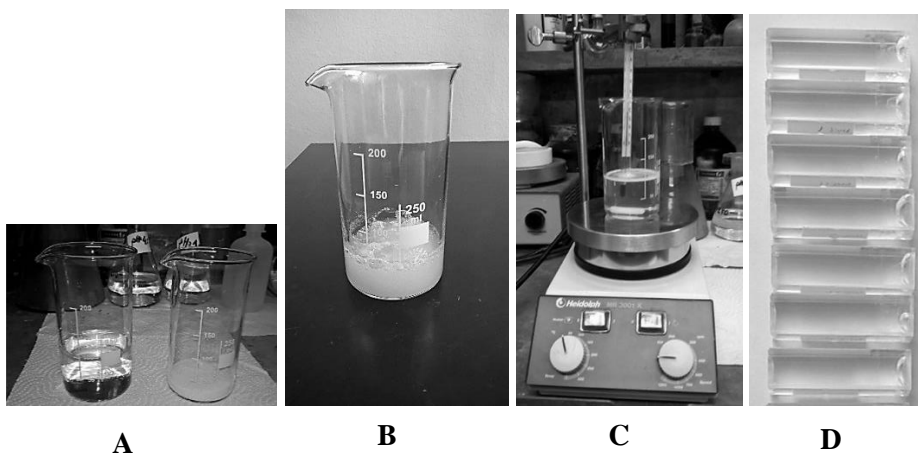


Fig. 14. A) pure materials, B) swollen gelatin, C) mixed and heated gel solution, D) prepared gel samples

Table 2. The chemical constituents of the investigated polymer gels

	nPAG	nMAG	VIPET
Water <i>Highly purified distilled (HPLC grade, Sigma Aldrich)</i>	89 %	86 %	80 %
Gelatin <i>From porcine skin (300 bloom, Sigma-Aldrich)</i>	5 %	8 %	7 %
Monomers <i>Acrylamide, (AAM, Sigma-Aldrich); Methacrylic acid (MAA, Sigma-Aldrich); N-vinylpyrrolidone, (VIPE, Sigma-Aldrich)</i>	3 %	5 %	4 %
Cross-linker <i>N,N- methylene-bis-acrylamide (BIS, Sigma-Aldrich)</i>	3 %	-	4 %
Oxygen scavenger <i>Hydroxymethyl phosphonium chloride (THPC, Sigma-Aldrich)</i>	10 mM	2 mM	10 mM

3.1.2 Irradiation of experimental gels

In order to highlight the irradiation procedure, the schematic outline is presented below by showing the photon and particles irradiation sources and beam energies (Fig. 15).

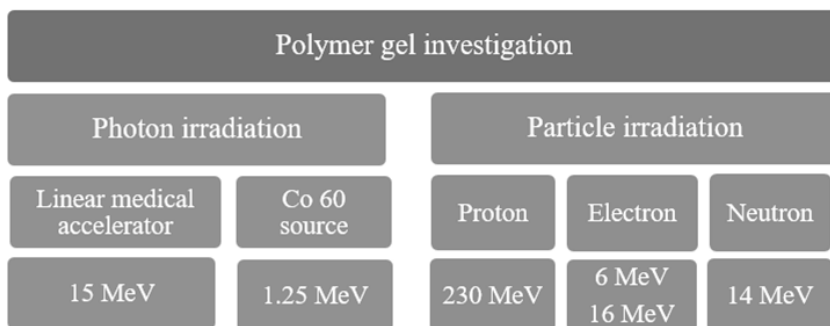


Fig. 15. The irradiation sources and their energies

The acrylamide (nPAG), methacrylic acid (nMAG), and *N*-vinylpyrrolidone (VIPET) based polymer gels were prepared by standard formulation as described in the previous section. Three batches of gels were prepared and marked as *m* for nMAG, *p* for nPAG, and *v* for VIPET dose gel (Fig. 16). The serial number, type of radiation, irradiation dose, and other important information was added when labeling the samples.

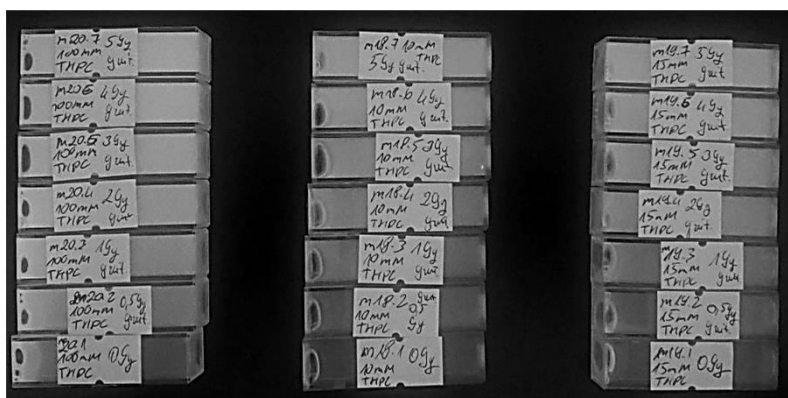


Fig. 16. The typical labelling of polymer gel samples

3.1.2.1 Photon irradiation of experimental gels

In order to investigate dose gel sensitivity to photons, experimental gel samples were irradiated by using X-ray beam of a medical linear accelerator and gamma rays of the medical teletherapy unit with ^{60}Co source.

Medical linear accelerator

The gels samples were irradiated to 2, 4, 6, 8, and 10 Gy doses to investigate the properties of the polymerized gels in the low-dose region. The step of 2 Gy was

set by following the standard fractionating practice that is used in radiotherapy [95, 96].

The irradiation of gel samples was performed in medical linear accelerator Clinac DMX (Varian) at the Hospital of Oncology of Lithuanian University of Health Sciences. The following irradiation parameters were used: max dose depth was 1.5 cm; source to surface distance, SSD, was set to 100 cm; field size $10 \times 10 \text{ cm}^2$; dose rate was 3 Gy/min. One monitor unit (MU) of the Linac corresponded to 0.01 Gy on average; however, when using calibrated ionization chamber, the value of MU in terms of Gy was adjusted for each treatment procedure separately. The schematic outline of samples in cuvettes that were prepared for irradiation is presented in Fig. 17. The location of samples during the irradiation procedure is presented in Fig. 18.

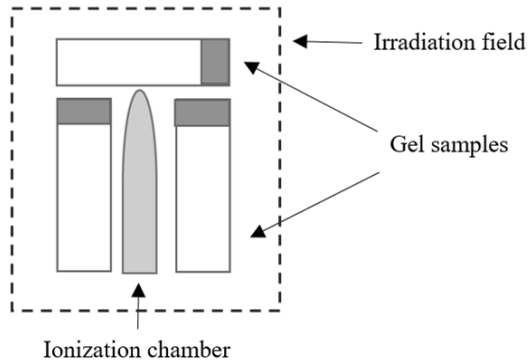


Fig. 17. Schematic outline of gel-filled cuvettes that were prepared for the irradiation with the indicated location of ionization chamber that was used as a reference dosimeter

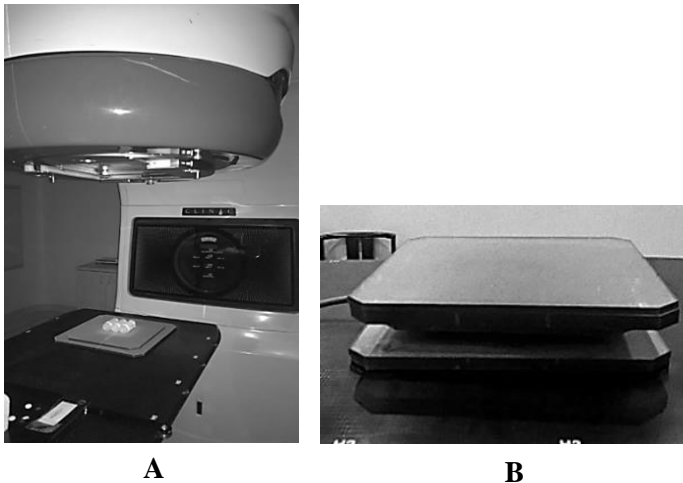


Fig. 18. A) Varian Clinac DMX linear accelerator that was prepared for samples irradiation, B) gel samples that were covered by PMMA sheets and prepared for irradiation

Medical teletherapy unit with ^{60}Co

A series of samples of nMAG, nPAG, and VIPET dose gels were prepared and irradiated in medical teletherapy unit ROKUS M with ^{60}Co source to doses: 0.5, 2, 4, 6, 8, 10 Gy. The average energy of 1.25 MeV of gamma photons was assumed, taking into account that ^{60}Co has two strong gamma lines at 1.17 MeV and 1.33 MeV. The actual ^{60}Co source activity and corresponding dose rate were calculated for the exact day of the treatment. Moreover, the irradiation time was calculated for each treatment separately in order to deliver precise doses to the samples. The source to surface distance (SSD) was set to 75 cm; the irradiation field size was 20×20 cm, and build up layer was 0.5 cm. The experimental setup for this type of irradiation is provided in Fig. 19. In order to minimize possible errors, three samples that were representing three different types of gels were irradiated to the same dose at once.

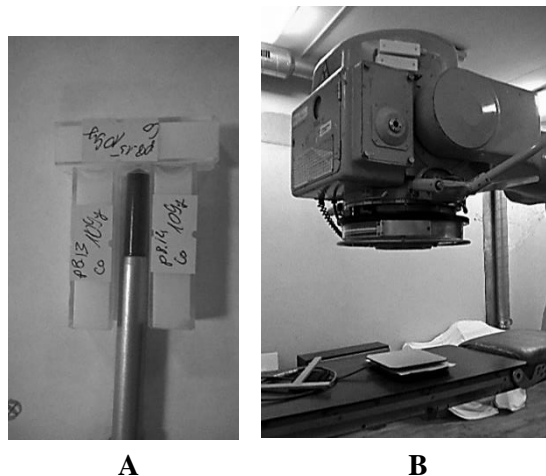


Fig. 19. The experimental setup for gel irradiation by using the teletherapy unit with ^{60}Co source. A) Samples that were prepared for irradiation, B) full setup for irradiation with PMMA bolus on top

3.1.2.2 Particle irradiation of experimental gels

nMAG, nPAG, and VIPET polymer gel samples were irradiated by high-energy protons and neutrons in order to assess the impact of high-energy particles on the polymerization processes in dose gels and investigate the radiation-induced changes of polymerized gel properties. Methacrylic acid based gel samples were irradiated by high-energy electrons additionally.

Proton irradiation

The experimental samples were irradiated in proton accelerator IBA PROTEOS C230 (Ion Beam Applications S.A) to doses from the interval 0.5–5.0 Gy at OncoRay Clinic in Dresden; 230 MeV proton irradiation was performed for 24 hours after gels' preparation by using standard snout 180 with the aperture diameter of 16.3 cm. Proton irradiation geometry was implemented by keeping gantry and treatment table orientations at 0° position. Farmer chamber PTW30013 with the build-up cap was fixed in the central position of the irradiation field, which was formed by applying snout of 15.00 cm. Ionization chamber was used as the reference dosimeter. Dose correction factor $k_0=1.022$ was calculated for this chamber, taking into account the atmospheric conditions: $p=1002.1$ hPa, and $T=23.1$ °C. During the irradiation of gel samples, three cuvettes from different batches, containing different gels, were positioned on the treatment table in the way, which was described above. The arranged cuvettes were surrounded by 1.50 cm thick PMMA blocks and covered by the additional 10.30 cm thick PMMA block (corresponds to the thickness of 11.19 cm in water) in order to secure 10.0 cm width of the modulated SOBPs with a total proton beam penetration depth of 17.0 cm. The performed experimental measurements showed no or only very small deviations between the absorbed dose values that were provided by the proton accelerator system and measured by Farmer chamber. The highest measured dose deviation was 0.005 Gy that was observed for 5 Gy absorbed dose.

Neutron irradiation

There are some specific dose gels that were used for dosimetry in neutron therapy [98]; however, the goal of this investigation was to assess the suitability of common dose gels (nPAG, nMAG, and VIPET) to be used in the neutron therapy.

Due to the limited access possibilities, the neutron irradiation of samples was performed with the aim to indicate the difference between the optical properties of the irradiated dose gels treated by neutrons and other particles. The neutron irradiation of gels was carried out at the Center for Physical Sciences and Technology (FTMC) in Vilnius. Two types of neutron sources were used: a) neutron generator that is exploring fission reaction: $D + T \rightarrow n + {}^4\text{He}$, max., energy of neutrons was 14.1 MeV; neutron flux was 10^8 n/s; dose rate was 1.08 Gy/h; neutron irradiation dose (equivalent dose) of gel samples was 0.3 Sv (see Fig. 20), and b) Pu(Be) neutron source that is producing broad spectra of thermal, epithermal, and fast neutrons in 3 different channels. The neutron energy distribution in each channel is shown in Fig. 21, and the corresponding parameters are provided in the Table 3.

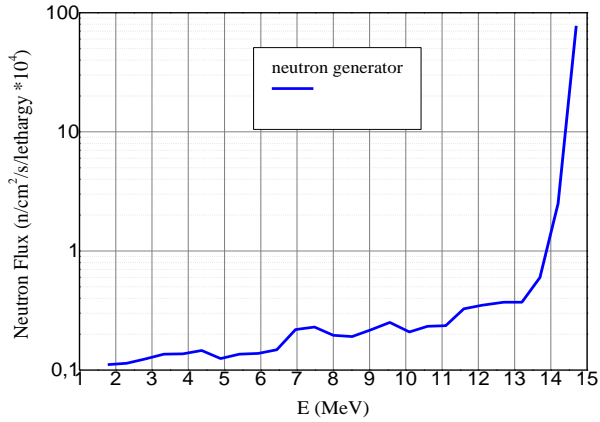


Fig. 20. The neutron generator spectrum at the irradiation position

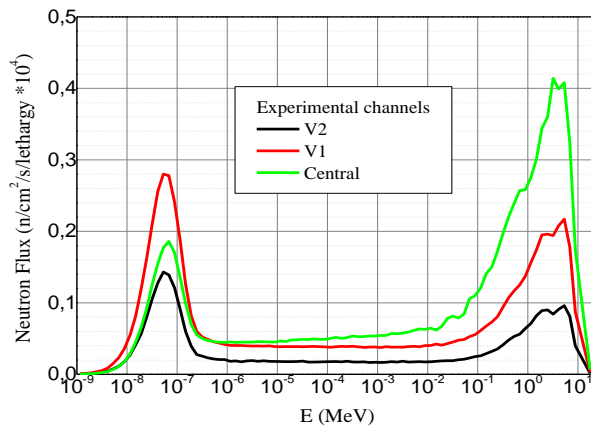


Fig. 21. Energy distribution in the experimental channels of Pu(Be) neutron unit

Table 3. The neutron related parameters in the experimental channels of Pu(Be) unit

Parameter	V2 channel	V1 channel	Central channel
Thermal neutrons	45 %	40 %	19 %
Epithermal neutrons	25 %	26 %	28 %
<u>Fast neutrons</u>	<u>30 %</u>	<u>34 %</u>	<u>53 %</u>
Flux, n/s	3.15E+04	6.76E+04	9.02E+04
Dose, mSv/h	17	37	40

The gel samples were placed in the V1 channel and irradiated with neutrons to 1.31 Sv, 2.7 Sv, 4.85 Sv doses (equivalent doses).

Electron irradiation

Two series of nMAG dose gel samples were irradiated with 6 MeV and 16 MeV energy electrons in medical linear accelerator Varian Clinac 2100C/D at the Hospital of Lithuanian University of Health Sciences of Kaunas Clinics. The experiment was performed with the aim to assess the impact of electron energy on the properties of the irradiated methacrylic acid based dose gels. The source to surface distance, SSD, of 100 cm was set in all the irradiation procedures. The irradiation field size was 6×6 cm². Moreover, 2.5 cm thick build up layer was used to focus the electron beam at the exact volume of the cuvette. The electron irradiation dose rate was 3 Gy/min. Monitor units (MU) of the linac were calculated in the same way as it was done in the case of photon irradiation: 1 MU = 0.01 Gy.

The experimental samples were irradiated to doses from the interval of 0.5–5.0 Gy. Some samples were irradiated to 5 Gy by applying dose fractioning strategy and splitting the whole dose in two fractions of 2.5 Gy each. The time interval between two fractions was 12 hours.

3.2 Irradiation dose measurements

The monitoring of radiation dose during the irradiation procedures was performed by the ionization chamber Farmer 30013 (PTW Freiburg) with a build-up cap that is connected to the electrometer UNIDOSE E (PTW Freiburg), calibrated for water. Room temperature and air pressure were measured with calibrated thermometer-barometer DELTA OHM HD2114B.0. The equipment used for the radiation dose monitoring is shown in Fig. 22. Pressure, temperature, and humidity correction were taken into account during the irradiation of samples, since they play an important role in the assessment of dose measurement uncertainty. Eq. 3.4 defines the calculation of pressure, temperature, and humidity correction coefficient k_{Tp} [98]:

$$k_{Tp} = \frac{273.2+T}{273.2+T_0} \cdot \frac{P_0}{P}. \quad (3.4)$$

Following the standard requirements, this coefficient was calculated for each irradiation procedure (IAEA-tecdoc-1585). Depending on the irradiation conditions, it varied from 1.018917 to 1.02039.

All measurements were performed by following international guidelines of IAEA protocol TRS-398 [98].

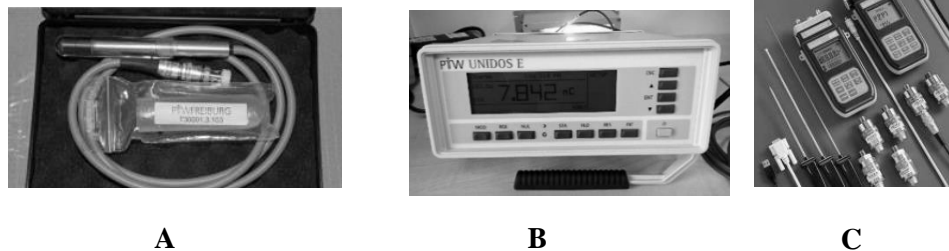


Fig. 22. A) Ionization chamber PTW Freiburg, B) electrometer UNIDOSE E (PTW), C) thermometer-barometer DELTA OHM HD2114B.0

3.3 Analysis of experimental gels

3.3.1 UV-VIS spectrometry

The optical properties of the irradiated dose gel samples were investigated by using UV-VIS spectrometer Ocean Optics with USB4000. The intensity of detector signal of dose gel samples was measured. The reflectance of the gel samples was not measured. The measurements of optical characteristics of the irradiated dose gels were performed 12–24 hours after the irradiation to be sure that the process of polymerization was fully completed. The research on polymerization process propagation in samples for nPAG, nMAG, and VIPET gels was performed prior to the main gels' optical parameter measurements. Firstly, the gel samples were prepared as shown in section 3.1.1. Gel samples were irradiated after 12 hours post preparation in linear accelerator and Co^{60} gamma source units as was mentioned in subsection 3.1.2.1. The relevant radiation doses: 0.5 Gy, 1 Gy, 2 Gy, 3 Gy, 4 Gy, 5 Gy, 6 Gy, 7 Gy, 8 Gy, 9 Gy, and 10 Gy, were applied. The UV-VIS spectra (transmittance and absorbance (registered intensity)) of irradiated gels were measured after 1 h, 3 h, 5 h, 7 h, 10 h, 12 h, 24 h, and 36 h post irradiation. The results revealed that “free polymerization” is continuing, when no radiation source was applied. The UV-VIS transmittance of the sample decreased from 69 to 47 % after 12 h for nMAG, from 75 to 45 % for nPAG, and from 81 to 69 % when 2 Gy dose is applied. Further, UV-VIS measurements of the same samples after 24 h and 36 h showed no significant decrease in transmittance.

The experimental setup for UV-VIS measurements is shown in Fig. 23.

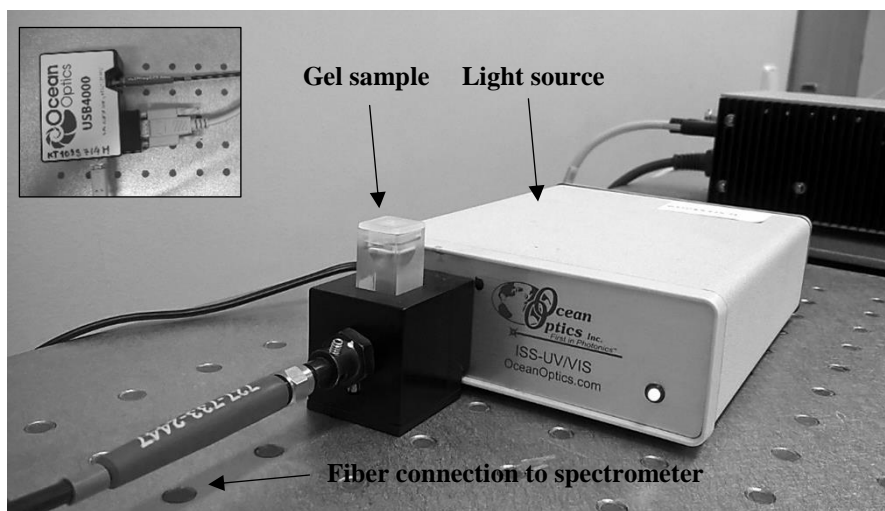


Fig. 23. The experimental setup for the measurement of optical characteristics of irradiated dose gels

Technical calibration of UV-VIS spectrometer was performed prior to the measurement start. The spectrum of empty reference cuvette was measured to get reference intensity (absorbance) and transmittance data of the PMMA cuvette. This reference spectrum was automatically subtracted from all the measured spectra of the irradiated dose gel samples. The spectrometer was recalibrated after every 5 measurements to eliminate the spectral variations of its light source. The transmittance and intensity (absorbance) spectra of the irradiated samples were measured in the wave range from 177 nm to 891 nm. The wave range was set by taking into account technical specifications of the spectrometer. The measurements in the wave length range from 177 nm to 891 nm was of the highest accuracy. The dose calibration curves for nMAG, nPAG, and VIPET gels were constructed by using registered intensity values at the wavelength of 650 nm. This wavelength was chosen due to the fact that new red light laser based photo-scanner was developed for the assessment of the absorbed dose in the irradiated gels. The gel evaluation at the same wavelength by using two different analysis methods might simplify the verification procedure of the new developed device.

3.3.2 Raman spectroscopy

Raman spectra of the experimental gel samples were measured by using a Renishaw inVia Raman spectrometer (Fig. 24), equipped with the DPSS laser ($\lambda=532$ nm) at the Institute of Materials Science of Kaunas University of Technology. The excitation beam from a diode laser was focused on the sample by using 20x magnifying objectives (NA=0.75, Leica). The laser power at the sample surface was 2 mW. The constant integration time of 10 s was used in all the measurements. The signal was accumulated 1–5 times and then averaged. The Raman Stokes signal was

dispersed with a diffraction grating (2400 grooves/mm), and the data was recorded by using a Peltier cooled charge-coupled device (CCD) detector (1024×256 pixels). This system yields a spectral resolution of about 1 cm^{-1} . Silicon was used to calibrate the Raman spectrometer setup in both Raman wavenumber and spectral intensity. Raman spectra of pure materials were measured additionally in order to assist the assignments of vibrational bands in Raman spectra of the irradiated gel samples.



Fig. 24. Renishaw inVia Raman spectrometer

3.3.3 Laboratory-made photo-scanner and scanning method

Steep dose gradients within millimeter range are common in brachytherapy; thus, this option shall be considered as well when evaluating dose gels. Furthermore, the spreading and diffusion of radiation polymerized species (clusters of polymer chains) from the initial irradiation location is possible. UV-VIS spectrometry was found not to be very suitable for high spatial resolution analysis along the longitudinal axis of the irradiated gel-filled cuvettes. MRI or, under circumstances, optical CT might be used, but both methods are expensive and not that handy, especially if talking about gel based dose assessment in catheter-based brachytherapy.

A prototype of the new photo-scanning system has been developed, which allows the dose evaluation along the longitudinal axis of the irradiated sample with a spatial resolution of 0.20 mm (Fig. 25). The scanning system consists of the moving motorized stage, sample scanner with sample holder, I/O board, adjusters, controller, integrated laser, and personal computer.

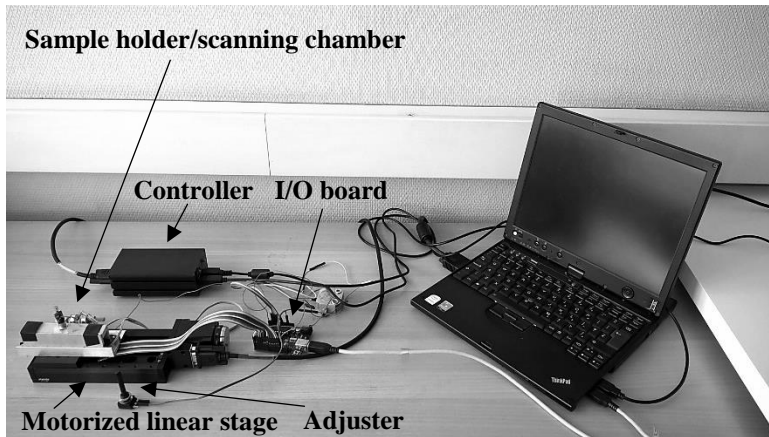


Fig. 25. Photo-scanning system for the evaluation of the transmitted light intensity in cuvette based samples

The measurement is performed as follows: cuvette with the irradiated dose gel inside is inserted and fixed in the sample holder of the scanner, which is designed to accommodate the standard cuvette. The diode laser (Thornlabs) is installed on the top of the scanning chamber. The photovoltaic elements (Thornlabs) are mounted on the opposite side of the scanner in front of the laser aiming to detect the intensity through the sample transmitted light, which changes with the irradiation dose of the sample. The scanning chamber is mounted on the 10 cm long motorized axial stage 8MT175 (Standa) with the space resolution of $0.31 \mu\text{m}$ ($1/8$ step); the resolution in full step is equal to $2.5 \mu\text{m}$; the scanning speed was set to 1 mm/s . I/O board is connected to a computer and scanning chamber. The system is driven by using a self-developed computer algorithm (Arduino and MatLab based) and is able to measure through the experimental sample transmitted laser light intensity and evaluate the intensity profile that is corresponding to the absorbed dose. The intensity profile measurement along the longitudinal axis of the cuvette samples is performed in several steps (see Fig. 26):

1. The cuvette with irradiated dose gel inside is fixed in the sample holder, which is loaded at the entrance position of the scanning chamber. The sample is moved in 0.20 mm steps, and the transmitted light intensity at each step is measured. The procedure continues until the laser scans the whole length of the cuvette. The scanning procedure is monitored, and the parameters are controlled by using the self-developed computer algorithm.
2. At each step, the scanned information about the intensity of the transmitted light is collected by photovoltaic elements, and the measured data is sent to the computer.
3. The sample related scanning data are archived and provided in the form of the graph.

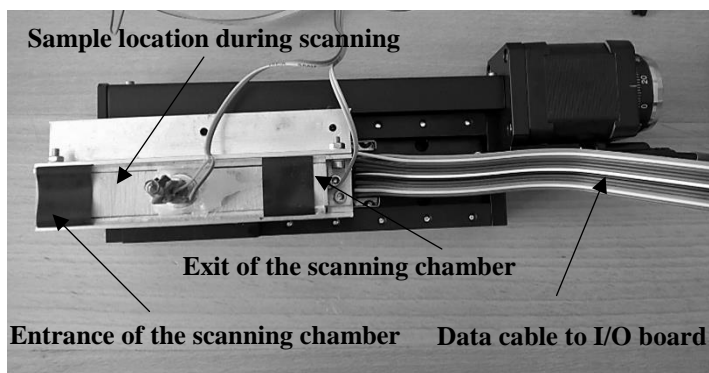


Fig. 26. The view of scanning chamber with a sample holder

Before starting the dose evaluation in the irradiated gels, the scanning system was calibrated. The empty PMMA cuvette was divided into 1 mm thick segments along the longitudinal axis (Fig. 27) and scanned in order to find geometric limits of the active volume (measurement window) and set the scanning step. The characterization of the dose profile with indicated zones for the scanned PMMA cuvette is provided in Fig. 28.

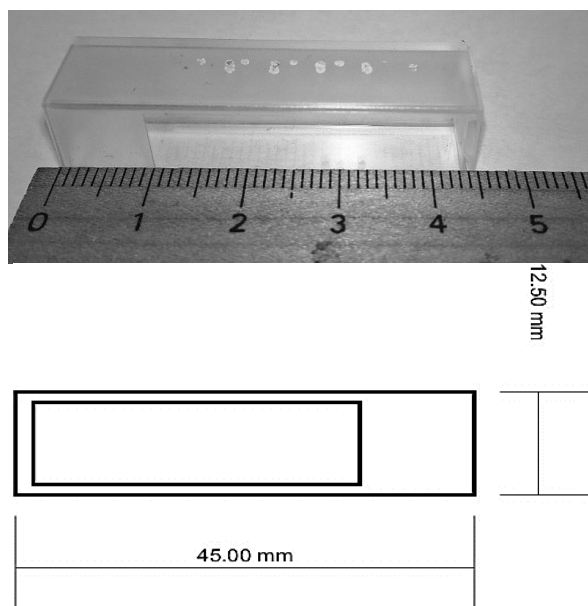


Fig. 27. First reference measurements to test system parameters

The analysis of the transmitted light intensity profile allowed the evaluation of the measurement window (the length of the active volume) for the scanner. It was set between 12 mm and 36 mm of the standard cuvette, where the registered transmitted light intensity profile was almost flat. Additionally, the reference cuvettes irradiated with 0.5 Gy, 1 Gy, 2 Gy, 3 Gy, 4 Gy, and 5 Gy were measured by photo-scanner by

10 times to find out the effective zone, the exact segment of cuvette where intensity profile is stable and flat as seen in Fig. 28. The cuvette related data as a background signal has been subtracted from each measurement data automatically.

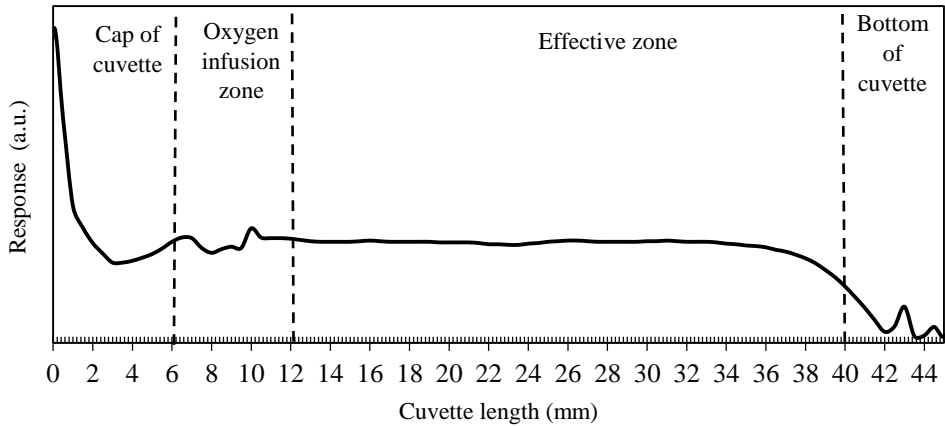


Fig. 28. Characterization of dose response scanning profile

Taking into account that not the whole information that was obtained during the scanning of gel samples was useful, the effective and ineffective zones for measurements were indicated. Fig. 29 shows a photograph of the cuvette with irradiated gel inside and 4 indicated zones in it. The most important is the effective Zone 3, which indicates the irradiated gel volume where information regarding gel's polymerization can be obtained. Zone 2 corresponds to the volume of possible oxygen infusion, which depends on the amount of oxygen scavenger in the gel and method that is used for the cuvette sealing. The oxygen infusion zone was determined by scanning the sample and analyzing the scanned response profile near the cuvette cap. The profile, where oxygen is infused (see Fig. 28 and 29), is leaping. This segment of gel cannot be used for dose measurement, because the oxygen affected segment cannot be polymerized. Higher concentrations of the oxygen scavenger prevent the expansion of oxygen infused zone [56]. Zone 1 and Zone 4 (see Fig. 29) are cuvette cap and bottom areas, which serves as reference points for photo-scanner to find out the beginning and the end of cuvette.

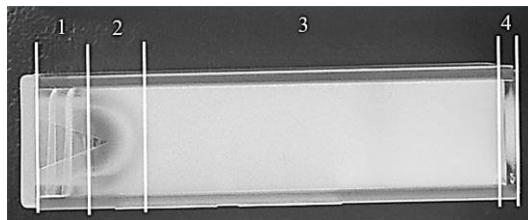


Fig. 29. Photograph of the irradiated dose gel cuvette with indicated zones: 1 the cap, 2 area of possible oxygen infusion, 3 area for effective measurements, 4 the bottom of cuvette

In order to obtain a dose calibration curve of the scanner, the intensity measurements of dose gels that are irradiated to different doses from the interval between 0 and 5 Gy have been performed. The corresponding intensity profiles are provided in Fig. 30.

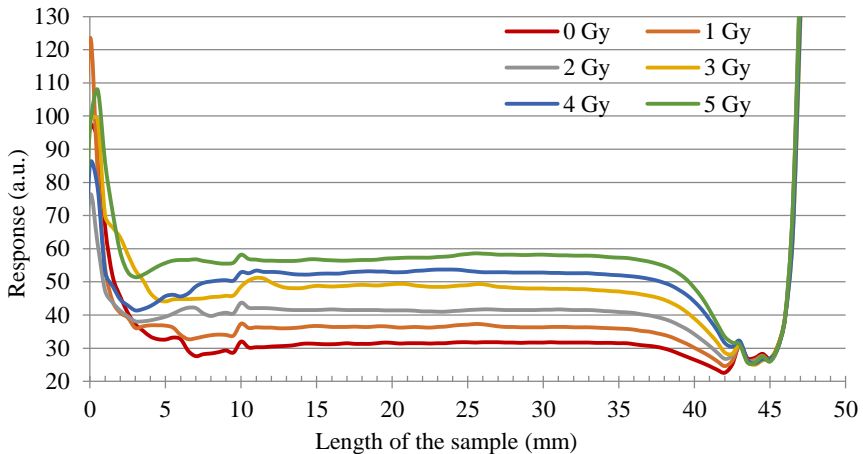


Fig. 30. Dose profile curves

The data that have been obtained within the measurement window (12–36 mm) were used for the construction of the calibration curve, which is presented in Fig. 31 together with the indicated standard deviations that were calculated for every measured dose at every scanning step. The standard deviation increased from 0.1 to 0.3 when the absorbed dose of the gel sample increased from 0.5 to 5 Gy. The samples irradiated <5 Gy doses were measured with higher precision.

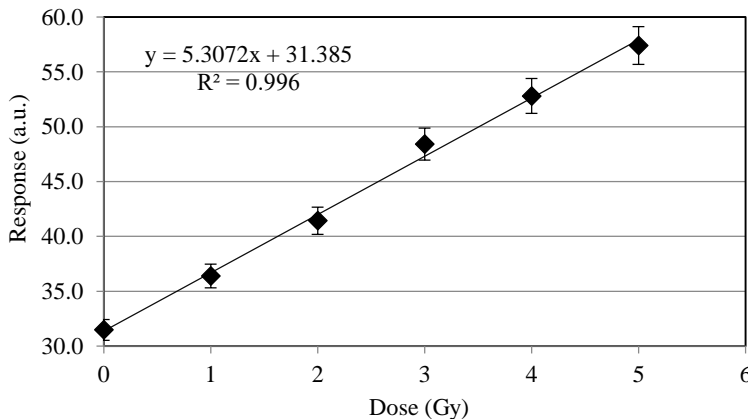


Fig. 31. Dose calibration curve of the photo-scanner

It was found that the calibration curve possessed good linearity between the irradiation dose and transmitted light intensity ($R^2 = 0.996$). The linear dependency

was seen in the irradiated dose versus measured response curve. This dependency (Fig. 32) is constructed to identify the gels' absorbed and scattered radiation dose by using photo-scanner response values.

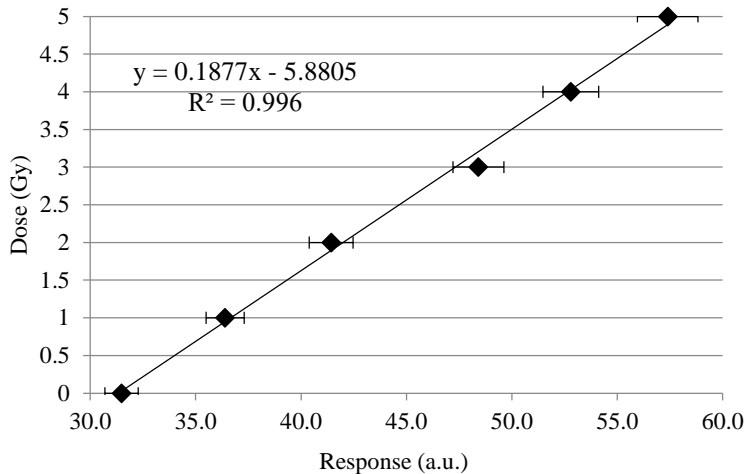


Fig. 32. The response curve to identify gels' absorbed dose

The dose values that were obtained from the response curve were compared with the ionization chamber (PTW Freiburg) measured dose values to find out the measurement accuracy of the constructed scanner. The radiation experiment was performed with nMAG, nPAG, and VIPET gel samples that are irradiated by medical linear accelerator by 15 MeV energy photons from 1 to 5 Gy doses. The applied dose was measured by the ionization chamber and dose gels at the same time during the exposure. The pressure, temperature, and humidity correction coefficient k_{tp} was calculated for linear accelerator and reached 1.018917. The irradiated dose values were multiplied by k_{tp} , and certain absorbed doses were determined. For irradiated 1 Gy dose, the actual absorbed dose was 0.947840 Gy, 2 Gy dose — 1.961920 Gy, 3 Gy dose — 2.981929 Gy, 4 Gy — 3.913134 Gy, 5 Gy — 4.904496 Gy.

After 12 hours, the dose gels were scanned by a photo-scanner. The dose values that were obtained from response curve: for irradiated 1 Gy, the estimated dose was 0.895 Gy, 2 Gy dose — 1.871 Gy, 3 Gy dose — 2.883 Gy, 4 Gy — 3.873 Gy, 5 Gy — 4.844 Gy. The calculated dose measurement accuracy by taking ionization chamber as reference device is from 9.2 to 10.4 %.

3.4 Preparation and evaluation of nanostructured polymer composites

3.4.1 Preparation of polymer nanocomposites

The aim of this study was to select most promising composites for the fabrication of transparent and lead-free radiation protection screens. The composites

with various ammonium metatungstate concentrations were examined in order to achieve the recommended lead equivalent of 0.5 mmPb, which is requested for the radiation shielding equipment. Before starting the experiments, the simulation of X-ray attenuating properties of composites has been performed. XCOM database was used for the simulation of various ammonium metatungstate concentrations [99].

The polymer composites that contain different concentrations of ammonium metatungstate were prepared by using a three neck flask (Fig. 33) that was placed in a water bath with heating function.

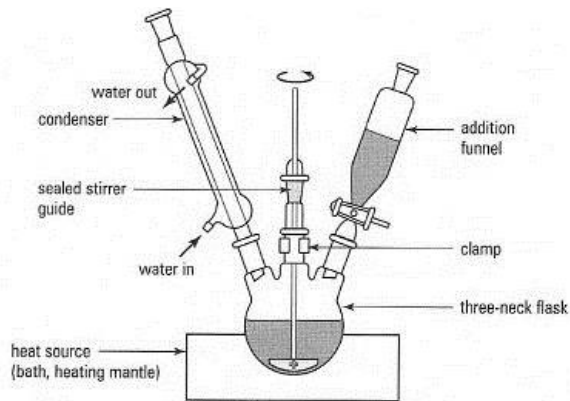


Fig. 33. Three neck flask for gel composition preparation [100]

A stirrer was integrated in one neck of this flask and condenser in another one. The third neck was left for the ingredients supply of composites. The calculated amount of non-ionic polyacrylamide PAA (Sigma-Aldrich, 32000 a.m.u) was added to the distilled water and left for 0.5 hour to swell. Then, the mixture was heated up to 70 °C under continuous stirring. Keeping this temperature, the mixture was stirred for another 0.5 hour. Then, the calculated amount of ammonium tungstate crystal hydrate $(\text{NH}_4)_6\text{H}_2\text{W}_{12}\text{O}_{40}\cdot x\text{H}_2\text{O}$ (Sigma-Aldrich, $\geq 85\%$ WO_3 basis (gravimetric) was added in small portions to the viscose mixture that was heated up to 80 °C under continuous stirring. Stirring was applied until the ammonium metatungstate salt was fully dissolved, and a homogeneous and transparent to the visible light composite was produced. Then, the three neck flask with the composite was placed in the thermostatic ultrasound bath Velleman VTUSC3 (vol. 2.6 L, 170 W) that was filled with water that was heated up to 50 °C. Ultrasound sonification at 42 kHz was performed for at least 15 min in order to remove air bubbles that were possibly produced during the composite preparation. Warm composite was poured into the standard cuvettes, and the prepared samples were left to set for at least one day. The name of AMWO-PX was assigned for these new developed composites, where X indicates concentration of ammonium metatungstate (Table 12).

First, four composites with different thickeners were produced in 10 mm thick plates. The sample of 10 mm thickness was prepared in order to evaluate lead equivalent (mmPb) by following measurement recommendation. The composition of the samples is as follows:

1. 65.9 % of $(\text{NH}_4)_6\text{H}_2\text{W}_{12}\text{O}_{40}\text{xH}_2\text{O}$, 32.9 % of H_2O , and 1.2 % of methyl carboxy cellulose;
2. 40 % of $(\text{NH}_4)_6\text{H}_2\text{W}_{12}\text{O}_{40}\text{xH}_2\text{O}$, 58.8 % of H_2O , and 1.2 % of $(\text{C}_3\text{H}_5\text{NO})_n$ (polyacrylamide);
3. 50 % of $(\text{NH}_4)_6\text{H}_2\text{W}_{12}\text{O}_{40}\text{xH}_2\text{O}$, 1 % of $(\text{C}_3\text{H}_5\text{NO})_n$ (polyacrylamide), and 49% of H_2O ;
4. 50 % of $(\text{NH}_4)_6\text{H}_2\text{W}_{12}\text{O}_{40}\text{xH}_2\text{O}$, 4.75 % of gelatin, and 45.25 % of H_2O .

Second, the AMWO-PX composites were prepared in PMMA cuvettes in varying concentrations of polyacrylamide (PAA), $(\text{NH}_4)_6\text{H}_2\text{W}_{12}\text{O}_{40}\text{xH}_2\text{O}$, and H_2O in order to find high visible light transparent (>85 %) and high lead equivalent (>0.5 mmPb) composite. Full composition of samples is presented as follows:

1. AMWO-P15: 1 % of PAA, 15 % $(\text{NH}_4)_6\text{H}_2\text{W}_{12}\text{O}_{40}$, and 84 % of H_2O .
2. AMWO-P30: 1 % of PAA, 30 % $(\text{NH}_4)_6\text{H}_2\text{W}_{12}\text{O}_{40}$, and 69 % of H_2O .
3. AMWO-P50: 1 % of PAA, 50 % $(\text{NH}_4)_6\text{H}_2\text{W}_{12}\text{O}_{40}$, and 49 % of H_2O .
4. AMWO-P60: 1 % of PAA, 60 % $(\text{NH}_4)_6\text{H}_2\text{W}_{12}\text{O}_{40}$, and 39 % of H_2O .
5. AMWO-P70: 1 % of PAA, 70 % $(\text{NH}_4)_6\text{H}_2\text{W}_{12}\text{O}_{40}$, and 29 % of H_2O .

A photograph of different lead-free and transparent AMWO-PX composites is provided in Fig. 34.

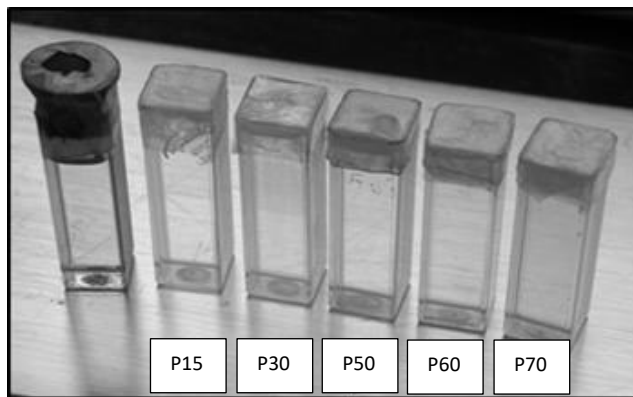


Fig. 34. AMWO-P composites. From the left: AMWO-DW (water and PAA only), AMWO-P15, AMWO-P30, AMWO-P50, AMWO-P60, AMWO-P70 [101]

3.4.2 Irradiation of composites

The main goal of this investigation was to develop lead-free and transparent composites as a material for radiation protection screens that are used for personnel's protection during the X-ray imaging procedures. Polymer composite samples were

irradiated with 150 keV photons by using X-ray therapy unit Gulmay D3225; 0.33 mm filter and cone applicator (No. 9, exit diameter 10 cm) were used. All samples were irradiated up to 10 Gy dose.

3.4.3 Experimental evaluation of composites

Evaluation of the X-ray attenuation of the experimental composites

The experimental measurements of X-ray attenuating properties of tungsten-containing nanocomposites and the evaluation of their lead equivalency were performed, according to the internationally accepted guidelines [102]. The experimental setup, shown in Fig. 35, was used for the measuring purposes [103].

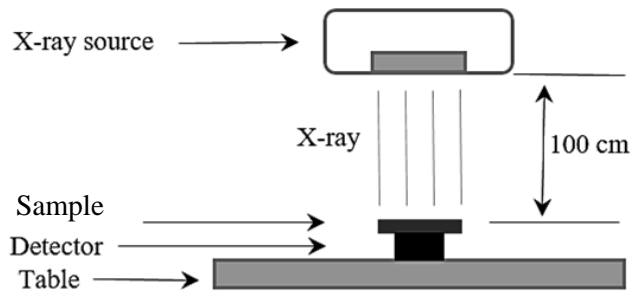


Fig. 35. Experimental setup for the estimation of lead equivalency of composites

The cuvettes that were filled with corresponding tungsten-containing composites (10-mm-thick shielding element) were irradiated by conventional external X-ray unit MULTIX PRO. The applied X-ray tube voltage was 120 kV. The distance of 100 cm was kept between X-ray tube focal spot and cuvette surface during all the investigations. ‘Barracuda’ multimeter with multi-purpose detector (RTI Electronics) was used for the voltage measurements in combination with point detector R100B for the dose measurements.

First, the transmission of the X-rays $B(x)$ was determined by measuring the air kerma $K(0)$ at the photon incidence point and the dose $D(x)$ beneath the x -thick shielding element (experimental cuvette with composite inside) that was placed on the detector (Eq. 3.5) [102]:

$$B(x) = \frac{D(x)}{K(0)}; \quad (3.5)$$

Second, lead equivalent thickness, x of the investigated structure, was calculated according to formula [102]:

$$x = \frac{1}{\alpha\gamma} \ln \left(\frac{B^{-\gamma} + \frac{\beta}{\alpha}}{1 + \frac{\beta}{\alpha}} \right); \quad (3.6)$$

where α , β , and γ are fitting parameters depending on the applied voltage. Measurement units are mmPb. The parameters were adjusted before each measurement. X-ray transmission measurements were performed in at least five different detector positions along the cuvette.

4. RESULTS AND DISCUSSION

4.1 Evaluation of dose gels

The purpose of this study was to identify the most suitable polymer dose gel for the detailed radiation sensitivity investigation. The research on dose sensitivity was performed by investigating different monomer based gels that were irradiated by photon and particle irradiation: photons, gamma rays, protons, electrons, and neutrons.

4.1.1 Influence of gel composition on the sensitivity of dose gels that were irradiated by different beams

The purpose of this investigation was to find out the dose sensitivity of differently composed nPAG, nMAG, and VIPET normoxic polymer gels that were irradiated to different beams. The steps of dose gel evaluation, regarding the sensitivity to irradiation with different beams, are as follows:

1. Preparation of nPAG, nMAG, and VIPET dose gels;
2. Irradiation of dose gels by X-rays, gamma rays, protons, electrons, and neutrons;
3. Measurement and evaluation of UV-VIS spectral characteristics of irradiated dose gels;
4. Selection of most promising dose gel compositions for further investigations.

UV-VIS spectroscopy was used for the evaluation of the absorbed dose related changes of optical properties in the irradiated dose gels. For the investigation of dose gels, beam energies, the same as in the clinical practice of cancer treatment procedures, were chosen; as those gels might be used for 3D dosimetry applications in radiotherapy. This research was focused on the development of dose gels which are sensitive to low-dose (<10 Gy) exposure.

Photon irradiation

nPAG, nMAG, and VIPET polymer gels were prepared and poured into PMMA cuvettes, according to the standard procedure that is described in Materials and Methods section of this dissertation. Cuvettes that were filled with experimental gels were irradiated, and their visible and ultraviolet light spectra intensity was analyzed by using UV-VIS spectrometer. The obtained spectra of gel samples were processed and analyzed using Origin 2016 PRO program package. The background subtraction was applied for the UV-VIS spectra prior to starting a detailed spectra analysis.

It is known [68, 69, 104] that the wavelengths that are corresponding to the absorption peaks in the UV-VIS spectrometry are correlating with the types of bonds in a given molecule and are valuable in determining the functional groups within a molecule. According to the Beer-Lambert law, the intensity of a solution is directly proportional to the concentration of the absorbing species in the solution and the path length of the light. It is known that the radiation-induced polymerization results in gel density changes [105]. The alteration and shifting of the intensity peak at λ_{\max} may identify the changes in concentration of the absorbing polymerized species in the polymer gel. The UV-VIS absorption spectra of the prepared nMAG, nPAG, and VIPET dose gels are presented in Fig. 36.

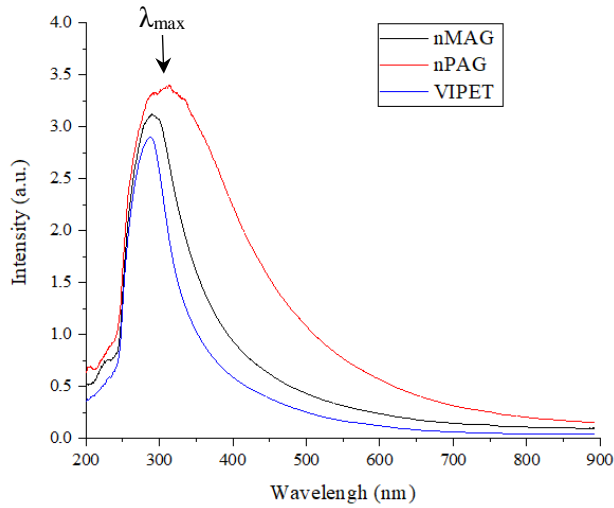


Fig. 36. UV-VIS intensity spectra of prepared VIPET, nMAG, and nPAG dose gels

The Gauss function (see Eq.4.1) was applied to fit peaks and full width of half maximum (FWHM), which allows evaluating the amount of light attenuating species, and it was calculated as follows [105]:

$$y = y_0 + \frac{Ae^{-\frac{4\ln(2)(x-x_c)^2}{w^2}}}{w\sqrt{\frac{\pi}{4\ln(2)}}}; \quad (4.1)$$

where y_0 is the base; x_c is the center; A is the area, and w is the full width of half maximum (FWHM). The curve fitting and evaluation of the λ_{\max} was performed for each UV-VIS intensity peak that is representing certain gel.

The following intensity peaks for the investigated dose gels were defined: $\lambda_{\max} = 288$ nm with FWHM= 120.9 nm for nMAG; $\lambda_{\max} = 286$ nm with FWHM= 83.4 nm for VIPET, and $\lambda_{\max} = 312$ nm with FWHM= 155.5 nm for nPAG. These data served as reference values, evaluating radiation-induced variations of optical properties in

the irradiated gels. It should be noted, that the Gauss function was applied to fit peaks and evaluate the full width of the half maximum (FWHM) [105].

Different monomer structures that were used for gel preparation and their molecular weight were responsible for different intensity registered in the experimental samples. Relatively broad intensity peak maximum was observed for nPAG and VIPET gels that were containing significant amount of two comonomers that are characterized by the high molecular density as compared to the maximum of nMAG dose gel that was produced by using only one methacrylic acid monomer. It is known that segmented polymer gel network structures are created in nPAG and VIPET when radiation-induced polymerization proceeds [1]. This leads to the formation of a number of non-uniformly polymerized gel clusters, which contribute to the increased optical density in the irradiated samples. Since the broadening and the red shift of the intensity peak in the irradiated gels are the consequences of polymerized gel cluster formation, the growth dynamic of the polymerized gel clusters should be taken into account. The intensity peaks of VIPET and nPAG gels were as well red-shifted as compared to the maximum of nMAG dose gel that was produced from gelatin and methacrylic acid [49].

In contrary to a number of investigations that were performed by other authors in the high dose region (10–100 Gy), this research was devoted to the development of dose gels, which are sensitive to low-dose (<10 Gy) exposure. The low-dose region is of special interest, since 2 Gy fraction is used for cancer treatment in radiotherapy [106–108]. According to this, 2 Gy step was used to change the irradiation parameters of nMAG, nPAG, and VIPET dose gels.

The irradiation dose related variations of registered intensity spectra for VIPET, nMAG, and nPAG gels are provided in Fig. 37–39. The full UV-VIS spectra of VIPET gel are presented to show the intensity peak broadening tendency and shift. As interest was indicated for 650 nm wavelength; therefore, nMAG and nPAG spectra are presented from 600 nm to 800 nm wavelength to focus only on the wavelength interval of interest; 650 nm wavelength was chosen to correspond to the constructed photo-scanner laser wavelength, which is close to 650 nm. The results of registered intensity of irradiated gels were used to compare to the response versus dose reading that was measured with photo-scanner. The λ_{\max} and full width of half maximum for VIPET, nMAG, and nPAG gels spectra are provided in Table 4. The intensity peaks shift towards longer wavelengths with the increased dose was observed from 274 nm to 310 nm for VIPET, from 312 nm to 358 nm for nPAG, and from 288 nm to 346 nm for nMAG. Therefore, the creation of cross-linked polymerized structures is indicated, and the gel tends to form a thicker polymer network when doses are increasing.

Table 4. λ_{\max} and FWHM of VIPET, nPAG, and nMAG gels that are irradiated by 15 MeV photons

VIPET			nPAG			nMAG		
Dose (Gy)	λ_{\max}	FWHM	Dose (Gy)	λ_{\max}	FWHM	Dose (Gy)	λ_{\max}	FWHM
0	274	95.4	0	312	155.5	0	288	120.9
0.5	277	108.5	0.5	318	159.8	0.5	297	128.5
2	287	119.2	2	325	178.9	2	308	141.5
4	289	134.9	4	328	197.2	4	317	162.0
6	303	152.5	6	333	213.1	6	329	189.3
8	308	169.2	8	345	238.7	8	334	200.1
10	310	189.3	10	358	251.0	10	346	233.7

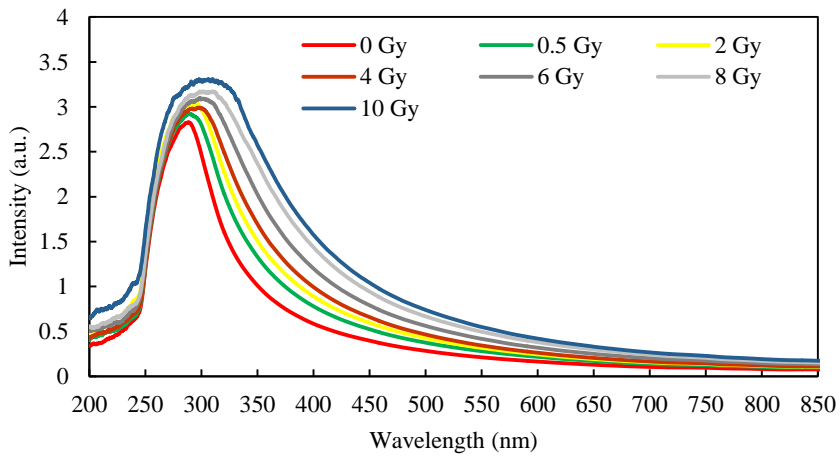


Fig. 37. The typical UV-VIS spectra of VIPET dose gel that is irradiated by 15 MeV photons

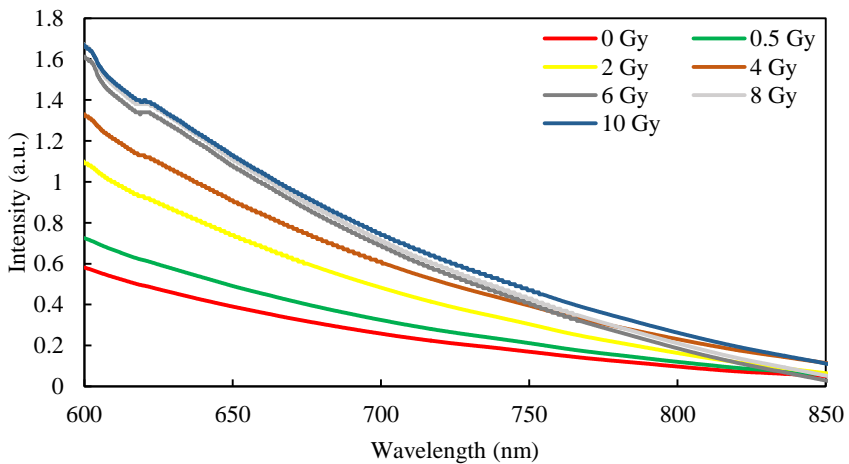


Fig. 38. The typical UV-VIS spectra of nPAG dose gel that is irradiated by 15 MeV photons

Methacrylic acid based dose gel composition is cross-linker free, but due to the irradiation, the created polymethacrylic acid forms insoluble polymerized particles. It results in the intensity peak broadening and red shift due to the irradiation. Absorption peak broadening to a lesser extent as compared with nPAG gel and the appearance of the red-side shoulder in the spectra were observed with the increasing absorbed dose in nMAG gels (Fig. 39). This agrees with the suggestions that were made [32] regarding the possible interaction of methacrylic acid with gelatin and formation of larger polymer clusters that are randomly distributed in the whole gel volume.

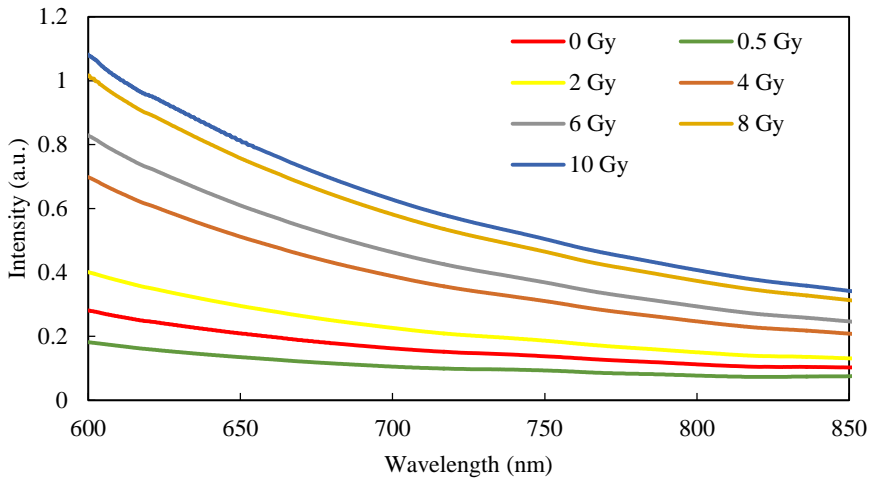


Fig. 39. The typical UV-VIS spectra of nMAG dose gel that is irradiated by 15 MeV photons

The analysis of the registered intensity spectra that was obtained after the irradiation of experimental gel samples (nMAG, nPAG, and VIPET) to 15 MeV X-rays revealed that differently composed dose gels were differently sensitive to the irradiation. The sensitivity parameter was evaluated by drawing tangents to dose response curves that derived at the same wavelength of $\lambda = 650$ nm in intensity spectra of each irradiated gel and estimating the slope values. Gel's optical sensitivity to radiation was calculated from dose response curves according to the formula (Eq. 4.2):

$$S = \frac{y_2 - y_1}{x_2 - x_1}; \quad (4.2)$$

where y_2 and y_1 are intensity values (a.u.) of the tangent, and x_2 and x_1 are corresponding values on dose (Gy) axis.

The attention was paid to the observed gel's optical density at 0 Gy, which was not equal to zero. This was explained by the fact that very weak polymerization may proceed when UV-VIS sensitive hydrogels are affected by the environmental light.

Dose sensitivity curves derived at the wavelength of 650 nm for nMAG, nPAG, and VIPET gels that were irradiated to 15 MeV X-ray are provided in Fig. 40. The wavelength of 650 nm for sensitivity analysis was chosen according to the recommendations of other researchers [68, 69] and due to the fact that the developed

photo-scanner was adopted to measure gel's dose response at 650 nm, which is close to the red light laser wavelength, which is used in a laboratory made photo scanner.

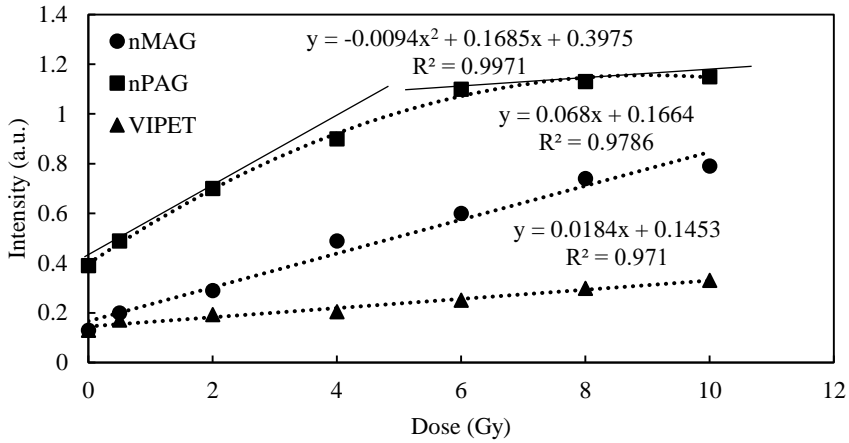


Fig. 40. Dose versus intensity (sensitivity) curves for nMAG, nPAG, and VIPET gels that were irradiated to 15 MeV X-ray and read out at the selected wavelength of 650 nm

The sensitivity of nMAG gel irradiated with 15 MeV photons was 0.068. The sensitivity of 0.018, which was found for VIPET gels, was the lowest. The dose sensitivity curve of nPAG gel was fitted with second order polynomial function and divided into two parts: rising part and saturated part. The rising part indicated slope value of 0.12. No significant difference in the sensitivity was found, when the gels were irradiated by 6 MeV instead of 15 MeV X-ray photons. This feature is very useful taking into account that the gel would be adopted to be stably sensitive to the medical range photon energies that were used for cancer treatment procedures.

The linearity in dose sensitivity functions in the low-dose range (0–10 Gy) was as well reported by the other authors (Fig. 41). There, ~0.24 dose sensitivity was indicated for acrylic acid based dose gel that was evaluated by MRI.

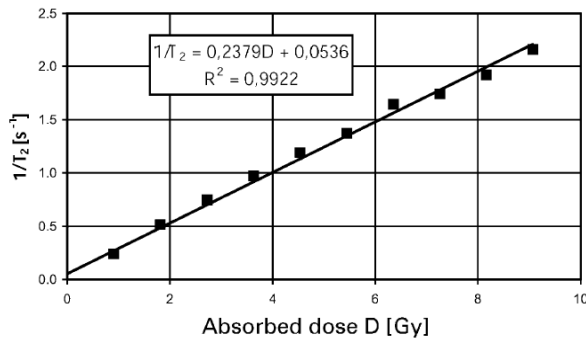


Fig. 41. The dose response of polymer gel dosimeter (linear part) [109]

This experiment revealed that liner part of the sensitivity curve is from 1 Gy to 9 Gy.

An additional investigation was performed by irradiating all three dose gels (nPAG, nMAG, and VIPET) to gamma photons in teletherapy unit with ^{60}Co source. The aim of this irradiation was to support the statement regarding the lowest sensitivity of VIPET gels. Both irradiation units: linear accelerator and teletherapy unit with ^{60}Co source produce high-energy photons; however, dose rates that play tremendous role in the polymerized structure formation are different. The dose rate of the teletherapy unit with ^{60}Co source on the day of the investigation was 0.152 Gy/min. The usual dose rate in linear accelerator is 3.000 Gy/min. Moreover, it should be noticed that X-ray photons represent a broad energy spectrum with maximum possible energy of 15 MeV, and gamma rays are of discrete origin with two energy lines at 1.17 MeV and 1.33 MeV (average 1.25 MeV). Due to the different photon energy, dose rate, and its distribution in both units, different polymerized structures may be created. It is known [110] that low-dose rate and relatively low photon energy are responsible for the creation of micro gels, i.e., gels with polymerized micro precipitates (clusters) in it. The cluster size and types of species highly depend on the type of irradiation and the energy of primary particles. According to the size of formed derivatives, the ultraviolet and visible light are absorbed differently. Due to the higher doses, the denser network structure is formed in polymerized gel, which leads to higher registered intensity at specific wavelengths. In the case of high dose rate and high-energy, nanogels (10–300 nm) that are consisting of tiny polymer nanoparticles (1–100 nm) are produced [111]. Moreover, they tend to create a well-defined 3D network structures when the irradiation dose increases [112]. Fig. 42 and Fig. 43 show absorption spectra of ^{60}Co irradiated VIPET and nPAG gels. The λ_{max} and full width of half maximum for VIPET, nMAG, and nPAG gels spectra are provided in Table 5.

Table 5. λ_{max} and FWHM of VIPET, nMAG, and nPAG gels that are irradiated by ^{60}Co source

VIPET			nPAG			nMAG		
Dose (Gy)	λ_{max}	FWHM	Dose (Gy)	λ_{max}	FWHM	Dose (Gy)	λ_{max}	FWHM
0	278	101.2	0	302	170.3	0	292	181.7
2	282	117.7	2	306	217.8	2	300	198.3
4	300	130.9	4	308	221.1	4	315	219.9
6	302	149.1	6	309	239.0	6	322	228.0
8	303	167.2	8	333	243.6	8	331	235.0

Intensity peaks are broadening and shifting to longer wavelength when the irradiation dose is increased. The peak broadening indicates that bigger amount of polymer was formed. In this case, nPAG and nMAG gels have shown quiet similar peak broadening. The investigation of dose sensitivity was done to find out which polymer gel is more sensitive to the gamma irradiation. This experiment corresponds to the other researchers' results [68], reporting the broadening of intensity peak registered by acrylamide based gels and its' shifting to higher wavelength from 300

nm to 450 nm when 12 Gy gamma irradiation dose was applied. Therefore, the main intensity peak position shift from 300 nm to 320 nm wavelength after 10 Gy photon dose application, as it was reported by the authors [69] for the methacrylic acid based gel.

Dose sensitivity curves for these gels are presented in Fig. 42.

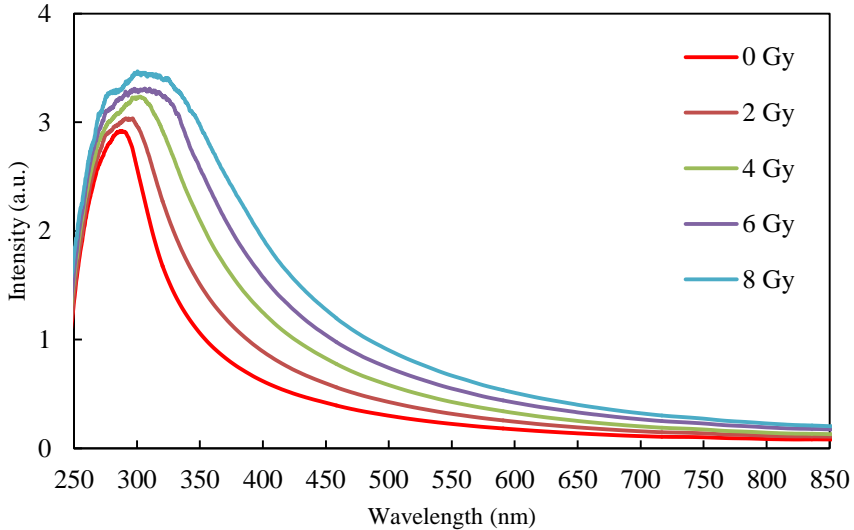


Fig. 42. The typical UV-VIS absorption spectra of VIPET dose gel that is irradiated by gamma photons from ^{60}Co source

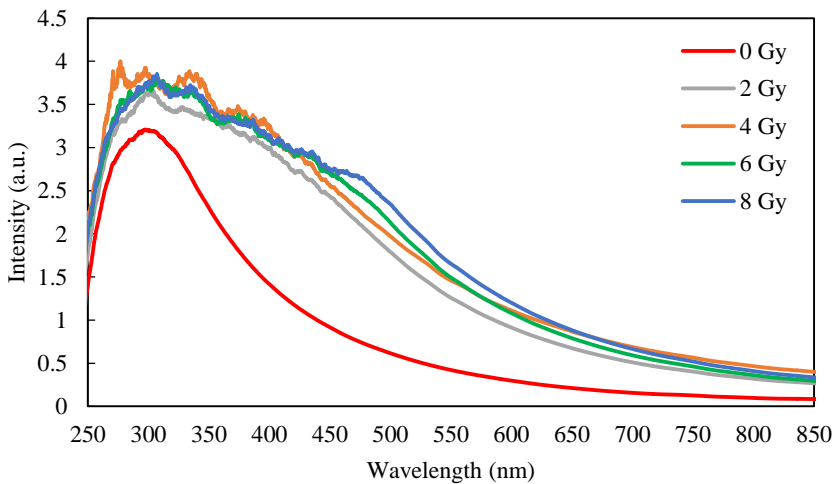


Fig. 43. The typical UV-VIS absorption spectra of nPAG dose gel that is irradiated by gamma photons from ^{60}Co source

Full UV-VIS spectra of nPAG gel are presented to show that due to the doses that are higher than 2 Gy, the intensity peaks are broad, and the periodic structure

could be seen. This may be a light scatter from the clusters, which was formed after the irradiation, when a cluster size is close to the incident light wavelength.

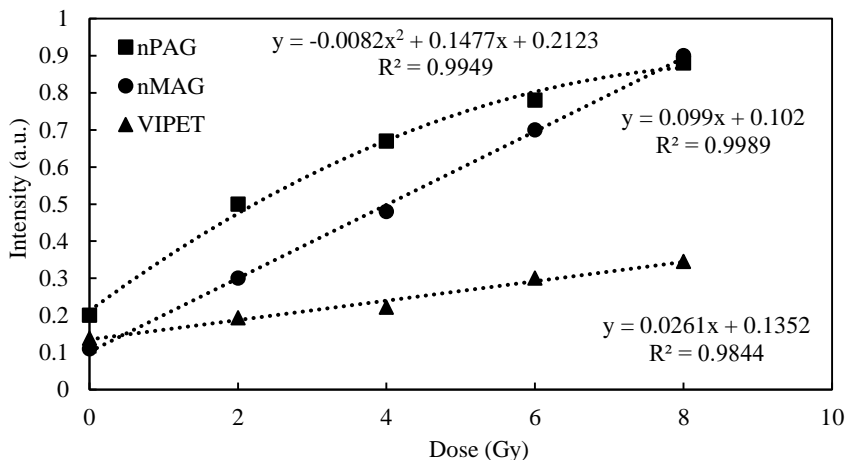


Fig. 44. Dose versus intensity (sensitivity) curves for nMAG, nPAG, and VIPET gels that are irradiated with ^{60}Co source. Intensity values at 650 nm wavelength

The slope calculations of the fitted lines revealed 0.099 sensitivity of ^{60}Co irradiated nMAG gels. The estimated sensitivity of 0.026 for VIPET gel was the lowest. As in the case of X-ray irradiation, the dose sensitivity curve of nPAG gel was fitted with second order polynomic function. The raising part indicated the slope value of 0.12. The dose sensitivity of gels that are irradiated to gamma photons was 1.5 times higher for VIPET and nMAG as compared to X-ray irradiated samples. The nPAG dose gel has the same sensitivity for X-ray and gamma irradiation in low (<10 Gy) dose range. This may be explained by the fact that low-dose rate (0.1–0.5 Gy/min) irradiation is responsible for the production of a number of different polymeric precipitates in gel volume that form clusters on the first but not uniform polymer networks [2, 113]. nMAG recorded almost linear, 0.99 for gamma and 0.97 for X-ray irradiation, dose response to the radiation-induced changes in the dose range up to 10 Gy. Taking into account that VIPET gel showed lowest dose response and nPAG gel is characterized by a saturation tendency at the doses >6 Gy, it was decided to select nMAG gel for the further more detailed development.

Electron irradiation

A batch of nMAG dose gels samples was prepared in the cuvettes and irradiated to the doses from the interval from 0 to 5 Gy. Since different energies may be responsible for different polymerization processes in the irradiated species, 6 MeV and 16 MeV electron energies were chosen for sample irradiation in order to assess possible energy dependence on the dose response. Dose response to the irradiation

and gel sensitivity derived from UV-VIS absorption spectra that are provided in Fig. 45 and Fig. 46.

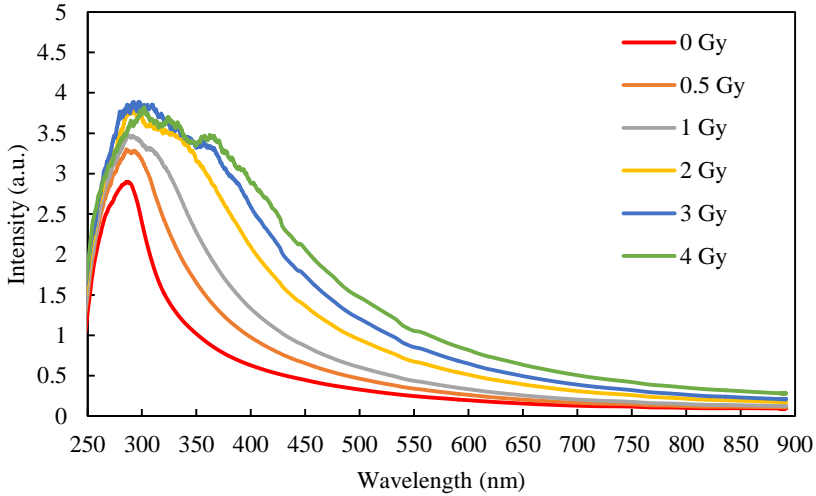


Fig. 45. The UV-VIS spectra of nMAG dose gel that is irradiated by 6 MeV energy electrons

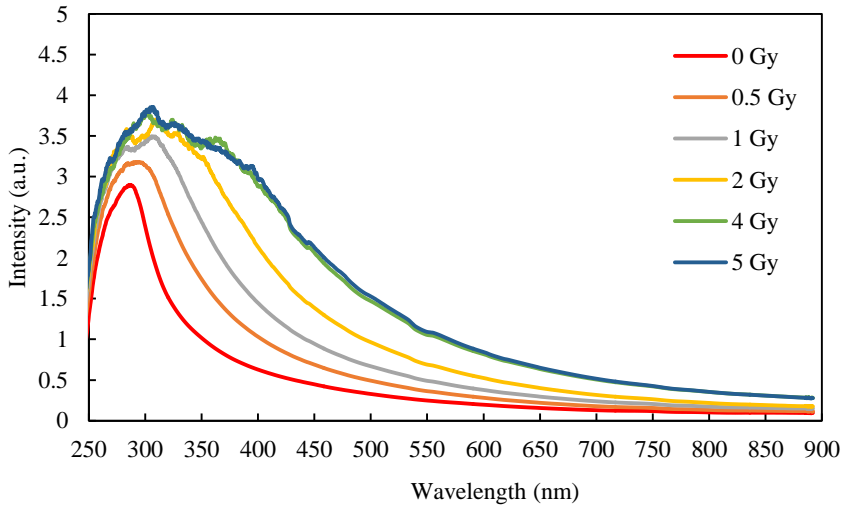


Fig. 46. The UV-VIS spectra of nMAG dose gel that is irradiated by 16 MeV energy electrons

The red-shift of the registered intensity peak and peak broadening with increased irradiation dose were clearly seen in both figures. The peak has shifted from 288 nm to 337 nm when 6 MeV were applied and from 288 nm to 349 nm when 16 MeV were applied. The same registered light intensity was observed in gels that were irradiated by 16 MeV energy electrons. When 4 Gy dose was applied for 6 MeV, the

FWHM was 191.7, and for 16 MeV, it was 200.9. Gauss absorption peak location λ_{\max} and FWHM of each sample for each irradiation dose are provided in Table 6.

Table 6. Spectral parameters of nMAG dose gel that is irradiated by electrons

Dose (Gy)	λ_{\max} (nm)		FWHM (a.u.)	
	6 MeV	16 MeV	6 MeV	16 MeV
0	288	288	83.4	83.4
0.5	300	302	110.3	114.5
1	311	313	128.1	137.1
2	327	329	171.8	173.5
3	336	-	182.5	-
4	337	337	191.7	200.9
5	-	349	-	211.3

Spectral parameters are directly linked to the amount of the created polymerized species. Higher doses introduce chemical reactions that are leading to the formation of denser polymer network structure in the irradiated gel. This is as well responsible for the increased registered intensity in gels that are irradiated by higher doses [1].

The comparison of the sensitivity of electron irradiated nMAG samples is provided in Fig. 47. The nMAG dose gel sensitivity to electron irradiation was estimated from the fitted dose response curves.

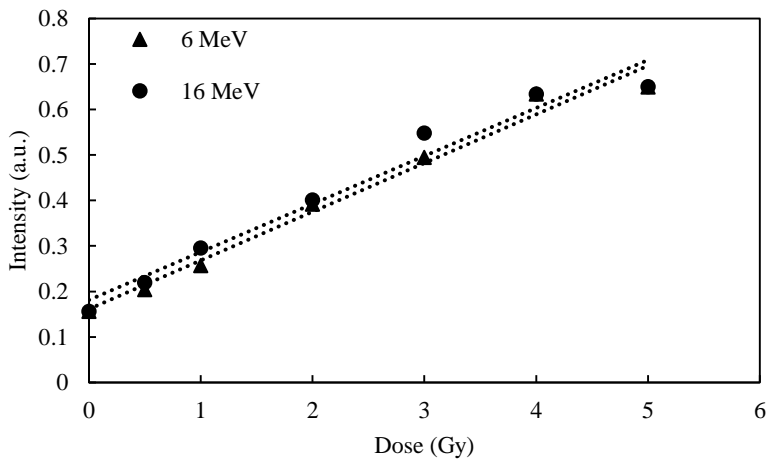


Fig. 47. The comparison of 6 MeV and 16 MeV energy electron irradiated nMAG gel, registered intensity at 650 nm

The performed sensitivity calculations confirmed that there is no significant difference between the sensitivity of gels that were irradiated by applying different electron beam energies. The estimated sensitivity parameter was the same for both electron energies and was equal to 0.11 (a.u.). This aspect makes the practical use of

nMAG for dose verification in electron therapy much easier, since there is no need for dosimeter calibration at different energies.

The performed investigation has shown the applicability of nMAG dosimeter in low-dose (<10 Gy) region when electron irradiation is applied. The required sensitivity of nMAG gel to electron beam irradiation in higher dose (>10 Gy) range might be achieved by varying dose gel composition and concentrations of dose gel constituents.

Proton irradiation

Taking into account that the proton dose that was delivered to the target per fraction may vary (is not fixed to 2 Gy) and the proton induced polymerization processes in low-dose region (0–5 Gy) have not been analyzed in details, the author of the dissertation has investigated low-dose radiation-induced polymerization related changes of UV-VIS spectral characteristic. VIPET, nPAG, and nMAG dose gels were examined to identify the most sensitive dose gels for proton detection.

VIPET, nPAG, and nMAG gel samples were prepared according to the standard procedure and irradiated with 230 MeV protons to different doses from the 0–5 Gy interval. Specific proton irradiation geometry, which is described in the Instruments and Methods section, was applied. Proton dose-dependent UV-VIS intensity spectra of dose gels are provided in Fig. 48, Fig. 49, and Fig. 50, respectively.

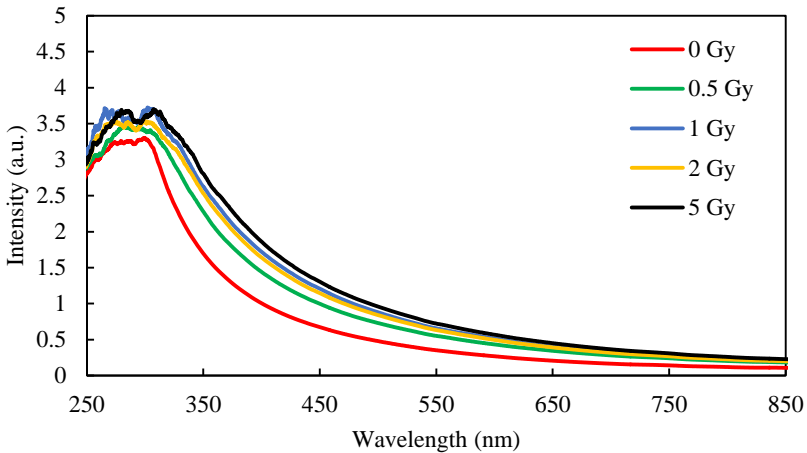


Fig. 48. The UV-VIS spectra of VIPET dose gel that is irradiated by 230 MeV energy

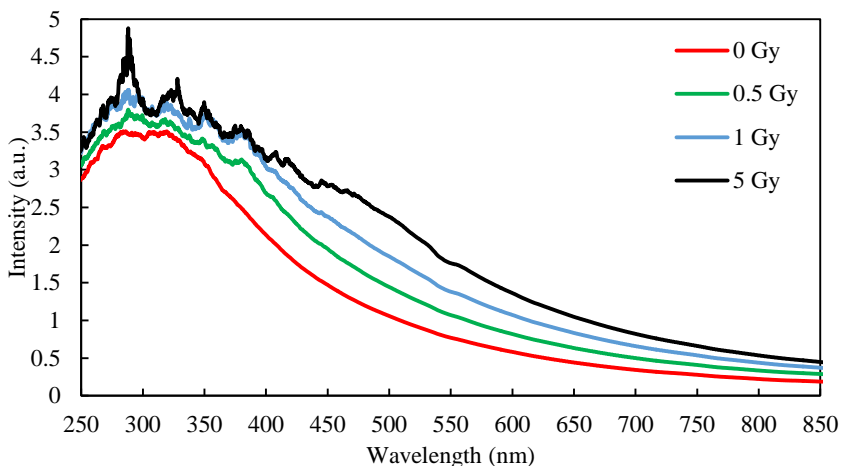


Fig. 49. The UV-VIS spectra of nPAG dose gel that is irradiated by 230 MeV energy protons

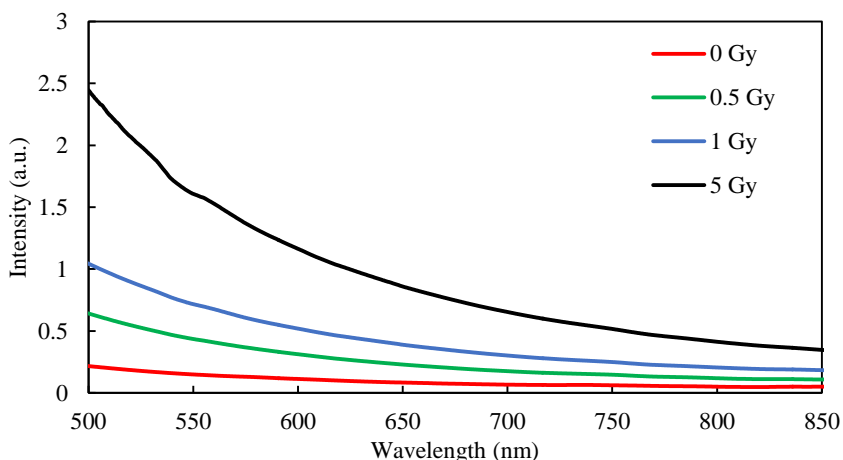


Fig. 50. The segment of the UV-VIS spectra of nMAG dose gel that is irradiated by 230 MeV energy protons

The red-shift of the absorption curve with the increased absorbed dose was observed for all the irradiated gels as a consequence of the specific polymerization process that was initiated by the proton irradiation in them. When high-energy protons travel through matter, they lose their energy by interacting with atoms along the short straight path (low LET interaction). However, they produce secondary delta electrons that contribute significantly to the polymerization processes. Interacting with water in hydrogels, delta electrons create a number of reactive species located near the main proton path. This leads to the clusters' creation locally in the gel volume near the particle path [27]. The localized polymerization (clusters) is not a problem for nPAG gels, since long cross-linked chains are produced that might connect different

neighboring fragments of polymerized gel and create polymer network structure. This behavior of the irradiated nPAG gel is reflected by broad and flat absorption peak. In contrary, the VIPET gels do not create long polymer chains; thus, the polymerized area is located close to the proton path. It becomes denser and larger with the increased absorbed dose. However, the growth of polymerized area is modest. This is clearly seen in narrow UV-VIS intensity peak of VIPET gel and its modest broadening. The most interesting case is the polymerization in nMAG dose gels. High optical density related UV-VIS registered intensity was out of the measurement region of UV-VIS spectrometer. It was impossible to get full spectra; thus, only fragments of spectra in the region of interest were measured. The absorption peak location, λ_{max} , and FWHM were estimated and calculated for all the spectra of proton irradiated gels, and they are presented in the Table 7.

Table 7. Spectral parameters of nMAG, nPAG, and VIPET dose gels that are irradiated by high-energy protons

Dose (Gy)	λ_{max} (nm)			FWHM (a.u.)		
	nMAG	nPAG	VIPET	nMAG	nPAG	VIPET
0	272	319	289	81.2	191.1	149.4
0.5	279	331	291	186.7	236.6	153.1
1	301	336	298	221.3	267.1	169.6
5	336	344	304	287.0	314.6	194.2

Gel sensitivity to proton irradiation was estimated by using dose versus registered intensity curves that are provided in Fig. 51.

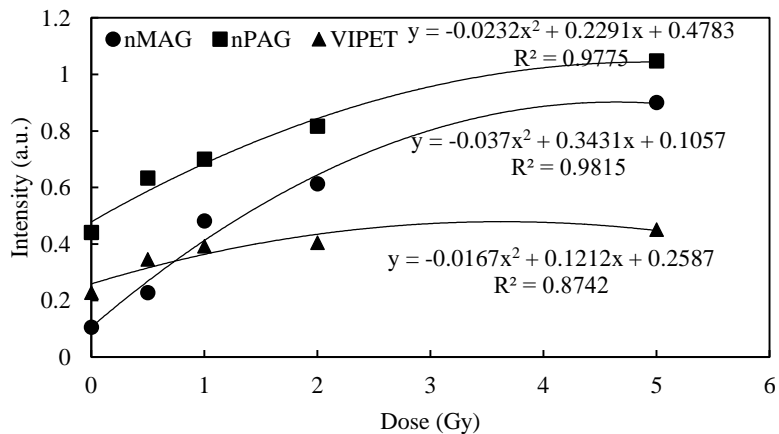


Fig. 51. The dose versus intensity (sensitivity) curves for 230 MeV proton irradiated nMAG, nPAG, and VIPET gels that are red out at 650 nm

It was found that the intensity of all the investigated gels measured at 650 nm was tending to saturate starting with 3 Gy dose; thus, the sensitivity was estimated from the rising part of the dose versus the intensity curves for the dose interval 0–3 Gy only. The irradiated VIPET gels recorded the lowest UV-VIS sensitivity of 0.058 to proton irradiation as compared to the other investigated gels. The UV-VIS sensitivity of 0.13 was estimated for nPAG gels. However, due to the prompt proton induced polymerization, it was especially complicated to follow the whole registered intensity spectrum of nMAG and analyze the polymerization processes in more details. This observation was in line with the research performed by the other authors who were investigating the cross-linked methacrylic acid gel [27]. The UV-VIS sensitivity of 0.22 was estimated for the irradiated nMAG gels.

Neutron irradiation

Two types of neutron sources were used in this experiment in order to observe the differences in UV-VIS spectral characteristics of polymerized gels that were irradiated by fast neutrons (14 MeV) and mixed neutron beam, including thermal, epithermal, and fast neutrons. The main parameters of the second neutron source are provided in subsection 3.1.2. Dose delivery was performed in the V1 channel with a defined low-dose rate of 0.617 mSv/min.

UV-VIS absorption spectra of VIPET, nPAG, and nMAG gels that were obtained by irradiating gel samples with different neutron sources are provided in Fig. 52, Fig. 53, and Fig. 54, respectively.

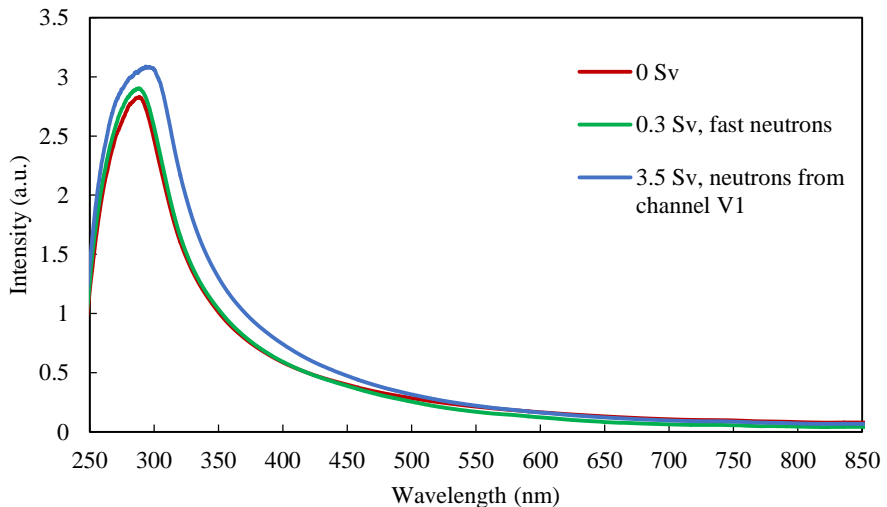


Fig. 52. UV-VIS absorption spectra of neutron irradiated VIPET gels

A clearly seen modest red-shift and the broadening of the intensity peak was seen for the neutron irradiated VIPET gels; however, at higher wavelength, the absorption spectra of gels that were irradiated to different doses were overlapping. A well-defined separation of dose versus registered intensity curves was seen in the case of nPAG (Fig. 53) and nMAG (Fig. 54) irradiation to neutrons.

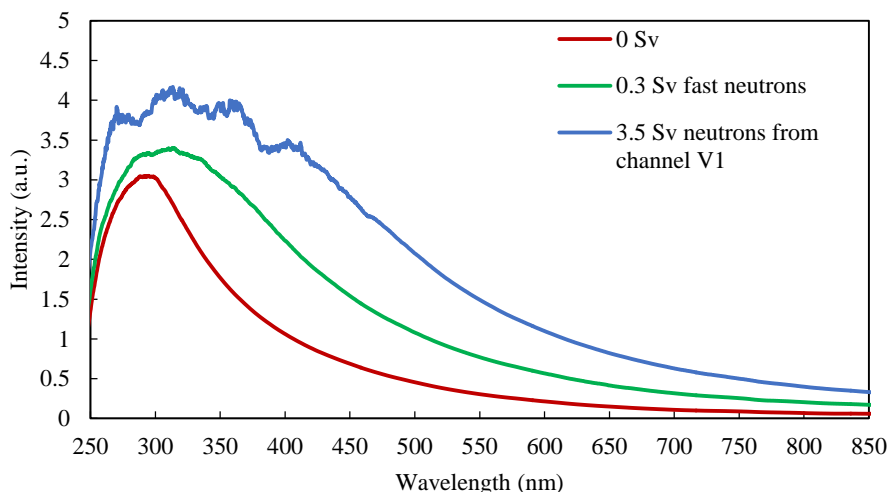


Fig. 53. UV-VIS registered intensity spectra of neutron irradiated nPAG gels

The differently shaped intensity peaks were found for nPAG gels that were irradiated by different neutron beams: peak was smooth for monoenergetic fast neutrons, but not uniform, the disordered peak for the mixed neutron beam was observed. The shape of the intensity peak was related to the possible development of more uniform polymerized gel structure after the irradiation to monoenergetic fast neutrons as compared to the creation of nonhomogeneous differently sized polymerized gel clusters that contribute to the significant broadening of the absorption peak in the case of mixed neutron beam irradiated dose gels.

The study of intensity spectra that are registered by neutron irradiated nMAG gel revealed that there was a difference between gel irradiation with fast (14 MeV, 0.3 Sv) neutrons and mixed beam of thermal+epithermal+fast neutrons (1.31 Sv, 2.7 Sv, and 4.85 Sv), as it is indicated in Fig. 54.

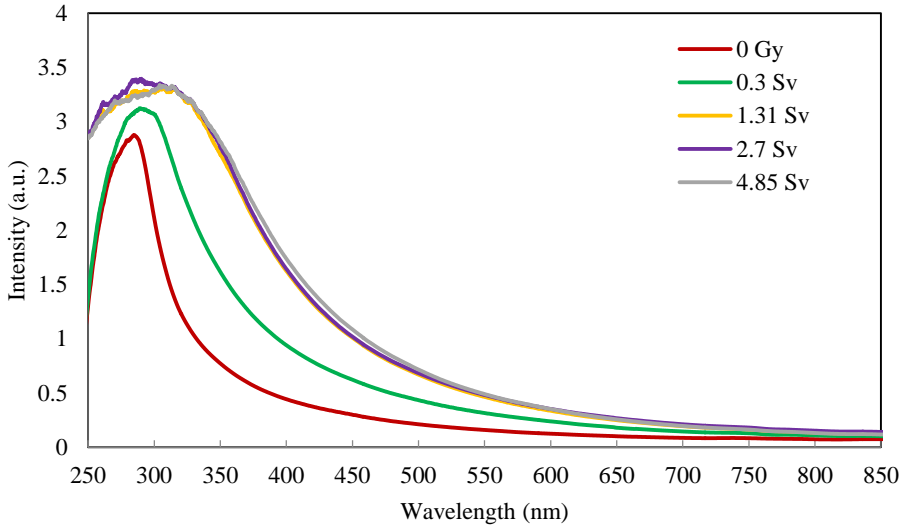


Fig. 54. The UV-VIS spectra of nMAG dose gel that is irradiated with neutrons

No significant difference was found between intensity spectra of nMAG gels that are irradiated to different doses by mixed neutron beam. The calculation results of the main peak characteristics that were performed after the application of the Gaussian fitting to the VIPET, nPAG, and nMAG intensity curves are provided in Table 8.

Table 8. Spectra parameters of nMAG dose gel that are irradiated by the neutron medical source

Dose (Gy)	λ_{\max} (nm)			FWHM (a.u.)		
	nMAG	nPAG	VIPET	nMAG	nPAG	VIPET
0	290	302	291	83.4	169.3	85.7
0.3	295	316	294	130.3	254.9	93.6
1.31	306	322	300	183.8	269.0	111.9
2.7	308	-	-	186.9	-	-
4.85	310	-	-	189.6	-	-

There can be seen the main intensity peak broadening and shift to the longer wavelength tendency for all the gels. The measured intensity peak of VIPET gel has shifted from 291nm to 300 nm. For nPAG gel, the peak has shifted from 302 nm to 322 nm. For nMAG gel, the intensity peak has shifted from 290 nm to 306 nm; 2.7 Gy and 4.85 Gy doses were applied only for nMAG. According to the results of FWHM calculations, the highest amount of polymer was formed in the nPAG gel when 1.31 Gy dose was applied. VIPET gel showed low sensitivity to neutron irradiation. It was impossible to construct dose versus registered intensity dependency for the gel UV-VIS sensitivity estimation due to the overlapping spectra, thus identifying nMAG gel as not suitable for neutron dose measurements.

The overall evaluation of the investigation results led to the conclusion that nMAG gel was the most sensitive dose gel to different types of irradiation.

The comparison of dose UV-VIS sensitivity of nMAG gel that is irradiated by high-energy X-rays, gamma photons, protons, and electron beams is provided in Fig. 55.

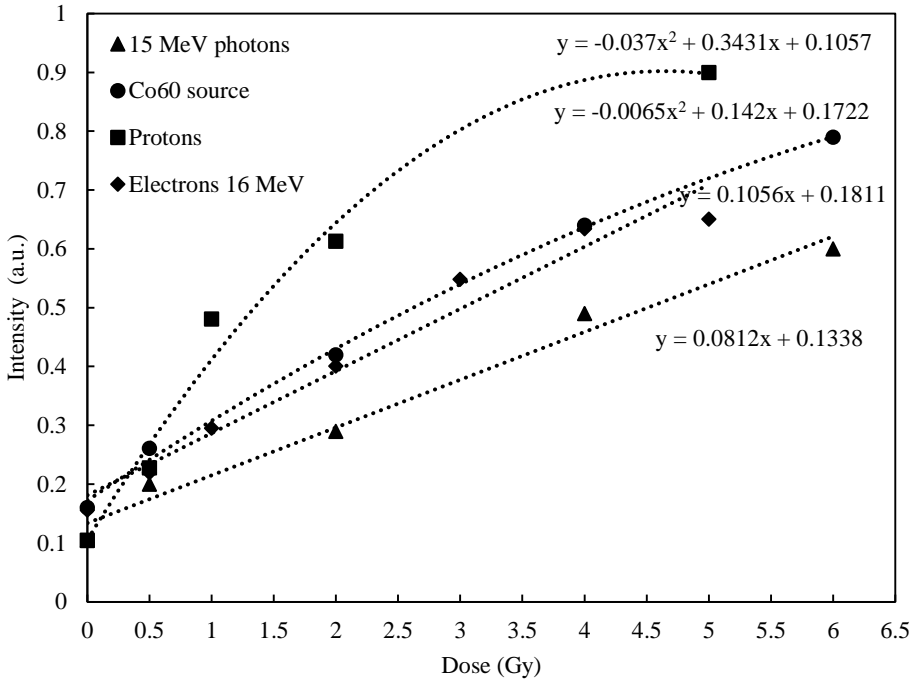


Fig. 55. The comparison of dose sensitivity of nMAG dose gel to different irradiation beams

According to the results provided in Fig. 55, nMAG gel that was evaluated at wavelength $\lambda_{max} = 650$ nm was mostly sensitive to proton irradiation. The slope was the steadiest, 0.34, for protons comparing to 0.08 for 15 MeV photons, 0.10 for 16 MeV electrons, and 0.14 for ^{60}Co source.

Summarizing the VIPET, nPAG, and nMAG polymer gels sensitivity to photon and particles <10 Gy doses irradiation, it is important to mention that VIPET gel has shown the lowest sensitivity to X-ray, gamma source, electron, proton, and neutron irradiation. nPAG gel had a tendency to reach saturation in dose sensitivity at 3 Gy dose, when medical 15 MeV X-ray and ^{60}Co source was applied. However, it should be noted that the high sensitivity of gel was a disadvantage when evaluating radiation-induced polymerization, since it was impossible to define the exact intensity peak position, which records the formation of different polymeric derivatives. Linear dose dependency of the intensity values in the nMAG UV-VIS absorption spectra was well pronounced in the case of gel irradiation with X-ray photons. Therefore, nMAG gels

were selected for further investigations that are devoted to the development of dose gels with enhanced sensitivity.

4.1.2 Influence of nMAG gel components' concentrations on the sensitivity of gel

Based on the results provided in the subchapter 4.1., nMAG gel was identified as being sensitive enough to high-energy electron, proton, and especially photon irradiation. Easy fabrication of nMAG gel and the universal feature to record the polymerization supported the choice of nMAG for further investigations.

In order to obtain the most sensitive to photon irradiation nMAG gel of advanced composition, three different sets of nMAG dose gel samples were prepared, varying the concentration of monomer, gelatin, and oxygen scavenger. The selected concentrations of nMAG gel components are presented in Table 9.

Table 9. Concentrations of nMAG gel components

nMAG gel component	Overall amount of material
Methacrylic acid, MA	2, 4, 6, 8 % w/w
Tetrakis-hydroxymethyl phosphonium chloride, THPC	3, 5, 10, 15 mM
Gelatin	4, 5, 6 % w/w

Gel preparation was performed following the procedure described in 3.1.1. In order to achieve homogeneous irradiation of the whole gel volume, the cuvettes filled gels were placed on their long side in the central position of the irradiation field. The 10 x 10 cm² field size was chosen in the linear accelerator; 15 MeV photon beam was applied for the irradiation, and the doses from the interval 0–5 Gy were delivered. The properties of the irradiated samples were analyzed in UV-VIS spectrometer and photo scanner that was developed in the laboratory. The standard error of UV-VIS spectra intensity measurements does not exceed 5 %. The standard error for constructed photo-scanner varies from 0.55 to 1.67 % when the irradiation doses are increasing.

Variation of methacrylic acid concentration

The selection of the interval for methacrylic acid concentrations (2–8 % w/w) (see Table 9) in nMAG gels was based on the research findings reported by the other authors [20, 49]. It was as well taken into account that a very small amount of methacrylic acid will not be sufficient to produce large polymerized structures, since nMAG gel does not contain any cross-linker, and polymethacrylic acid precipitates itself to form small insoluble polymeric structures. Methacrylic acid concentrations that were used in the experiment were calculated and added to the solution, keeping the concentrations of other gel components as it was indicated for the standard nMAG gel.

In order to analyze the dose dependency to the registered UV-VIS spectra intensity values of the irradiated gels at 650 nm wavelength, the intensity versus dose curves were constructed (Fig. 56), from which the gel sensitivity parameter to

irradiation derived by drawing tangential to the fitted curve. It was found that MMA concentration of 4 % was limiting the observation of the spectral characteristic changes due to the saturation of radiation-induced polymerization at the absorbed dose >3 Gy. No polymerization saturation was observed for the nMAG gels, containing 8 % w/w of methacrylic acid. The dose sensitivity was found to be 0.55 for gels that are containing 8 % w/w of methacrylic acid. It was impossible to evaluate the sensitivity parameter for nMAG that is containing 6 % w/w of methacrylic acid unmistakably. The polymerization process was slowed down at 3 Gy dose and is faster at higher doses (4–5 Gy) to form larger polymerized gel clusters. However, the polymerization proceeds in smaller extent as compared to the gels with higher concentrations of methacrylic acid.

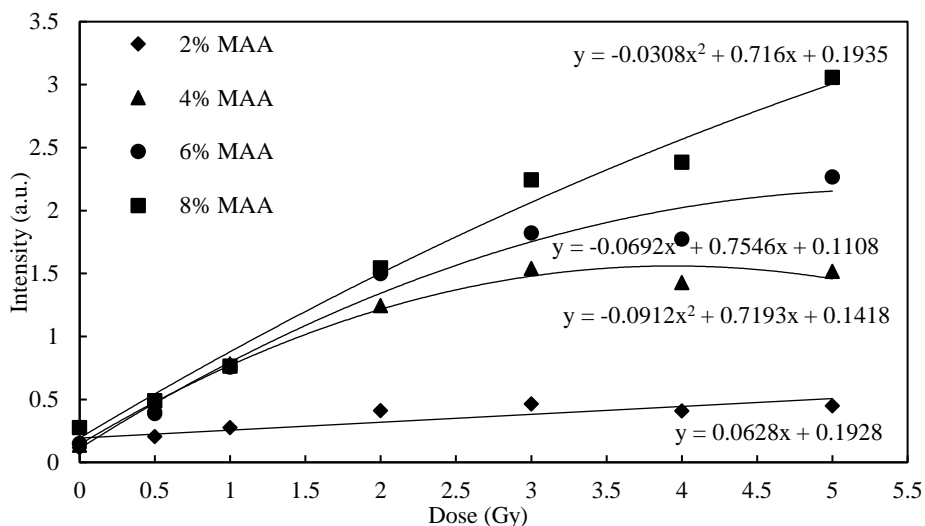


Fig. 56. Methacrylic acid concentration dependent nMAG gel sensitivity curves. Registered intensity values were red out at the wavelength of 650 nm

In order to verify the results that were obtained by analyzing UV-VIS intensity spectra, the independent measurement of the same samples was performed by using newly made photo-scanner. Not overlapping and well-distinguished curves that are possessing linear character in the active region of the measurements were set as the main criteria for the selection of the most suitable methacrylic acid concentration in nMAG. According to results that are presented in Fig. 56, the most relevant to the set requirements was the gel that contains 8 % w/w of methacrylic acid.

Fig. 57 provides scanned profiles of dose gel that is containing 8 % w/w of MAA and is irradiated to different doses. The informative segment from 15 mm to 40 mm of measured profile is provided. It is clearly seen that the scanned dose response profiles are flat and almost linear, indicating that the effective volume of the cuvette was irradiated homogeneously. The sensitivity parameter for nMAG gels that is containing different concentrations of MAA derived from the dose response curves of

the scanner (Fig. 58). It was found that the sensitivity parameter 0.128 was the highest for the gels that are containing 8 % w/w MAA, indicating coincidence of the results that were obtained by applying two different methods.

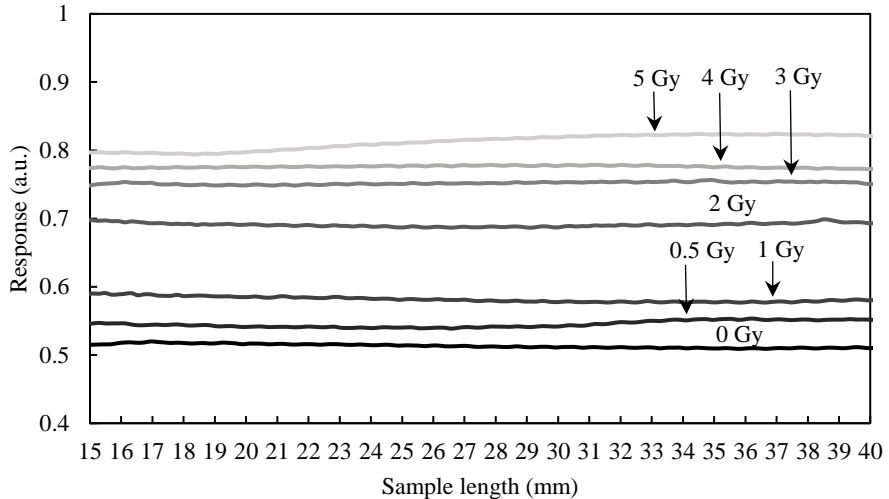


Fig. 57. Scanned dose response profiles of nMAG gels that are containing 8 % of MAA and irradiated to different doses

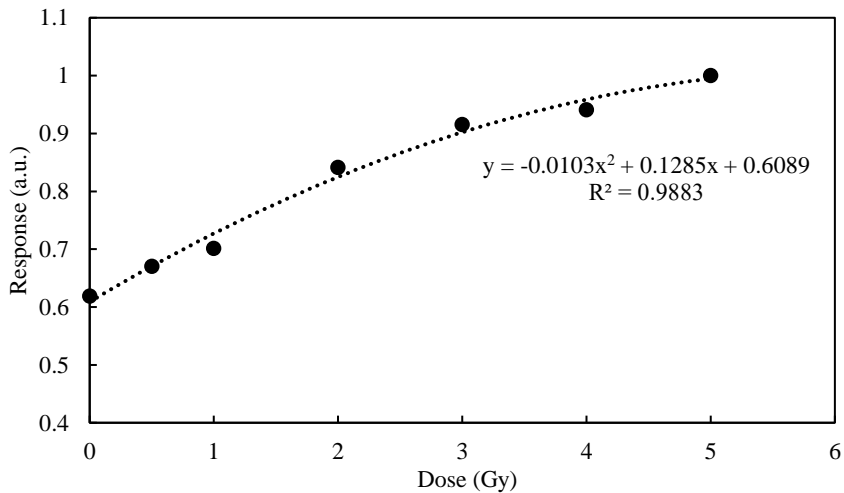


Fig. 58. Scanner dose response in the irradiated nMAG gels that are containing 8 % of MAA

Similar profiles of gels response to 18 MeV photon irradiation were observed by the other authors (Fig. 59 [114]) that evaluated dose response of irradiated methacrylic acid based dose gels by using MRI. The dose sensitivity was examined up to 10 Gy, and the effect of fractionation was observed when the dose is higher. They found 6–8 % concentrations as the most promising.

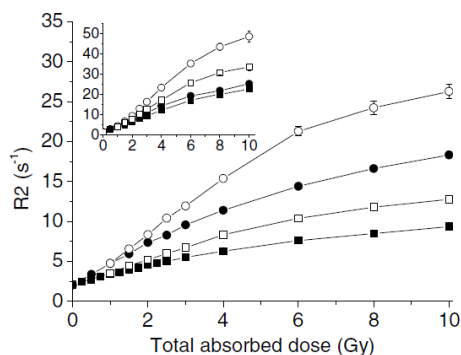


Fig. 59. R2 dose response for nMAG (2 % MAA (filled), 4 % MAA (open), 6 % MAA (insert, filled), 8 % MAA (insert, open)) that is irradiated to the absorbed doses up to 10 Gy [114]

In the system like methacrylic acid based gel, the polymer chain growth is stopped through the termination and chain transfer processes. The termination occurs when due to the interaction of free radicals, a disproportionation reaction occurs that stops further propagation. In the termination-by-combination process, the two growing free radical chains combine to form a single long polymer chain with two free radical electrons that are participating in a new covalent chemical bond. In the termination-by-disproportionation process, two dead polymer molecules are formed after one of the free radicals abstracts a hydrogen atom near the free radical on the other chain, leading to a new covalent bond between the carbon at the end of the first chain and the abstracted hydrogen. A new unpaired electron, which is left behind when the hydrogen atom is abstracted, contributes to the formation of a carbon-carbon double bond at the end of the second chain, which consumes both free radicals. In methacrylic acid system, the kinetic parameters for the bimolecular termination processes, i.e., combination and disproportionation, have been reported to be relatively small and of similar magnitudes [114].

The bigger registered UV-VIS intensity values that were observed for the higher monomer concentrations may be explained by employing the polymerized gel density theory. This theory suggests that the observed intensity changes of irradiated nMAG are due to the density changes that occur after the irradiation. Since irradiation of methacrylic acid initiates polymerization, it is to assume that the polymerization of nMAG causes the density change. The density change that is occurring in nMAG ($\Delta\rho_{gel}$) can be expressed as a function of the weight fraction of the polymer that is formed in the gel and an intrinsic density change that occurs per weight fraction of monomer converted to polymer ($\Delta\rho_{polymer}$). The density change that occurs in gel after the irradiation can be expressed as follows:

$$\Delta\rho_{gel} = \%T \Delta\rho_{polymer} = \%T_{0Gy}(1 - f_m) \Delta\rho_{polymer}, \quad (4.3)$$

where $\%T$ is the weight fraction of the formed polymer in the gel. The term polymer yield will be used when referring to $\%T$ for the simplicity. Nearly all the available monomer in the system is consumed when the gel is irradiated with the higher doses. It means that $\%T = 0$ for an un-irradiated gel and $\sim\%T$, as given in the initial gel composition ($\%T_{0Gy}$) for a fully polymerized gel. The equation 4.3 indicates that for a given dose, the total density change that occurs in nMAG depends on the amount of monomer in the initial gel composition, $\%T_{0Gy}$, the fraction of consumed monomer (f_m), and an intrinsic density change that occurs per weight fraction conversion of the monomer to polymer, $\Delta\rho_{polymer}$ [115].

Variations of the oxygen scavenger amount

Further development of advanced nMAG gel focused on the adjustment of oxygen scavenger, oxygen scavenger hydroxymethyl phosphonium chloride (THPC), amount. Since oxygen scavenger plays an important role in the polymerization process of hydrogels by preventing the termination of developed polymeric chains due to interaction with reactive radicals in water, it is assumed that the larger amount of oxygen scavenger in the gel may contribute to the enhancement of dose gel sensitivity to the irradiation dose/time. Moreover, the higher concentration of oxygen scavenger prevents the expansion of oxygen infused zone. This is extremely important when high dose gradients are present in the irradiated gel [56]. However, smaller amount of oxygen scavenger contributes to the reduction of the saturation dose, which is important for evaluating dynamics of the polymerization processes.

For the investigation, 3 mM, 5 mM, 10 mM, and 15 mM concentrations of THPC were selected. The performed analysis of UV-VIS spectra of irradiated nMAG gels revealed that the gels that are containing higher amount of THPC, 10 mM and 15 mM, were absorbing light better than others (Fig. 60). However, a more uniform tendency of radiation-induced changes was observed at THPC concentrations of 5 mM and 10 mM. Applying the linear regression method R^2 , the values of 0.9895 and 0.9509 were estimated for 10 mM and 5 mM of THPC in nMAG gels with corresponding tangential values of 0.16 (16 %) and 0.11(11 %). For 15 mM and 3 mM of THPC, these values were 0.23 (23 %) and 0.08 (8 %).

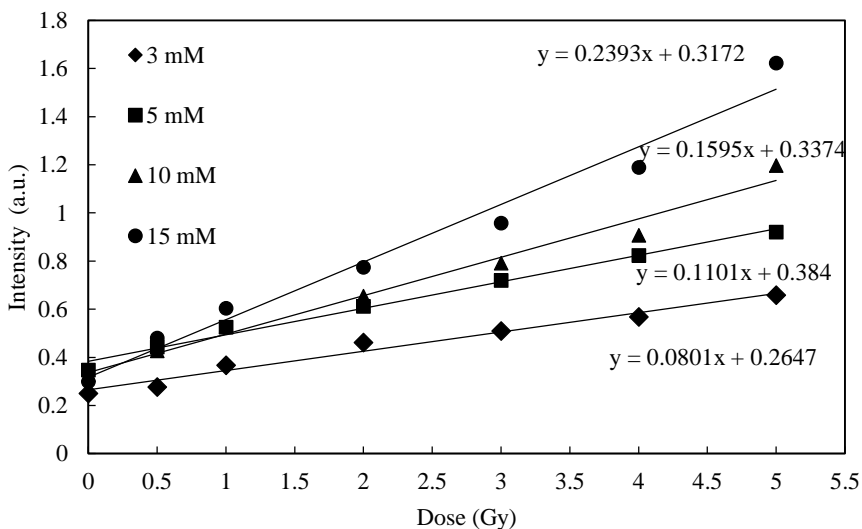


Fig. 60. Dose-dependent registered intensity values of the irradiated nMAG dose gels that are containing various THPC concentrations (registered at $\lambda=650$ nm)

The analysis of irradiated nMAG gel samples that are containing various concentrations of the oxygen scavenger by using photo scanning method revealed that 3 mM and 5mM of THPC containing samples were characterized by low-flatness and thus overlapping dose response profiles. Low concentrations of oxygen scavenger in gels were responsible for relatively fast saturation of polymerized gel, therefore making impossible to distinguish between gels that were irradiated to higher than 2 Gy doses. The investigation of scanned dose response profiles of gels containing 10 mM and 15 mM of THPC indicated good linearity, and it was possible to distinguish between curves that are corresponding to gels which are irradiated to different doses (Fig. 61). The tendency of slight saturation was observed as well, which is an advantage when analyzing low-dose induced changes in the polymerized gels (Fig. 62). Based on the obtained results, 15 mM of THPC were identified as suitable amount developing nMAG gels of enhanced sensitivity. The experimental results in line with other authors [34], who had analyzed the concentrations of THPC from 2 mM to 15 mM for normoxic polymer hydrogels. It was concluded that the most suitable THPC concentration varies from 4 mM to 15 mM and depends on gel type and post-manufactory irradiation time.

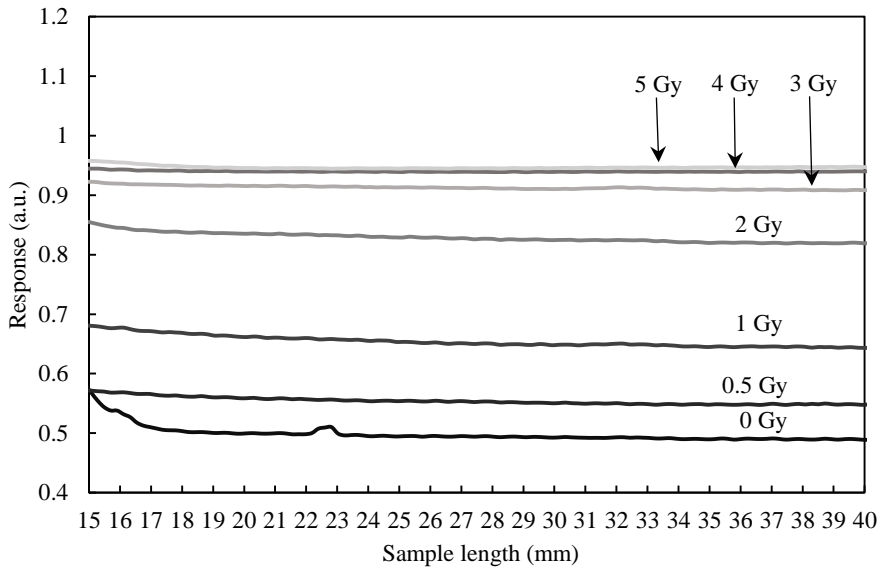


Fig. 61. Scanned dose response profiles of nMAG gels that are containing 15 mM of oxygen scavenger and irradiated to different low doses

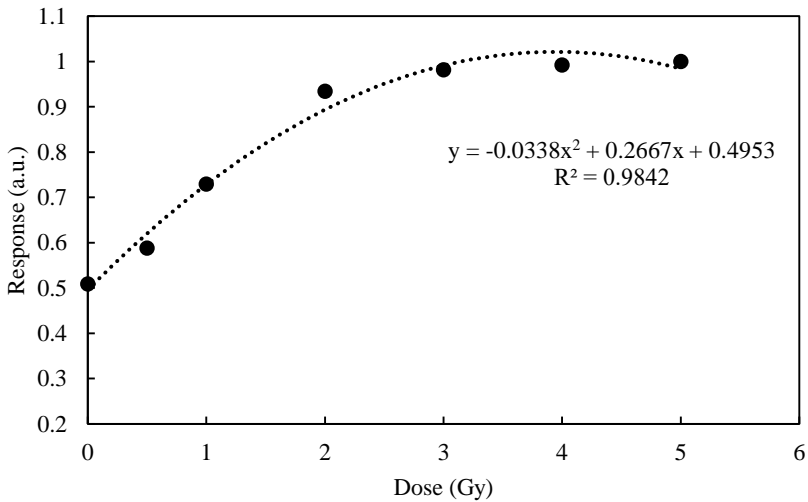
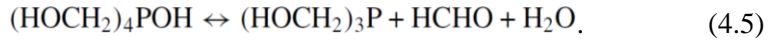
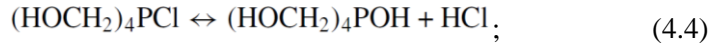


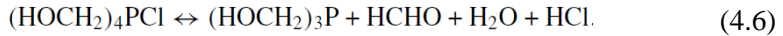
Fig. 62. Intensity to dose response in the irradiated nMAG gels that are containing 15 mM of oxygen scavenger

The THPC ((HOCH₂)₄ PCI) scavenging reactions with O₂ and gelatin are as well presented in this section to assess the potential limitations in gel's stability through possible reactions of THPC. THPC is a monoprotic acid that is having acid-ionization constant pK_a = 5.5. It is likely that proton exchange with water creates

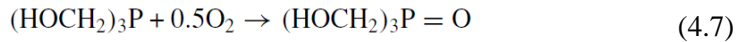
tetrakis (hydroxymethyl) phosphonium hydroxide (THPOH) and tris(hydroxymethyl)phosphine (THP) [34]:



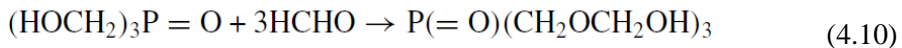
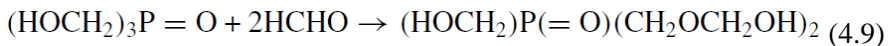
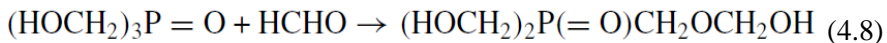
The dissociation of THPOH is followed by the appearance of THP ((HOCH₂)₃P) and formaldehyde. These reactions are combined to form Eq. 4.6 [34].



The THP can scavenge O₂ through reaction to produce tris(hydroxymethyl)phosphine oxide (THPO) [34].



Eq. 4.5 and the subsequent scavenging of O₂ rely on the fact that the P–CH₂OH linkage is weak and is lightly split. Both THPOH and THPO can be neutralized with formaldehyde to produce hemiacetals such as presented in Eq.4.8, 4.9, 4.10 [34].



The neutralization of THPC includes the reaction presented in Equation 4.5 and subsequent 4.7–4.10 reactions. The raw calculation of THPC 5 mM concentration taking into account Eq. 4.6 and the equations above reveal that an initial THPC:O₂ molecule ratio is 5:1 in the polymer gel. As a result, even after all O₂ has been scavenged from the gel, there may be unreacted THPC remaining in the solution. Therefore, it is possible that THPC may react with gelatin and methacrylic acid by using this rough calculation [34].

Variation of gelatin concentration

It is known that the increased concentration of the gelatin in nMAG gel may lead to the reduction of gel sensitivity to irradiation [49]. Irradiated to higher doses gelatin starts interacting with methacrylic acid and forms polymer derivatives that are complicating the evaluation of dose gels. Moreover, the polymerization level of dose gel will be reduced due to the additional consumption of methacrylic acid monomers in reactions with gelatin; too low amount of gelatin in dose gel will result in loss of its function as a scaffold for hosting polymer derivatives. Lower than standard (8 %

w/w) concentrations of gelatin (4 %, 5 %, and 6 % w/w) were investigated in order to alter gel's sensitivity. Dose-dependent UV-VIS intensity values of the irradiated nMAG dose gels that are containing various gelatin concentrations are provided in Fig. 63.

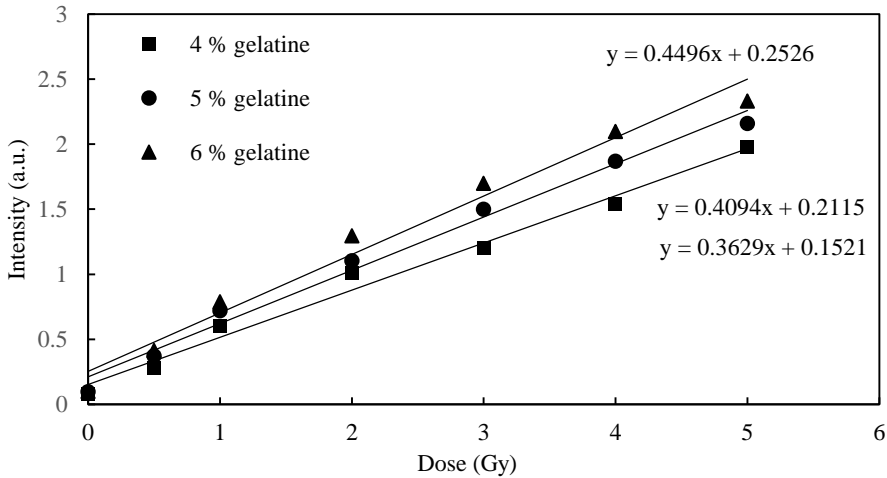


Fig. 63. Dose-dependent UV-VIS light intensity values of irradiated nMAG dose gels that are containing various gelatin concentrations

The performed analysis has shown that the gels which are containing 4 % and 5 % of gelatin were less sensitive (0.36 for 4 %, 0.41 for 5 %) to irradiation as compared to the gels that are containing 6 % of gelatin, but the whole gel was tending to get thin (liquefy) after the irradiation, indicating unstable gelatin scaffold. This might be a big disadvantage in gel dosimetry, since in this case, it is impossible to obtain 3D dose distribution images as it can be done in the solidified gels. In contrary, dose gels containing 6 % of gelatin were sensitive enough (0.45) to the irradiation and more stable. Analyzing the scanned dose response profiles of the irradiated nMAG gels that are containing different gelatin concentrations, the best linearity and well-defined distinguishability of curves was found in gels that are containing 6 % of gelatin (Fig. 64).

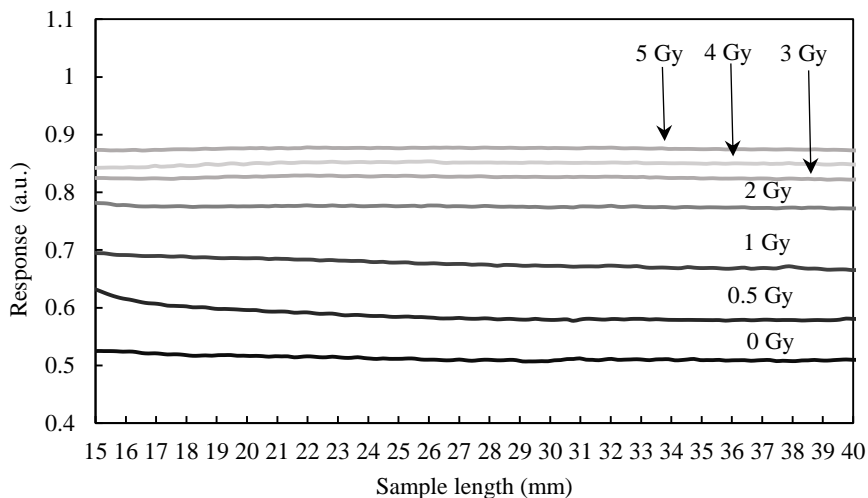


Fig. 64. Dose-dependent intensity response profiles along the cuvettes that are filled with the irradiated nMAG gels that are containing 6 % w/w of gelatin (scanned by using $\lambda=650$ nm laser wavelength)

The dose sensitivity curve for nMAG gels that are containing 6 % of gelatin (Fig. 65) tends to saturate slightly with the increasing irradiation dose. The gel saturation at the relatively low doses, which is up to 5 Gy, is one of the requested parameters when discussing gel's sensitivity in low-dose irradiated polymerized gels.

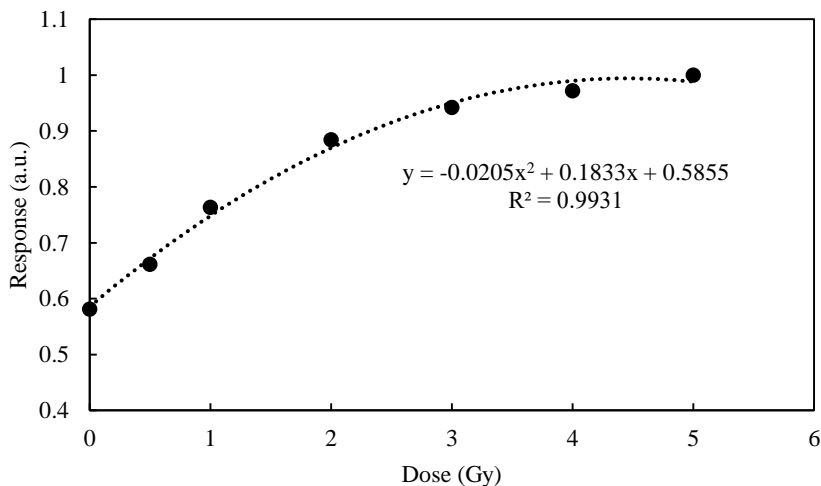


Fig. 65. Dose response that is registered at the same scanning position for nMAG gels that are containing 6 % of gelatin and irradiated to different low doses

There are two assumptions that are concerning gelatin concentration contribution to the polymerization process of methacrylic acid. First assumption states that methacrylic acid monomers polymerize by grafting onto the gelatin matrix [49]. In this scheme, the radiolysis products (e.g., OH radicals) abstract a hydrogen atom from gelatin, and the created gelatin radical is an initiator for the polymerization of methacrylic acid. Then, a free radical on the gelatin polymer matrix acts as initiator, and a polymer branch grows from there. The second assumption states that the template polymerization is responsible for gelatin's contribution to the polymerization in the nMAG systems [32]. In the template mechanism, the monomer complexes with the dissolved polymer, and polymerization progresses along the polymer matrix, using the polymer as a template. However, other authors [49] have shown that the polymerization of methacrylic acid in the nMAG type dosimeter does not require the polymeric structure of gelatin as a template. Gelatin is a single or multistranded polypeptide chain that contains groups of amino acids. These amino acids are typically linked together in several hundred units and in helical form to give the gelatin strands. The amino acids contain amine units within the larger molecule. The amino acid arginine (Arg) is presented in Fig. 66.

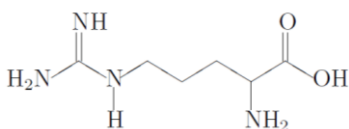


Fig. 66. Amino acid arginine in gelatin [49]

The unreacted oxygen scavenger THPC can react with primary and secondary amines and polymerize it. The reactions of monomeric amines and THPC at room temperature are exothermic and take place readily. THPC may react with the amine groups in gelatin polypeptide chains. For example, in the case of arginine, THPC+arginine would yield structures as it is shown in Fig. 67.

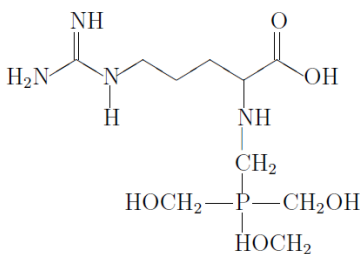


Fig. 67. THPC and arginine structure [49]

The THP can be reduced under the reaction of amines with the hydroxy groups in THPC to the polymer unit as given in Fig. 68A. The reduction of THPC allows reacting with moieties on the gelatin chains to increase the gelatin coagulation and crosslinking further. The possible gelatin that is cross-linked to the THPC structures is presented in Fig. 68B.

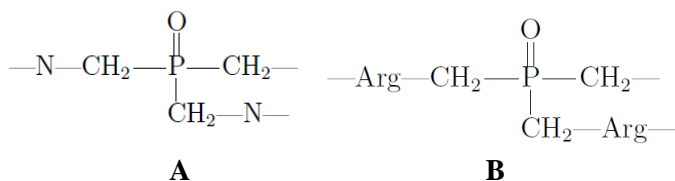


Fig. 68. A) polymer units, B) gelatin that is cross-linked to THPC structures [49]

The increase of coagulation of polypeptides by the induction of the THPC has been reported by the other authors [116]. This coagulation process may help to explain the reduction in dose response in polymer gel that is containing THPC. The more crosslinked gelatin network makes monomer diffusion more difficult in these types of gels. Further support for this theory is found in studies that indicate that an increasing gelatin concentration decreases the apparent diffusion coefficient of water in gelatin gels [34, 116].

The increased amount of gelatin in nMAG gels contributes to the higher dose sensitivity of gel because growing polymethacrylic acid chains do not readily undergo chain transfer to gelatin, and gelatin is important for the precipitation of polymethacrylic acid particles from the solution [115].

Summarizing the “reference” and “advanced” nMAG gels’ sensitivity changes due to its chemical composition, the following relations (see Fig. 69 and Fig. 70) are presented. The dose sensitivity curves were constructed by taking registered intensity values from UV-VIS spectra at 650 nm wavelength. Gel dose response values were measured by the laboratory made photo-scanner and were taken from the middle of measurement window (effective zone) at 30 mm of cuvette axial length.

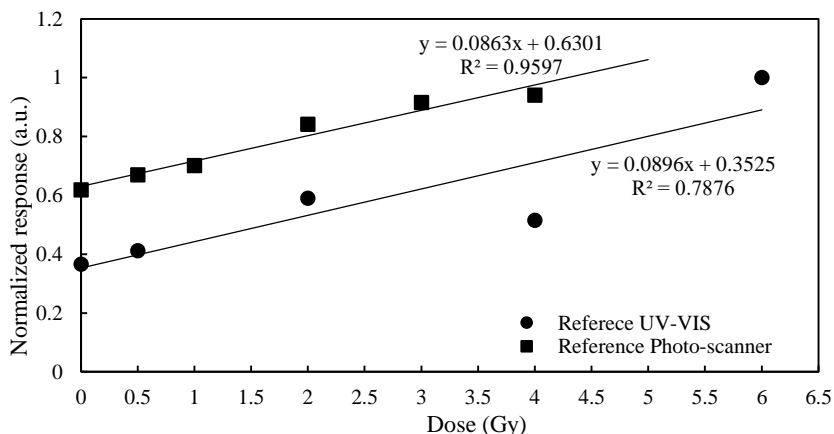


Fig. 69. Dose response of reference nMAG gel that is investigated by the UV-VIS spectroscopy and photo-scanning methods

As it can be seen in the Fig. 70, the reference gel sensitivity to low doses (<10 Gy) is increasing the linear function for both measurement methods, i.e., UV-VIS

spectroscopy and photo-scanning. Sensitivity parameters are as well similar: 0.089 for UV-VIS spectroscopy and 0.086 for photo-scanning method.

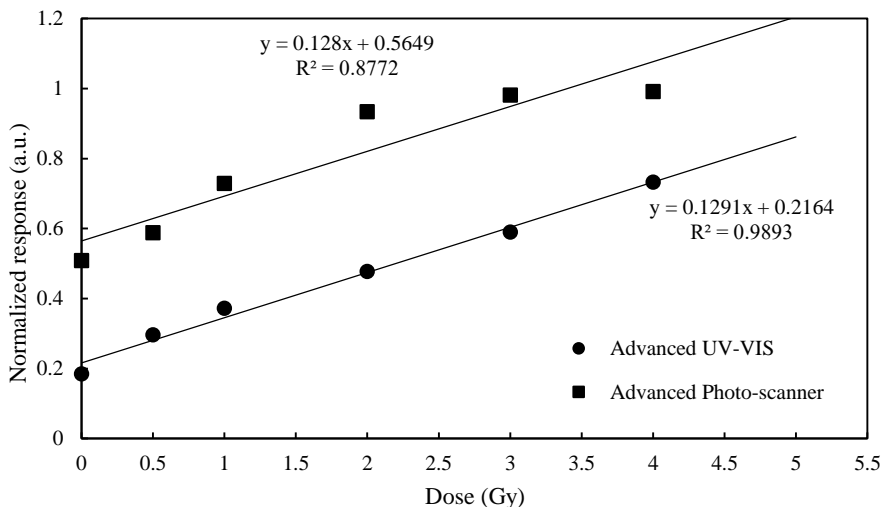


Fig. 70. Dose response of advanced nMAG gel that is investigated by the UV-VIS spectroscopy and photo-scanning methods

The linear increasing tendency is seen in Fig. 70 where advanced nMAG gel's sensitivity to low doses is presented. The sensitivity parameters are 0.129 (a.u.) for UV-VIS spectroscopy and 0.128 (a.u.) for photo-scanning method. The overall nMAG gel sensitivity to low-dose photon irradiation was increased by 30 % (from 0.09 (a.u.) to 0.13 (a.u.)).

Photo-scanning method allows the corrections of dose response curves as compared to those obtained from the results of UV-VIS measurements. Due to the high spatial sensitivity of the proposed photo scanning method, the intensity was evaluated in 0.2 mm steps along the gel-filled irradiated cuvette that is covering the whole irradiated gel length, and the average intensity value for the whole range was provided for the construction of the dose response curve. In the case of UV-VIS spectra, the measurements were performed only at one certain position of cuvette. The results that were obtained by using photo-scanning method are in accordance with the results of the other authors [109, 114].

The performed analysis of dose gel sensitivity varying concentrations of gel constituents led to the selection of the possibly most sensitive nMAG dose gel composition: 8 % w/w of methacrylic acid as a monomer, 15 mM of (hydroxymethyl) phosphonium chloride, as oxygen scavenger, 6 % w/w of gelatin as a scaffold for hosting polymeric derivatives, and 86 % w/w of purified water.

4.1.3 Investigations of nMAG gel polymerization processes by using Raman spectroscopy

It is known, that Raman spectroscopy and FTIR allow the examination of structural changes on the molecular level; however, Raman spectroscopy is a more sensitive technique for the analysis of molecular structures that are containing nonpolar species such as C-C and C=C, which commonly make the backbone of synthetic polymers [117]. According to this knowledge, Raman spectroscopy was applied for the examination and comparison of polymerization processes in the irradiated reference nMAG gels (5 % w/w of methacrylic acid, as monomer; 2mM of hydroxymethyl phosphonium chloride, as oxygen scavenger; 8 % w/w of gelatin, as a scaffold for hosting polymerized derivatives, and 89 % of pure water) and advanced nMAG gels (8 % w/w of methacrylic acid, 15 mM of hydroxymethyl phosphonium chloride, 6 % w/w of gelatin, and 86 % of pure water).

nMAG gels represent hydrogels that are tending to polymerize when the supplied amount of external energy is sufficient to initiate breaking or the formation of new molecular bonds. According to this definition, the characteristic molecular bonds and their performance under high-energy photon irradiation provide important information about the changes in polymerized gel structure. Before starting Raman analysis, the main monomers that were used and the basic polymerization products that were formed should be known in order to focus on the most important Raman peaks that show the structural changes of polymerization product. The characteristic frequencies (Raman peaks) of every single functional group in the methacrylic acid and nMAG dose gels were assigned by analyzing information that was provided by the other researchers [72, 75, 77, 118]. The obtained Raman spectra were analyzed by using Origin PRO 2016 program package.

The Raman peaks of the most important bonds of pure methacrylic acid (Fig. 71) that may contribute to the analysis of photon irradiation-induced polymerization processes were identified as follows: 801 cm^{-1} - $\nu(\text{C-COOH})$, 1403 cm^{-1} - $\delta(\text{CH}_2)$, 1441 cm^{-1} - $\nu(\text{CO})_s$, 1640 cm^{-1} - $\nu(\text{C=C})$, 2937 cm^{-1} , and 2997 cm^{-1} - $\nu(\text{CH}_2)_s$. Their positions were taken into account when analyzing the irradiated reference nMAG gels (5 % w/w of methacrylic acid, 2 mM of tetrakis-hydroxymethyl phosphonium chloride, 8% w/w of gelatin, and 89 % of pure water) and advanced nMAG gels (8 % w/w of methacrylic acid, 10 mM of tetrakis(hydroxymethyl) phosphonium chloride, 6 % w/w of gelatin, and 86 % of pure water).

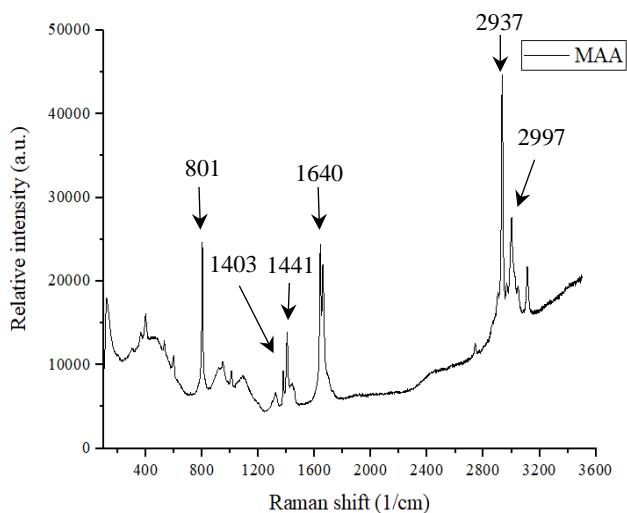


Fig. 71. Raman spectra of pure methacrylic acid

Raman spectra of reference and advanced nMAG dose gels after the photon irradiation up to 5 Gy dose are presented in Fig. 72 to represent the relative Raman peaks' increase and decrease due to 0.5–5 Gy doses that are irradiated by 15 MeV energy photons.

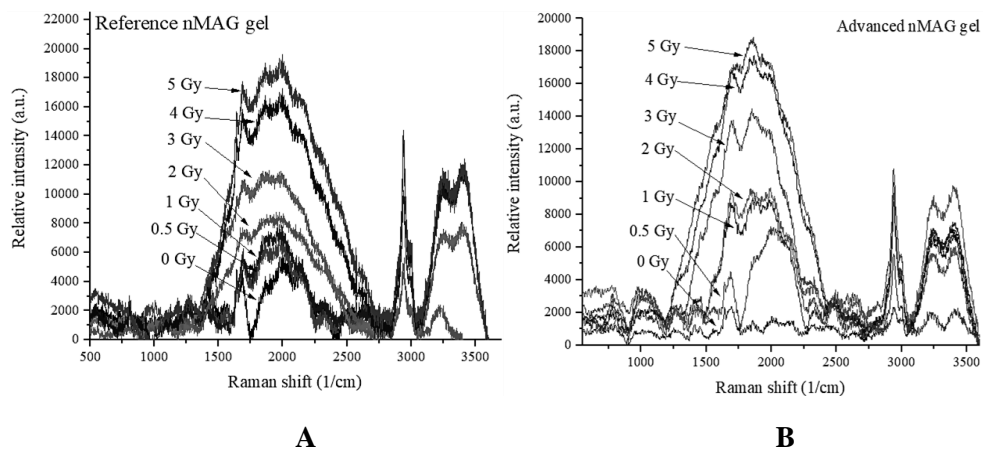


Fig. 72. A) Raman spectra of reference nMAG dose gel, B) Raman spectra of advanced nMAG dose gel

As it was expected, Raman spectra of gel samples had a different shape as compared to the spectrum of pure methacrylic acid. This is due to the presence of gelatin and water components, which are represented in the broad band seen between 1200 cm^{-1} and 2500 cm^{-1} (gelatin and imparted structures) and between 3100 cm^{-1}

and 3500 cm^{-1} (water). A tendency of growing Raman intensity with increasing photon irradiation dose was observed as well as the broadening of the “gelatin” band, which indicates rearrangements in the gel structure and the formation/disintegration of polymer fragments that are embedded in the gelatin matrix. In order to compare polymerization in reference and advanced nMAG gels, the Gaussian function was fitted under the total Raman peak of the “gelatin” band for each dose gel sample. The central peak position, its intensity, and the calculated FWHM for reference and advanced gels that are irradiated to doses up to 5 Gy are shown in the Table 10.

Table 10. The Gaussian function fitting parameters of total peak from 1200 cm^{-1} to 2400 cm^{-1} which shows the amount of polymer that was formed for reference and developed nMAG gel

Dose (Gy)	Raman peak position (cm^{-1})		Raman peak intensity (a.u.)		FWHM (a.u.)	
	Reference	Advanced	Reference	Advanced	Reference	Advanced
0	1861	1875	3822	1399	143	78
0.5	1906	1989	5873	5556	622	326
1	1943	1947	6158	8050	650	526
2	1948	1957	6350	8248	695	677
3	1952	1962	11639	13633	781	723
4	1959	1965	16528	17032	799	750
5	1969	1977	18766	21402	832	762

The increase of Raman peak intensity and FWHM may have derived from the data provided in Table 10. Moreover, it can be seen that the exact positions of Raman peaks are slightly altering with the dose. This may happen, since the increase in the concentration of a specific molecule after the higher dose irradiation leads to the increased vibrational intensity of corresponding molecular bands. In the case of overlapping with neighboring band, the position of the corresponding peak may be slightly shifted [3]. The increasing intensity of Raman peak with the increased absorbed dose in gels indicates the growing level of the gel polymerization as well as increasing FWHM records that are growing the amount of formed polymerized derivatives. The central peak intensity of the advanced nMAG gels increases 15 times at 5 Gy absorbed dose as compared to the intensity at 0 Gy dose, but the Raman peak intensity of a reference gel increases only 4 times at the same irradiation levels. This may happen due to the higher concentration of methacrylic acid in the advanced dose gel. Moreover, the increase of FWHM in both gels was observed with the increasing absorbed dose. Nevertheless, the FWHM values that were obtained for the irradiated advanced gels were in general lower as compared to those of reference gels. This indicates that the polymerization in the advanced gels proceeds faster and the produced structures are more uniform. It is an advantage when a well-developed polymer network structure is formed. Some tendency for saturation at higher

irradiation doses was observed when analyzing FWHM of both gels (Fig. 73). It indicates that the gelatin matrix is getting filled up with the polymer derivatives that contribute significantly to the polymer networking process.

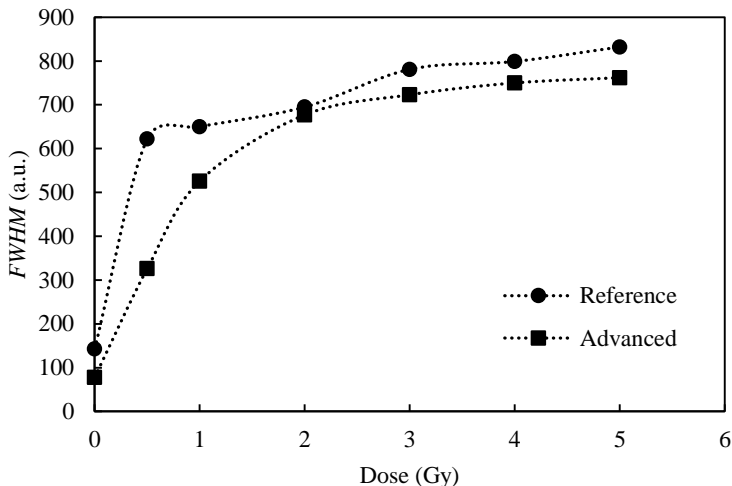


Fig. 73. Variations of FWHM with irradiation dose of nMAG gels within the area between 1200 cm^{-1} and 2400 cm^{-1}

As it was mentioned before, the analysis of relative Raman peaks intensity after the irradiation of gel is focused on specific molecular bonds. The specific bonds in nMAG gel identified: 807 cm^{-1} , 1409 cm^{-1} , 1640 cm^{-1} , 2940 cm^{-1} , and 3114 cm^{-1} . Gauss function was used to fit Raman peaks as was recommended by the authors [119–122]. Typical nMAG spectra are presented in Fig. 74 to get a closer look at the peak separation. All Raman spectra of 0–5 Gy irradiated nMAG gels were fitted in the same manner.

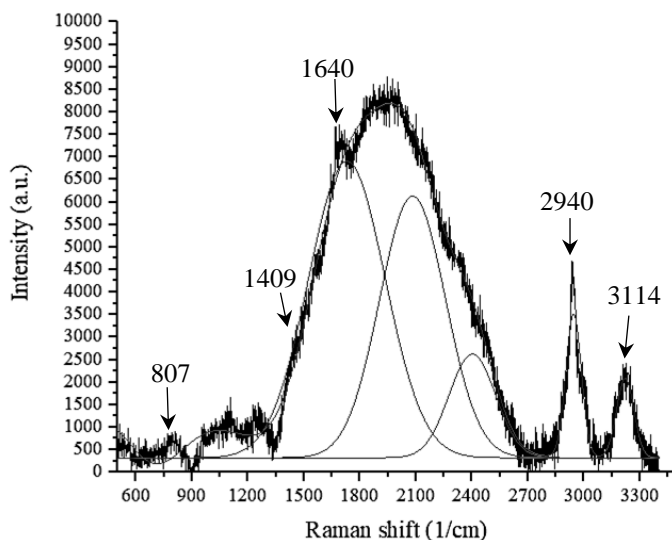


Fig. 74. Raman spectra of 4 Gy irradiated nMAG gel with fitted Gauss function

For a more detailed analysis of molecular bonds, the changes in the irradiated nMAG dose gels Raman spectra were divided into four segments: 700–900 1/cm, 1350–1440 1/cm, 1600–1750 1/cm, 2800–3300 1/cm.

A band at 807 cm^{-1} is caused by the symmetric stretching mode of C-COOH, which corresponds to a bond between carboxylic carbon and double bond carbon. This mode is a polarized one, which is known to be very sensitive to the environmental change such as the dissociation of carboxylic acid. The bond connecting two carbons is formed by the participation of a SP^2 hybrid orbital. After photon irradiation, it changes to a SP^3 hybrid orbital, while the polymerization proceeds and becomes weaker. Monomer consumption, in general, should lead to the decrease of intensity for the vibrational mode with the increasing dose; however, it was hard to distinguish this peak in reference dose gels (Fig. 75A). Due to the higher concentration of methacrylic acid in the advanced nMAG gel, the peak corresponding to the bond at 807 cm^{-1} between carboxylic carbon and double bond carbon was better pronounced in this gel. It should be noticed that the overall peak intensity did not drop to zero, indicating that not all monomer was consumed by absorbing the highest, at this investigation, 5 Gy dose.

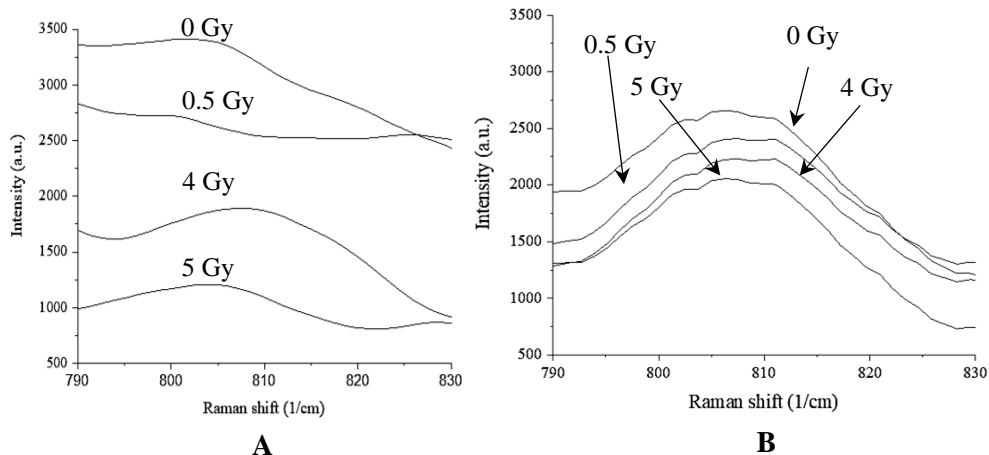


Fig. 75. A) Raman spectra fragments with indicated specific peaks of reference and B) advanced nMAG dose gels in the range of 790 1/–830 1/cm

The peak at 1411 cm^{-1} that is clearly seen in Fig. 76B most probably may be attributed to the CH_2 vibrational bending mode of polymethacrylic acid (PMA).

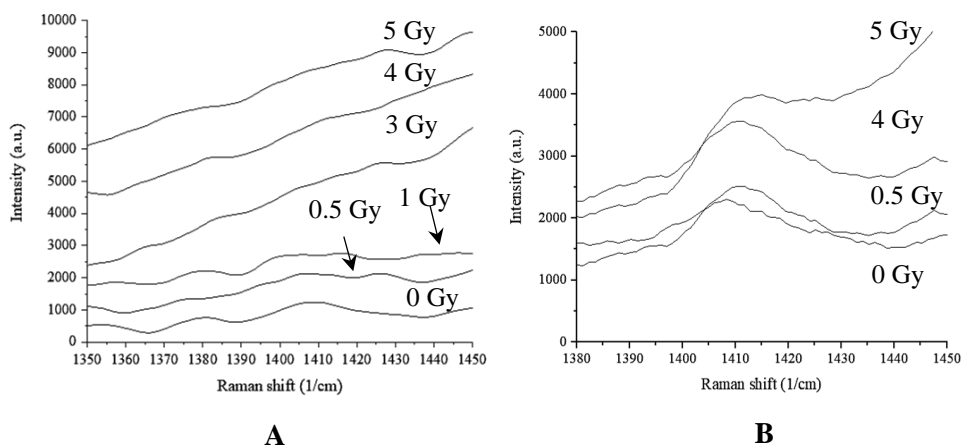


Fig. 76. A) Raman spectra fragments with indicated specific peaks of reference and B) advanced nMAG dose gels in the range of 1350 1/–1440 1/cm

It is expected that the intensity of this bond should increase with the increasing photon irradiation dose, since it records the formation of polymeric structure. However, despite the fact that the tendency of increasing Raman intensity with the increasing radiation dose over the investigated range was clearly seen, it was impossible to define an exact CH_2 peak location in reference nMAG gels. A small shift from 1411 cm^{-1} to 1414 cm^{-1} of the peak corresponding to CH_2 bending mode was observed in the irradiated advanced nMAG dose gels. However, the peak itself was well pronounced and indicated the presence of polymerization in gels.

Since the level of polymerization can be derived from the area under the fitted Gaussian peak, it is trivial that the changes in FWHM will follow the same tendency and provide information regarding the polymerized amount of gel. The tendencies for monomer consumption (at 808 cm⁻¹) and polymer production (at 1414 cm⁻¹) in the irradiated advanced nMAG gel are provided in Fig. 77.

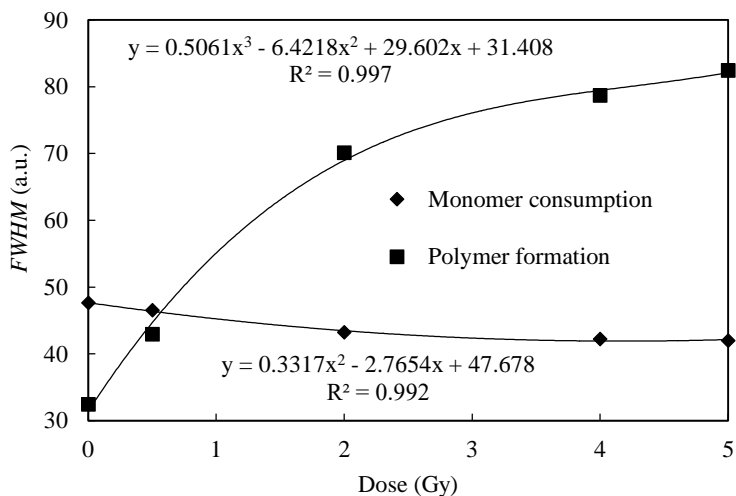


Fig. 77. Monomer consumption (corresponding peak at 808 cm⁻¹) and polymer formation (corresponding peaks at 1411–1414 cm⁻¹) tendencies in the irradiated advanced nMAG gels

The stabilization of consumption of methacrylic acid is most likely due to a combination of two factors: (1) the physical amount of monomer is low beyond 2 Gy, and (2) polymer formation impedes migration of monomer radicals. According to the other researchers, only beyond 20 Gy monomer is completely consumed [117].

C=C is another bond for verifying the transformation from monomer to polymer. It appears at 1640 cm⁻¹ in nMAG dose gels (Fig. 78). As the polymerization proceeds, it gradually changes to a single bond, therefore causing a weakening of the band intensity [123].

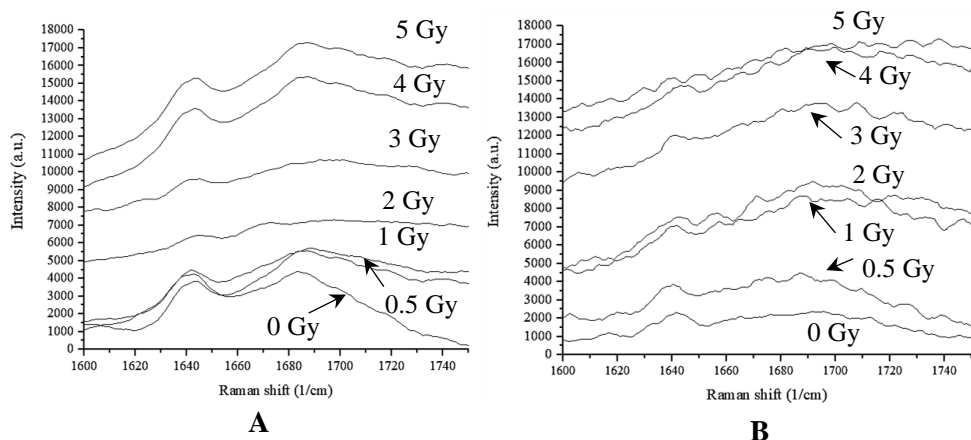


Fig. 78. A) Raman spectra fragments with indicated specific peaks of reference and B) advanced nMAG dose gels in the range of 1600 1/–1750 1/cm

The main problem when evaluating C=C Raman peak is caused by the presence of gelatin and its constituents in dose gels that record a broad Raman peak, which may overlap with the C=C peak. This problem was not acute during the performed investigation, since the Raman peak at 1642 cm^{-1} was found in all the analyzed nMAG gels that were irradiated to different doses. The peak at 1642 cm^{-1} was less intense for gels with higher concentration of methacrylic acid. It was decreasing smoothly with the increasing radiation dose, indicating effective consumption of monomer. In contrary, well-pronounced and relatively intense peak at 1642 cm^{-1} was observed in the reference gel samples. However, the decrease in the amount of methacrylic acid was not a well-expressed tendency. According to the intensity variations of the Raman peak 1642 cm^{-1} , the monomer consumption was faster up to 3 Gy, and then it was slowed down. Further smooth decrease of the monomer amount could be achieved at the higher irradiation doses than 5 Gy. According to the other authors [117], in the case of low (0.1–0.5 Gy/min) and modest (1–3 Gy/min) dose rate irradiation, the termination of polymerization, leading to increased amount of monomer, is possible as well [117, 124].

The spectral information regarding the photon induced polymerization behavior of methacrylic acid was as well obtained by analyzing a band appearing at 2940 cm^{-1} , which is assigned to symmetric vinyl stretching mode $\nu(\text{CH}_2)_s$. This vibrational mode is the only one, which does not overlap with other bands according to literature, therefore providing “true” information about the polymerization process [125, 126]. Gradual decrease of Raman peak at 2940 cm^{-1} was observed in both advanced and reference dose gels (Fig. 79).

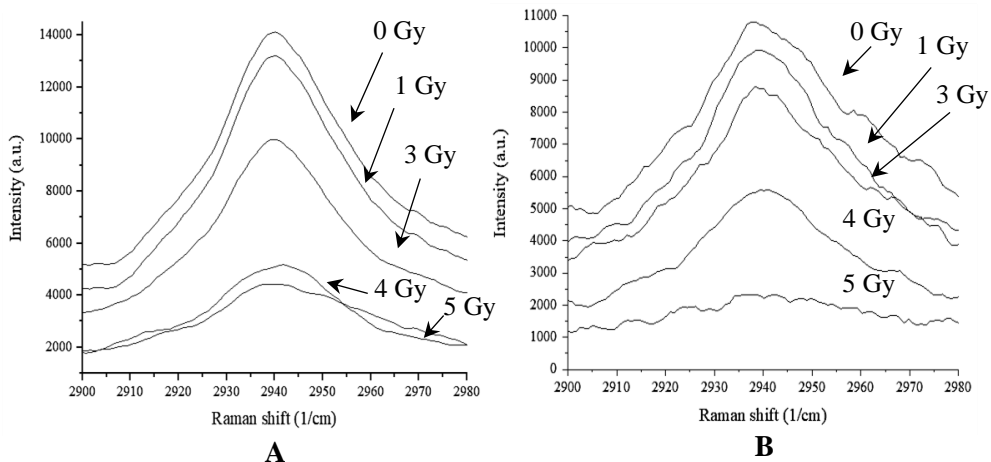


Fig. 79. Raman spectra fragments with indicated specific peaks of reference (A) and advanced (B) nMAG dose gels in the range of 2900 1/–2980 1/cm.

Other researchers [117] have as well divided the irradiated gel Raman spectra to a few segments to analyze peaks in a closer view, because some peaks are overlapping. Broad peaks that are representing specific 1450 cm^{-1} CH_2 and 2936 cm^{-1} CH_2 stretching mode, which are responsible for polymerization, are presented in Fig. 80.

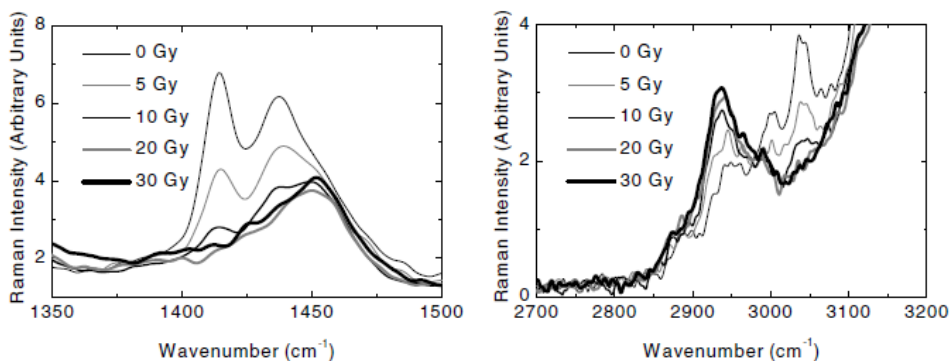


Fig. 80. Segmented Raman spectra of polyacrylamide dose gel [118]

It was concluded that peaks 1450 cm^{-1} and 2936 cm^{-1} , which are representing polymer formation in methacrylic acid based gels, are increasing due to the increasing absorbed dose up to 30 Gy. The Raman spectra profiles were similar to this research, and the same tendency of peaks broadening were reported.

The analysis of Raman peak intensity at 2940 cm^{-1} has shown that its decrease in advanced dose gel samples was smooth over the whole dose range (Fig 81).

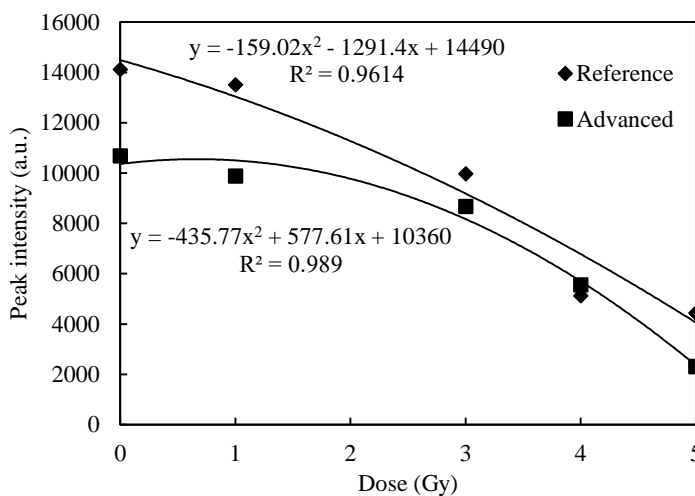


Fig. 81. Analysis of Raman peak intensity at 2940 cm^{-1}

A faster peak intensity decrease that is corresponding to faster consumption of monomer was observed in reference gels up to 4 Gy. At higher irradiation doses, the intensity variation tendency became very modest. The obtained results supported the obtained findings that are regarding possible recreation of methacrylic acid during the irradiation to higher doses due to the possible termination of polymerization. The monomer consumption and polymer formation tendency due to the irradiated dose is reported by the other authors and presented in Fig. 82 [71].

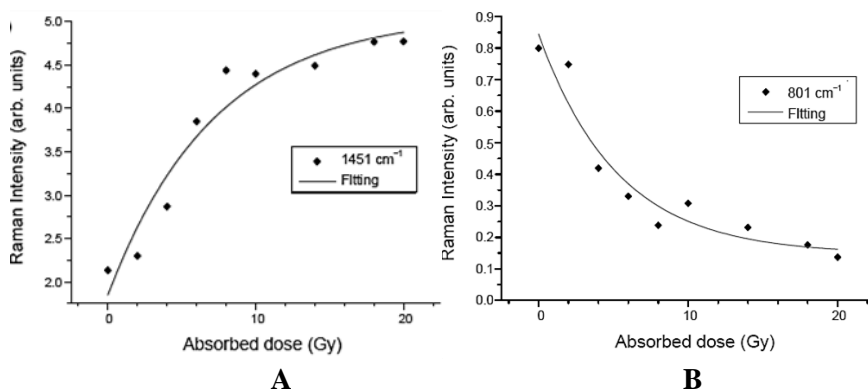


Fig. 82. Trend of variation A) 1451 cm^{-1} , B) 801 cm^{-1} [71]

It could be seen that at higher irradiation doses, the polymer formation representing Raman peak increases and reaches the plateau for dose near 20 Gy. Moreover, the peak representing monomer consumption decreases steady, until it reaches slowing down point near 18 Gy. It was reported that the increase and decrease

speed is faster up to 10 Gy [72]. The same tendency was found in this investigation (Fig. 77 and 81)

Summarizing the Raman spectroscopy analysis results, it is important to mention that the new composition (advanced) nMAG gel was characterized by more homogeneous structural changes when reference gel up to 5 Gy dose. Faster consumption of methacrylic acid up to 4 Gy, but steady polymer formation at 0-5 Gy dose range show that spatial resolution and stability of advanced gel are satisfying to measure low doses.

4.2 Application of photo-scanning method for the evaluation of spatial distribution of polymerized derivatives in the irradiated gels

The investigation of spatial distribution of polymerized derivatives in photon irradiated advanced nMAG dose gels and the analysis of the polymerization expansion to the neighboring space around the irradiated volume are presented in the following section.

The research steps that were carried out to evaluate the spatial distribution of polymerized derivatives in the irradiated gels are as follows:

1. Preparation of nMAG gel varying components' concentrations;
2. Irradiation of advanced nMAG gels by 15 MeV photons to low doses from interval 0–5 Gy;
3. Analysis of irradiated advanced nMAG gels by using developed photo scanning-method;
4. Investigation of spatial distribution of polymerized derivatives in the irradiated advanced nMAG gels;
5. Defining limits for the spatial resolution of the photo-scanner.

Advanced nMAG dose gel samples that are containing 8 % w/w of methacrylic acid, 15 mM of (hydroxymethyl) phosphonium chloride, 6 % w/w of gelatin, and 86 % w/w of purified water and irradiated by 15 MeV photons to doses up to 5 Gy were investigated. The developed photo scanning method was used for the assessment of spatial distribution of polymerized derivatives in gel and the evaluation of the polymerization expansion out of the irradiated area due to the diffusion of radiation produced reactive radicals in the water.

Three irradiation scenarios were applied: 1) irradiation of a well-defined, 1 cm long part of the gel volume to doses up to 5 Gy and leaving the rest of the volume irradiation free; 2) dividing the gel volume in two well-defined parts and irradiating one part of the gel to one selected dose and another part of the gel to different doses up to 5 Gy; 3) irradiation of well-defined (0.5 cm long) part in the middle of the gel sample to 4 Gy and 5 Gy doses. The first scenario was applied to find out whether polymerization expands to non-irradiated gel volume and how this expansion depends

on the radiation dose. The second scenario was applied to identify the boundary shift between two irradiated parts of the sample and find out the interception of different doses. The third scenario was used to find out the polymerization propagation to non-irradiated volume when there is no container wall limitation. The polymerization propagation to non-irradiated site and possible shift of the polymerization boundary to gel volume that is irradiated by lower dose are the essential characteristics in the case when polymerized gel is used as a radiation detector.

4.2.1 Scenario no. 1: Partially irradiated dose gel volume

Implementing this scenario, 1 cm thick part of dose gel volume inside the cuvette was irradiated to doses from 0.5 to 5 Gy, and another part of the gel was left non-irradiated. The sharp irradiation geometry, the boundary between irradiated and non-irradiated area, was achieved by adjusting parameters of a medical linear accelerator as it is shown in Fig. 83.

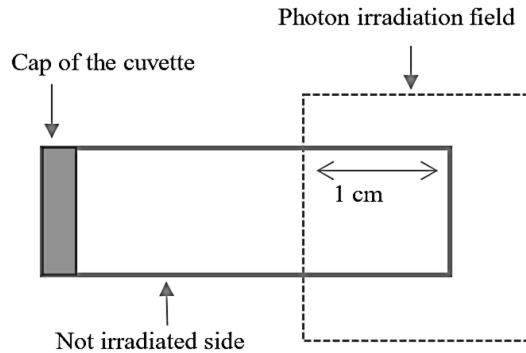


Fig. 83. Irradiation geometry of the advanced nMAG dose gel samples (scenario no.1)

The photograph of some advanced nMAG dose gel samples after the irradiation to doses up to 5 Gy are provided in Fig. 84. As it was discussed in the previous section (3.1), the radiation-induced polymerization causes changes in the optical density of the irradiated gels. The provided photograph indicates that the main radiation-induced changes are present in the region up to 1 cm from the bottom of cuvette; however, some expansion of the polymerized area with less intensity is clearly seen.

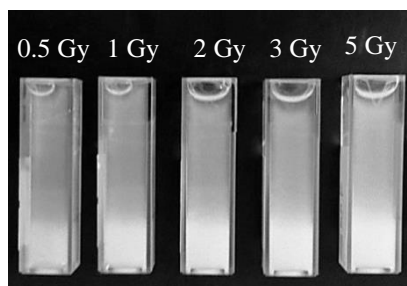


Fig. 84. Some advanced nMAG dose gel samples after the irradiation to different doses

The sample was scanned along the longitudinal axis, and the dose response profiles of the irradiated cuvettes that were filled with advanced nMAG dose gels are shown in Fig. 85. The irradiated zone is marked by dashed lines. Scanning was performed in 0.20 mm step.

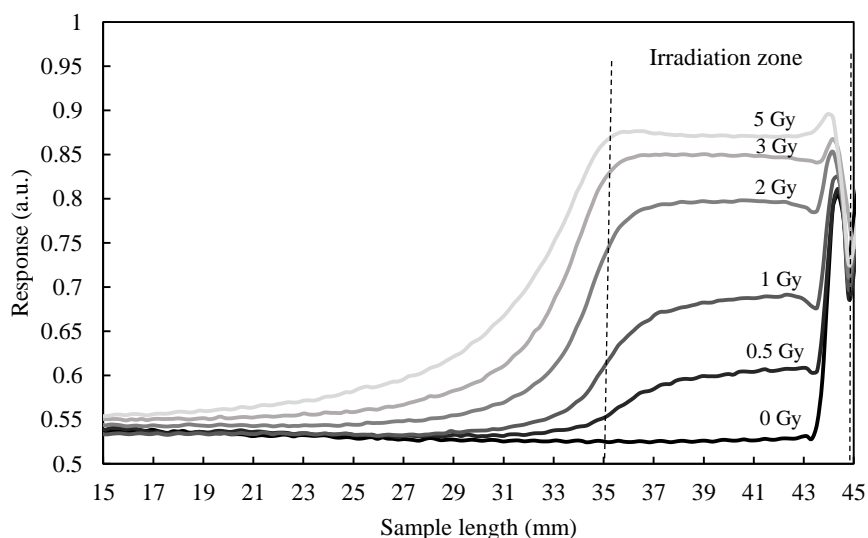


Fig. 85. Scanned dose response profiles of the advanced nMAG dose gels that are irradiated according to scenario no. 1 with indicated 1 cm thick irradiation zone

The scanned dose response profiles clearly indicated the absence of a sharp edge between the irradiated and non-irradiated zones. This confirms non-uniform distribution of the polymerized derivatives that are close to the boundary in the irradiated area due to the diffusion of the created reactive radicals from the irradiated zone towards the zone without irradiation. The profile near the boundary between two zones becomes steeper with the increased absorbed dose, and the distribution of the polymerized derivatives becomes more uniform in the whole irradiated area, because higher doses are responsible for the formation of well-developed polymer network structure. The penumbra that appears due to the curve slopes of different doses was

calculated. A quantitative measure of the penumbra, ΔP , can be defined as the distance over which the dose increases from 10 to 90 % of its maximum value [60]. The penumbra appears due to the polymerization propagation towards the non-irradiated gel volume. The evaluated ΔP values were as follows: 5 Gy — 6 mm, 3 Gy — 5 mm, 2 Gy — 4 mm, 1 Gy — 3 mm, 0.5 Gy — 2 mm. The non-linear but monotonic tendency of increasing penumbra due to the increased irradiation dose is presented in Fig. 86. It could be assumed that for the higher doses (>5 Gy), the penumbra may reach the saturation level, which means that the penetration of polymerized derivatives into the non-irradiated area is finite.

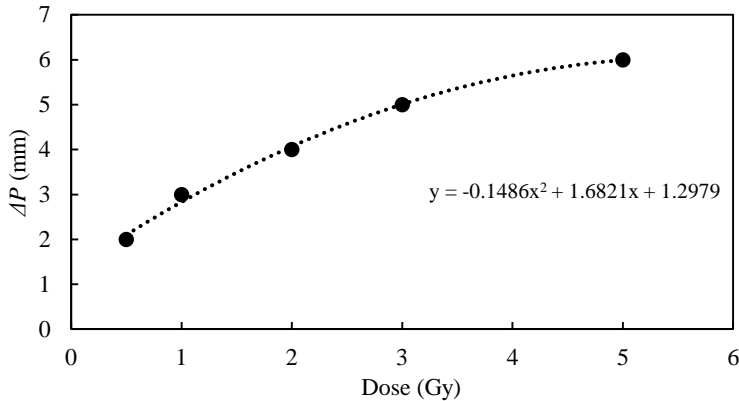


Fig. 86. The increase of penumbra due to the irradiation dose

The measured profiles of the irradiated samples were in a good agreement with the results of the other researchers who had reported penumbra variations from 2.2 mm to 4.6 mm when small amounts of oxygen scavenger (0.05 mM HQ) were mixed into the methacrylic acid based gel [59]. Their irradiation geometry together with the obtained results are presented in Fig. 87.

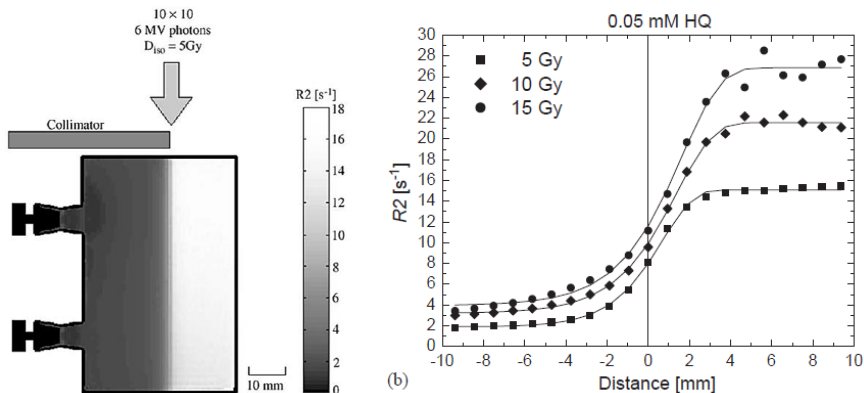


Fig. 87. The irradiation scheme of container that is filled with gel (left) presented the profile of scanner gel that is irradiated by 5, 10, 15 Gy doses [59]

In the presented study, the collimator similar to the built-in medical linear accelerator was used to form sharp irradiation geometry. Low doses in the range from 5 to 15 Gy were applied.

4.2.2 Scenario no. 2: Two differently irradiated parts of dose gel volume

In order to evaluate the “overlapping” of polymerizations in the boundary region between two zones that are irradiated to different doses, another batch of advanced nMAG gel dose samples was fabricated. The procedure is described in Instruments and Methods section. The concentrations of gel components were the same as in section (3.2.1): 8 w/w% of methacrylic acid, 6 w/w% of gelatin, 15 mM of tetrakis (hydroxymethyl) phosphonium chloride, and 86 w/w% of pure water. Fabricated samples were irradiated in linear accelerator by adjusting its parameters to the geometry that is shown in Fig. 88. Gel-filled cuvette was divided in two parts: the A part of the cuvette was dedicated for the irradiation to doses from 0.5 to 5 Gy; the B part of the cuvette was dedicated for the irradiation of all samples to the constant 2 Gy dose.

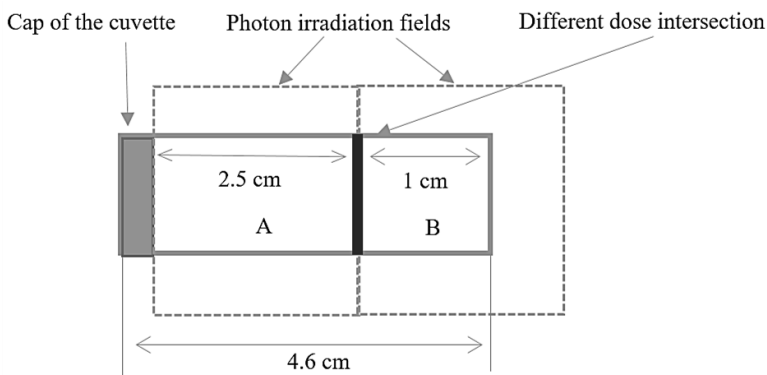


Fig. 88. Irradiation geometry of the advanced nMAG dose gel samples (scenario no. 2)

First, the corresponding zone of each sample was irradiated to 2 Gy and then immediately after the first irradiation, to doses from 0.5 to 5 Gy. A photograph of irradiated advanced nMAG doses is shown in Fig. 89. It is visually seen that the bottom part of the cuvette was irradiated to various doses and the upper part to the same dose in all the samples.

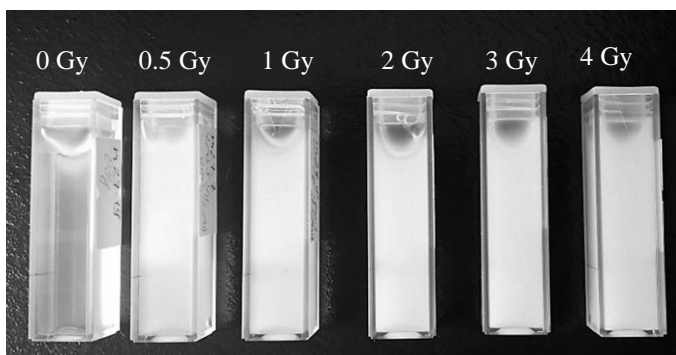


Fig. 89. Photograph of some advanced nMAG dose gel samples after the irradiation, according to scenario no. 2

The irradiated advanced nMAG gel samples were scanned by using photo scanning method along the longitudinal axis. The scanning step of 0.20 mm was applied. The scanned dose response profiles of advanced nMAG dose gel samples are provided in Fig. 90.

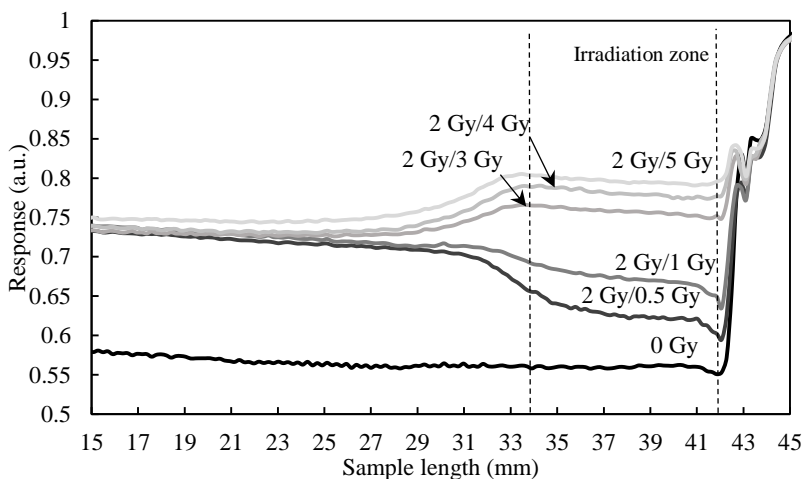


Fig. 90. Scanned dose response profiles of the advanced nMAG dose gels that are irradiated according to scenario no. 2 with indicated 1 cm thick irradiation zone

The scanned dose response profiles indicated the presence of transition zone close to the boundary between differently irradiated parts of the cuvette. The width of this zone depends on the irradiation doses; the polymerization expansion up to 3.2 mm was estimated for samples part, which was irradiated to 0.5 Gy and 1 Gy doses. Moreover, the increase of the spread was observed up to 4.1 mm close to the boundary between two zones for samples part, which was irradiated to higher (3 Gy, 4 Gy, 5 Gy) doses as compared to the standard 2 Gy dose. This might be explained by two-way diffusion of free radicals in gel from one cuvette part to another, depending on

the irradiation doses. Taking into account that the irradiation of gel in both cuvette parts was not performed simultaneously, the radiation-induced diffusion of free radicals to non-irradiated part started immediately (in a time period of 10^{-15} s to 10^{-14} s) after the first irradiation. After 10^{-11} s, a local thermal equilibrium in the recombination of reactive particles may be reached. Taking into account that the average diffusion coefficient of the reactive particles in water is $4 \times 10^{-9} \text{ m}^2 \text{ s}^{-1}$; then, it is probable that after 10^{-11} s, the root mean square displacement of the particles from the point of creation is 0.28 nm [1]. It is only one tenth of the intermolecular distance of the methacrylic acid monomer.

When the irradiation doses to both cuvette parts were the same (2 Gy and 2 Gy), an insignificant (0.20 mm) increase just behind the boundary was observed. Additional number of diffused free radicals contributed to the faster polymerization saturation in higher dose part and was responsible for the formation of a polymerization transfer zone backwards to the 2 Gy zone. The measured response, which was estimated along the longitudinal axis of 2 Gy irradiated sample part (from 15 mm to 25 mm), is varying insignificantly from 0.12 to 0.18 a.u. It shows that only 2 Gy irradiation contributes to the response, and there may be no diffused radical from 0.5 Gy, 1 Gy, 3 Gy, 4 Gy, and 5 Gy irradiation in this gel volume.

4.2.3 Scenario no. 3: Irradiated dose gel volume with no boundary restrictions

In order to find out the complete polymerization propagation profile to non-irradiated volume, the gels were irradiated to 4 and 5 Gy doses in the middle of the sample. These doses were chosen for the visualization of polymerization penumbras, which was first studied in 4.2.1 section. The zone of 0.5 cm length was chosen in the middle of measurements' window of the cuvette (Fig. 91). The expansion of polymerized zone was clearly seen in each irradiated sample.

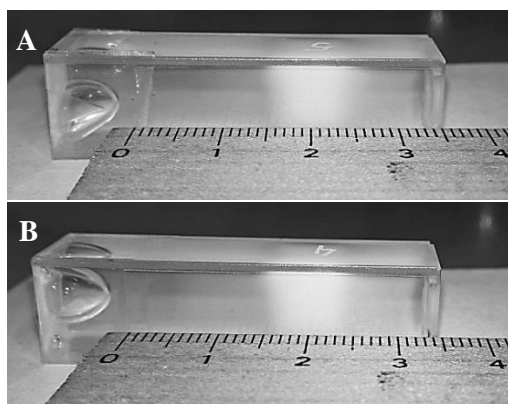


Fig. 91. A) 5 Gy, B) 4 Gy irradiated gel samples with no polymerization spread restrictions along the cuvette

The cuvettes were scanned by using a constructed scanner along the longitudinal axis, and the dose response profiles were established for the evaluation of polymerization propagation penumbra ΔP . The measured profiles (Fig. 92) had the same shape, but ΔP for 4 Gy and 5 Gy irradiated samples were different.

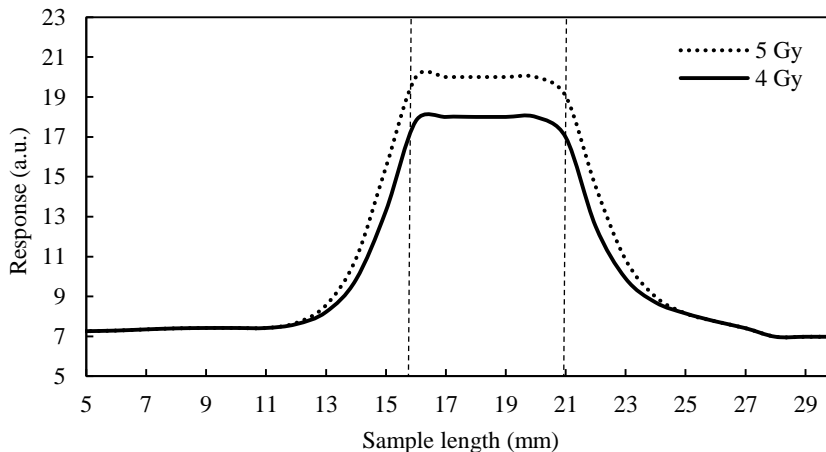


Fig. 92. The polymerization spread profiles of 5 and 4 Gy doses

The performed calculations revealed that ΔP was equal to 2 mm for 4 Gy dose and 5 mm for 5 Gy dose. Equal ΔP to both sides from the polymerized zone identified that the polymerization defuses equally to both non-irradiated sides of gel if there are no restrictions within cuvette. At the sample length zones from 5 mm to 11 mm and 28 mm to 30 mm, no significant increase was observed in response, which is showing polymerization propagation (“dark polymerization” when no additional radiation dose is applied) to non-irradiated samples’ side.

In order to explain the polymerization spread to non-irradiated gel volume, the model that is clarifying polymer molecules’ migration is presented. The model was suggested by the authors [27] and indicates that the expansion of polymerized derivatives to non-irradiated volume could be explained by using spur propagation theory. The polymerization propagation kinetic model of the polymer molecules is defined as a localized microscopic area. As it was mentioned before, the radiolytic products appear in clusters that are called “spurs”. They are produced along the path of an incident of ionizing irradiation and ejected secondary electron (Fig. 93) [28].

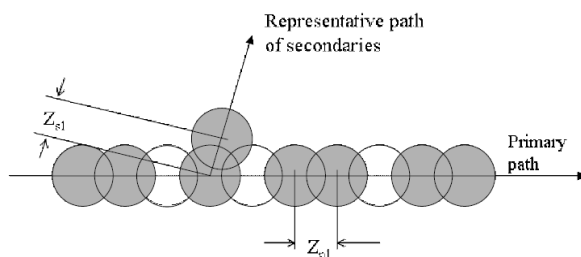


Fig. 93. “Spurs” along the incident path and the representative secondary path. Z_{p1} and Z_{s1} are the average distances between the spurs

The propagation of the “spurs” into a medium is presented simplified as a spread of the elementary wave. In this model, it was assumed that initial “spur” has constant size and the same number of radical. The radical inside the “spur” reacts only with neighbor “spur” when both spreading “spurs” interact with each other. The interaction model is shown in Fig. 94.

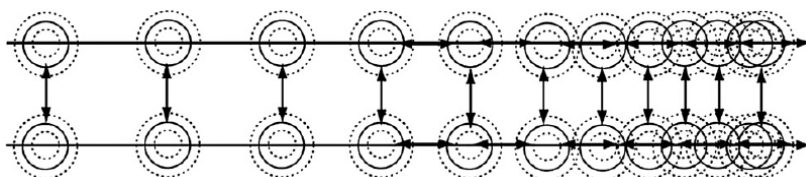


Fig. 94. The “spur” interaction model [28]

There (Fig. 94), the long horizontal arrows show the path of ionizing particle or wave; small arrows show the interaction between “spurs”; spheres are representing constant size “spurs”. The yields of radical depend on the localized energy loss in the interaction area of ionizing irradiation. When the energy is consumed, the interactions of radicals increase; therefore, the distance between the “spurs” decreases. Such a behavior of radicals affects the yield of polymerization and the propagation of produced polymers [27]. When the radiation dose is higher, the higher amounts of “spurs” are formed in the same volume. This effect leads to denser polymerized volume.

To sum up the experimental results of the polymerization spread to non-irradiated gel volume, it is important to mention that when there is no polymerization spread restrictions, the polymerization propagation is symmetric, ΔP is similar in geometry. Penumbra is increasing from 2 to 6 mm when 0.5–5 Gy doses are applied monotonically and saturates at >5 Gy. The polymerization expansion at the different dose boundary between two zones was from 3.2 mm (0.5 Gy, 1Gy) to 4.1 mm for samples part, which was irradiated to 3 Gy, 4 Gy, 5 Gy doses. This feature proves that the polymerization in nMAG gel is symmetric; the boundaries and intersection could

be detected by photo-scanning method in good accuracy, and dose gel could be used as a radiation dosimeter.

4.3 Evaluation of polymeric nanocomposites as filler materials for transparent radiation protection screens

The exploration of the radiation absorption feature of radiation-sensitive polymeric composites may lead to several applications: radiation-sensitive materials for dose measurements that are used in 3D dosimetry and radiation-sensitive materials for radiation attenuation that are used in shielding equipment for radiation protection purposes. The difference between two applications is related to the fact that in the dosimetry case, the alteration of the characteristics due to the radiation-induced polymerization of compounds is used. In the radiation attenuation case, the focus is on the development of nanocomposite by using the already existing polymer. The results of the development of advanced dose gels with enhanced sensitivity to photon irradiation are provided and discussed in the chapters 3.1 and 3.3 of this dissertation. In this chapter, the results on the development of polymer-based composites that are possessing corresponding sensitivity to attenuate X-rays are presented. The aim of this investigation was to develop, investigate, and verify lead-free, transparent polymer based nanocomposites that are meeting radiation protection requirements and might be used as the filling for the radiation protection screens.

4.3.1 Differently composed polymeric $(\text{NH}_4)_6\text{H}_2\text{W}_{12}\text{O}_{40}\text{xH}_2\text{O}$ composites

As it was already stated, a new generation of radiation protection equipment is based on lead-free materials. Polymer based materials that contain nanostructures (particles, precipitates, etc.) and are possessing required radiation attenuation properties have the advantage of their relatively simple fabrication. Polymer based transparent and solid compounds for the fabrication of radiation protection screens in medical environment are in high demand.

Before starting differently composed ammonium metha-tungstate polymeric composites $((\text{NH}_4)_6\text{H}_2\text{W}_{12}\text{O}_{40}\text{xH}_2\text{O})$ investigations in depth, the radiation protection was tested by estimating the lead equivalent. Polymeric composites were produced by using gelatin, polyacrylamide, and methyl carboxy cellulose to compose a thicker composition. The lead equivalent measurement results are presented in Table 11. The evaluation of polymeric nanocomposites was done in a frame of the project “Optically transparent nanocomposites for radiation protection screens”, MIP- 091/12 (Final report, 2014).

Table 11. Lead equivalent of $(\text{NH}_4)_6\text{H}_2\text{W}_{12}\text{O}_{40}\text{xH}_2\text{O}$ containing polymeric composites that are produced by using different thickeners

Experimental composite	Sample thickness (mm)	Lead equivalent (mmPb)		Sample image
		Before the irradiation	After the irradiation to 10 Gy	
65.9 % $(\text{NH}_4)_6\text{H}_2\text{W}_{12}\text{O}_{40}\text{xH}_2\text{O}$ +32.9 % H_2O +1.2 % (methyl carboxy cellulose)	10	0.42	0.40	
40 % $(\text{NH}_4)_6\text{H}_2\text{W}_{12}\text{O}_{40}\text{xH}_2\text{O}$ +58.8 % H_2O +1.2 % $(\text{C}_3\text{H}_5\text{NO})_n$ (polyacrylamide)	10	0.36	0.26 (irradiated to 50 Gy)	
50 % $(\text{NH}_4)_6\text{H}_2\text{W}_{12}\text{O}_{40}\text{xH}_2\text{O}$ +1 % $(\text{C}_3\text{H}_5\text{NO})_n$ (polyacrylamide) +49 % H_2O	10	0.49	0.39	
50 % $(\text{NH}_4)_6\text{H}_2\text{W}_{12}\text{O}_{40}\text{xH}_2\text{O}$ +4.75 % gelatin +45.25 % H_2O	10	0.49	0.49	

The visual inspection of samples as well as the performed UV-VIS scanning lead to the conclusion that composites that are containing gelatin and methyl carboxy cellulose were not transparent enough to be used in the radiation protection screens. On the contrary, highly viscose solid composites that are produced by using polyacrylamide as a thickener were announced as a promising candidate materials for the radiation protection.

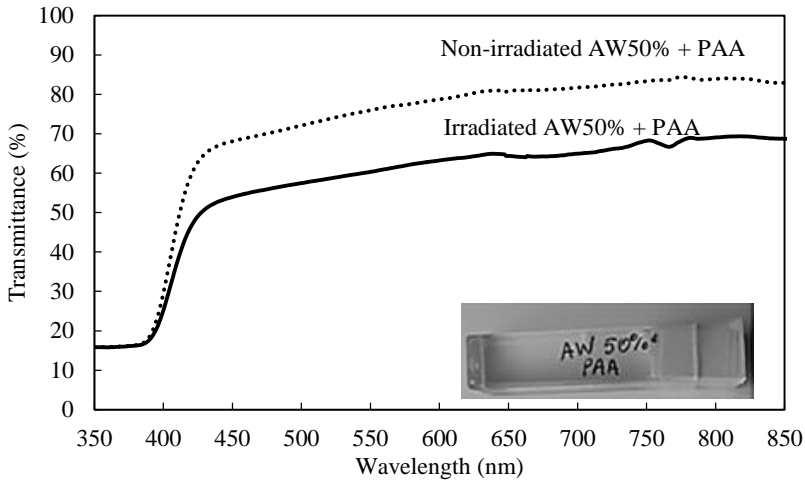


Fig. 95. Comparison of optical transparency spectra of composites that are containing polyacrylamide before and after the irradiation

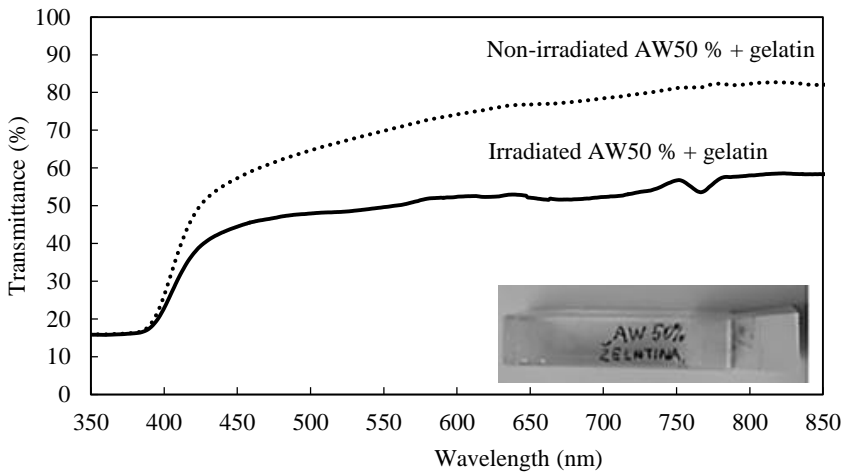


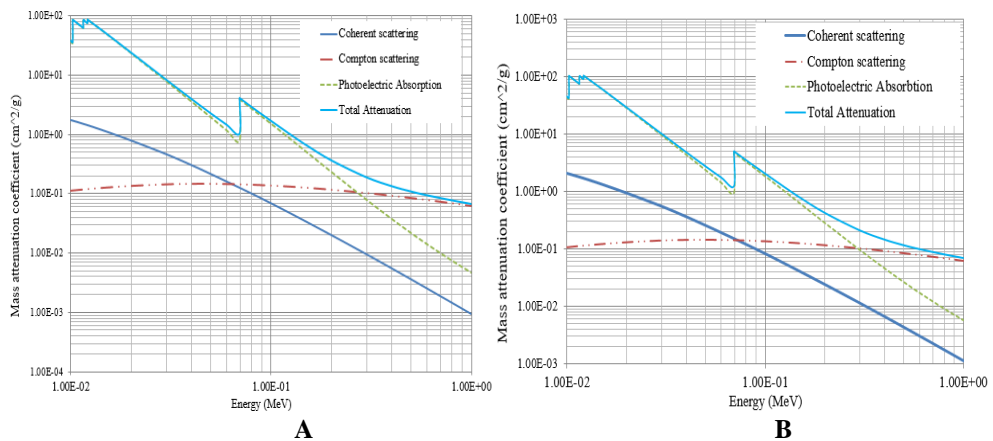
Fig. 96. Comparison of optical transparency spectra of composites that are containing gelatin before and after the irradiation

As it can be seen in Fig. 94 and Fig. 95, the 50 % $(\text{NH}_4)_6\text{H}_2\text{W}_{12}\text{O}_{40}\cdot x\text{H}_2\text{O} + 1\%$ $(\text{C}_3\text{H}_5\text{NO})_n$ (PAA) +49 % H_2O composite has reduced its transmittance by 15 % after 10 Gy photon irradiation. While composite made of 50 % $(\text{NH}_4)_6\text{H}_2\text{W}_{12}\text{O}_{40}\cdot x\text{H}_2\text{O} + 4.75\%$ (gelatin) +45.25 % H_2O reduced its transmittance by 24 %. The experiment proved that polyacrylamide as a thickener is most suitable for the composition of transparent radiation protection screen.

4.3.2 Polymeric composites containing different concentrations of $(\text{NH}_4)_6\text{H}_2\text{W}_{12}\text{O}_{40}\text{xH}_2\text{O}$

The analysis of composite formation features, stability, and state of fabricated polymeric composites, intrinsic properties of composites that are characteristic of radiation shielding materials, and changes of these properties due to the irradiation revealed that polymer composite (AMWO-PX), containing ammonium methatungstate and polyacrylamide, were most suitable to be used as a filler material for the radiation protection screens.

In order to optimize radiation-shielding properties of AMWO-PX nanocomposites, various concentrations of $(\text{NH}_4)_6\text{H}_2\text{W}_{12}\text{O}_{40}\text{xH}_2\text{O}$ were used as an input data for the simulation of radiation attenuation processes in the irradiated composites by using XCOM database [127]. Mass attenuation coefficient (μ/ρ) versus photon energy is presented in the following graphs. The modelling results for some composites and lead are shown in Fig. 97. The comparison of total attenuating properties for AMWO-PX compositions and lead are provided in Fig. 98. There, the main processes such as coherent scattering, Compton scattering, photoelectric absorption, and total attenuation were presented.



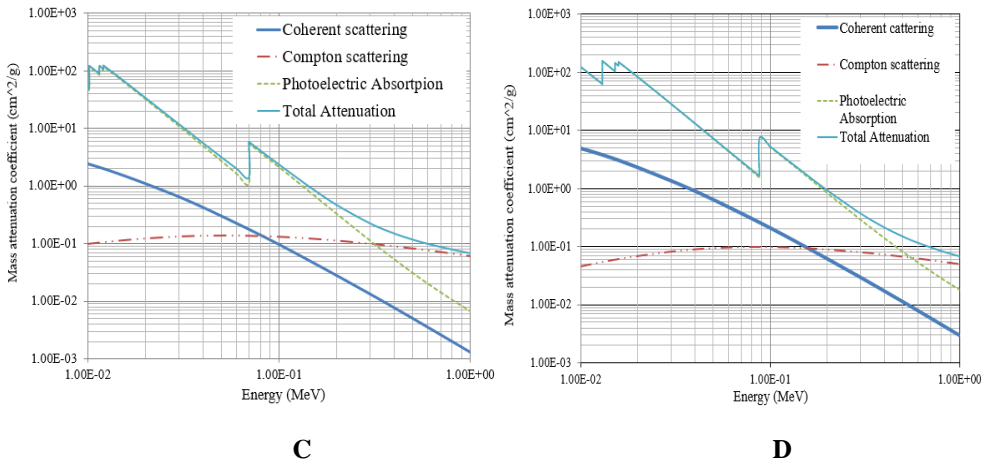


Fig. 97. X-ray attenuation properties in AMWO -PX composites that contain various concentrations of $(\text{NH}_4)_6\text{H}_2\text{W}_{12}\text{O}_{40} \times \text{H}_2\text{O}$: coherent scattering, photo effect, Compton scattering, and total attenuation. A) AMWO-P50, B) AMWO-P60, C) AMWO-P70, D) Lead

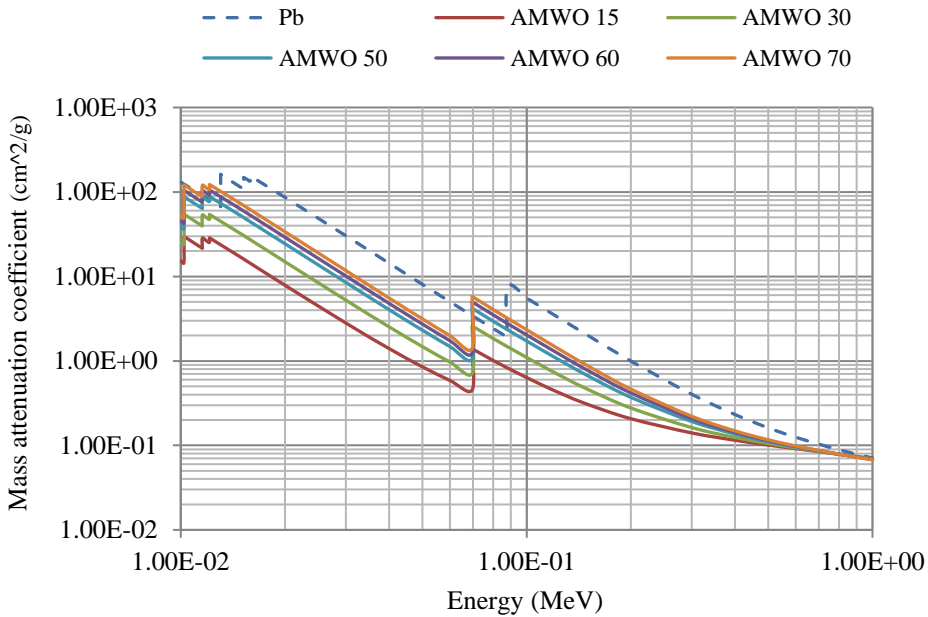


Fig. 98. The comparison of various AMWO polymer gel composites' attenuation parameters

The modelling results revealed that X-ray attenuation in the whole range of investigated energies for MWO-PX composites were lower, but curve profile was very similar to those obtained for lead. Additionally, more detailed analysis of absorption edges of the investigated composites (Fig. 98) has shown that within a small energy range of 70–88 keV, the attenuation properties of composites AMWO-

P50, AMWO-P60, and AMWO-P70 were even better than in the lead, which has a characteristic K_{α} absorption edge at $E=69.5$ keV.

Based on the simulation results, the series of the experimental AMWO-PX composite samples with different $(\text{NH}_4)_6\text{H}_2\text{W}_{12}\text{O}_{40}\cdot x\text{H}_2\text{O}$ concentrations were composed, irradiated to 150 keV X-ray photons, and analyzed experimentally. The comparison of lead equivalent that is estimated by simulation and performed experimental measurements are provided in Table 12.

The compositions of AMWO-PX composites are patent protected (LT patent No. 6292) [128]. No significant difference between the lead equivalents in irradiated and non-irradiated samples were found, indicating that the radiation attenuation properties of AMWO-PX, containing $\geq 50\%$ of $(\text{NH}_4)_6\text{H}_2\text{W}_{12}\text{O}_{40}\cdot x\text{H}_2\text{O}$, were most effective from all the investigated samples.

Table 12. Attenuating properties of AMWO-PX composites

Experimental composites	Density (g/cm^3)	Linear attenuation coefficient (cm^{-1})	Optical transmittance (%)	Lead equivalent (mmPb)		
				XCOM	Before the irradiation	After the irradiation to 10 Gy, 150 KeV
<u>AMWO-P15:</u> 1 % PAA +15 % $(\text{NH}_4)_6\text{H}_2\text{W}_{12}\text{O}_{40}$ +84 % H_2O	1.189	0.52	90	0.13	0.17	0.15
AMWO-P30 1 % PAA +30 % $(\text{NH}_4)_6\text{H}_2\text{W}_{12}\text{O}_{40}$ +69 % H_2O	1.390	1.00	90	0.26	0.30	0.28
<u>AMWO-P50</u> 1 % PAA +50 % $(\text{NH}_4)_6\text{H}_2\text{W}_{12}\text{O}_{40}$ +49 % H_2O	1.849	2.19	89	0.56	0.57	0.57
AMWO-P60 1 % PAA +60 % $(\text{NH}_4)_6\text{H}_2\text{W}_{12}\text{O}_{40}$ +39 % H_2O	2.046	2.47	89	0.63	0.62	0.61
AMWO-P70 1 % PAA +70 % $(\text{NH}_4)_6\text{H}_2\text{W}_{12}\text{O}_{40}$ +29 % H_2O	2.475	3.63	86	0.75	0.72	0.71

Taking into account that for 10 mm thick AMWO-P15 and AMWO-P30 samples (cuvette with composite filling), the estimated lead equivalent did not meet

the requirement (>0.5 mmPb), and optical transparency of AMWO-P70 was relatively low, some additional experiments were performed with samples AMWO-P50 and AMWO-P60. The lead equivalent of 0.61 mmPb has not changed as compared with the lead equivalent of non-irradiated sample.

Moreover, the optical transmittance spectra of cuvettes filled up with AMWO-PX composites were investigated before and after 10 Gy dose irradiation. It was found that all the investigated spectra were characterized by spectral Plato in the visible light region and were more transparent in AMWO-PX composites, containing smaller (15 % and 30 %) concentrations of ammonium tungstate (Table 12). The optical transparency of AMWO-P50 and AMWO-P60 samples before the irradiation were similar, but after the irradiation to 10 Gy and especially to 50 Gy, the transparency of AMWO-P50 has reduced from 91 % to 89 %. The lead equivalent of AMWO-P60 after 10 Gy dose irradiation remained almost the same and reduced only from 0.62 mmPb to 0.61 mmPb. This sample was tested by additionally applying thermos-test: sample was cooled at the refrigeration to -25 °C for 12 hours and then uniformly heated up to $+25$ °C for 12 hours. The same cycle was repeated 7 times to check composite's thermal stability; the UV-VIS transmittance spectra were measured before thermos-test and after. The results showed that the transmittance to visible light was reduced by 2 %.

Based on the performed research, 60 % of ammonium methatungstate, containing hybrid organic-nonorganic polymeric composite, was selected as a filler material for the radiation protection screens. The prototype of the radiation protection screen that is filled with AMWO-P60 composite was tested in the medical environment and approved for further commercialization of the product.

5. CONCLUSIONS

1. The analysis of the optical characteristics of dose gels that are irradiated to low doses (<10 Gy) has shown that the sensitivity of gels was directly dependent on the type of irradiation that is responsible for the gel's polymerization and chemical content of gels. It was found that the standard nMAG gel was most sensitive to all types of irradiation as compared to nPAG and VIPET gels. The sensitivity parameter of nMAG gel to 15 MeV X-rays was 0.068 (a.u.), to gamma photons (^{60}Co source) — 0.099 (a.u.), to electrons — 0.11 (a.u.), to protons — 0.22 (a.u.).
2. By varying concentrations of the nMAG gel components, the dose gel of advanced composition was developed, which recorded the enhanced by 30 % sensitivity to high-energy photons. The composition of the advanced nMAG gel was as follows: 8 % w/w of methacrylic acid as a monomer, 6 % w/w of gelatin, 86 % w/w of purified water, and 15 mM of hydroxymethyl phosphonium chloride, as an oxygen scavenger.
3. A new photo scanning dosimetry instrumentation for dose evaluation in the irradiated gels was developed, constructed, and implemented for the experimental measurements. The constructed system allowed the scanning of irradiated polymer gel samples with a spatial resolution of 0.20 mm.
4. It was shown that the polymerization spread out in the irradiated dose gels was dependent on the proliferation of the radiation produced reactive radicals within the gel. The polymerization spread out was smooth and varied from 2 mm (0.5 Gy) to 6 mm (5 Gy) away from the irradiated volume.
5. The development and investigation of different lead-free polymeric composites, recording X-ray attenuation properties that are similar to those of lead, revealed that most promising composites contained water, 1 % $(\text{C}_3\text{H}_5\text{NO})_n$ (polyacrylamide), and different concentrations of $(\text{NH}_4)_6\text{H}_2\text{W}_{12}\text{O}_{40}\cdot x\text{H}_2\text{O}$. It was shown that $(\text{NH}_4)_6\text{H}_2\text{W}_{12}\text{O}_{40}\cdot x\text{H}_2\text{O}$ concentration of 60 % in the composite was sufficient enough for its application in the radiation protection equipment, since the estimated lead equivalent of the composite was 0.63 mmPb, and UV-VIS transparency was 89 %.

LIST OF REFERENCES

1. BALDOCK, C. Polymer gel dosimetry. *Physics in Medicine and Biology*. 2010, 55, R1–R63. doi: 10.1088/0031-9155/55/5/R01.
2. MCAULEY, K. Fundamentals of polymer gel dosimeters. *Journal of Physics: Conference Series*. 2006, 56, 35–44. doi: 10.1088/1742-6596/56/1/004.
3. GUSTAVSSON, H., et al. Linear energy transfer dependence of a normoxic polymer gel dosimeter investigated using proton beam absorbed dose measurements. *Physics in Medicine and Biology*. 2004, 49, 3847–3855.
4. YAO, T. and L.H. LUTHJENS. A study of four radiochromic films currently used for (2D) radiation dosimetry. *Radiation Physics and Chemistry*. 2017, 133, 37–44.
5. MARINI, A., et al. Fricke gel dosimeters with low-diffusion and high-sensitivity based on a chemically cross-linked PVA matrix. *Radiation Measurements*. 2017, 106, 618–621. doi: 10.1016/j.radmeas.2017.02.012.
6. ANDREWS, H.L., et al. Gel dosimeter for depth dose measurements. *Review of Scientific Instruments*. 1957, 28, 329–332. [accessed on 2017-03-25]. Available from: <https://doi.org/10.1063/1.1715877>.
7. GORE, J.C., et al. Measurement of radiation dose distributions by nuclear magnetic resonance (NMR) imaging. *Physics in Medicine and Biology*. 1984, 29, 1189–1197. [accessed on 2017-04-07]. Available from: <https://www.ncbi.nlm.nih.gov/pubmed/6494247>.
8. ALEXANDER, P., et al. The degradation of solid polymethylmethacrylate by ionizing radiations. *Proceedings of the Royal Society. A*. 1954, 223–392.
9. YALE UNIVERSITY (US). Three dimensional detection, dosimetry and imaging of an energy field by formation of a polymer in a gel. Inventors: Marek MARYANSKI, John GORE, Robert SCHULZ. US Patent US5321357. 1992-08-07. United States Patent and Trademark Office. [accessed on 2017-08-12]. Available from: <https://patents.google.com/patent/US5321357>.
10. DE DEENE, Y., et al. Validation of MR-based polymer gel dosimetry as a preclinical three-dimensional verification tool in conformal radiotherapy. *Magnetic Resonance in Medicine*. 2000, 43, 116–125.
11. DUTHOY, W., et al. Clinical implementation of intensity-modulated arc therapy (IMAT) for rectal cancer. *International Journal of Radiation Oncology, Biology, Physics*. 2004, 60, 794–806.
12. PAPPAS, G., et al. The globalization of leptospirosis: Worldwide incidence trends. *International Journal of Infectious Diseases*. 2008, 12(4), 351–7. doi: 10.1016/j.ijid.2007.09.011.
13. WATANABE, Y., et al. Image distortion in MRI-based polymer gel dosimetry of Gamma Knife stereotactic radiosurgery systems. *Medical Physics*. 2002, 29, 797–802.
14. MASOUMI, H., et al. Determine the dose distribution using ultrasound parameters in MAGIC-f Polymer Gels. *Dose Response*. 2016, 14(1), 1–7. doi: 10.1177/1559325815625647.
15. RINTOUL, L., et al. Radiation dose distribution in polymer gels by Raman spectroscopy. *Applied Spectroscopy*. 2003, 57, 51–57.
16. PARWAIE, W., et al. Evaluation of MRI-based MAGIC polymer gel dosimeter in small photon fields. *International Journal of Radiation Research*. 2016, 14, 60–65.

17. FONG, P.M., et al. Polymer gels for magnetic resonance imaging of radiation dose distributions at normal room atmosphere. *Physics in Medicine and Biology*. 2001, 46, 3105–13.
18. MASSILLON, J.G., et al. Characteristics of a new polymer gel for high-dose gradient dosimetry using a micro optical CT scanner. *Applied Radiation and Isotopes*. 2010, 68, 144–154.
19. SENDEN, R.J., et al. Polymer gel dosimeters with reduced toxicity: A preliminary investigation of the NMR and optical dose–response using different monomers. *Physics in Medicine & Biology*. 2006, 51–14. doi:10.1088/0031-9155/51/14/001.
20. HUANG, Y.R. and Y.J. CHANG. Dosimetry study of diagnostic X-ray using doped iodide normoxic polymer gels. *Radiation Physics and Chemistry*. 2014, 104, 414–419.
21. GAFAR, S.M., et al. Toluidine blue O-gelatin gel dosimeter for radiation processing. *Open Journal of Polymer Chemistry*. 2014, 04(03), 56–61. doi: 10.4236/ojpcem.2014.43007.
22. MATTEA, F. and D. CHACÓN. Polymer gel dosimeter based on itaconic acid. *Applied Radiation and Isotopes*. 2015, 105, 98–104.
23. VANDECASTEELE, J., et al. Radio-physical properties of micelle leucodye 3D integrating gel dosimeters. *Physics in Medicine and Biology*. 2011, 56, 627–651.
24. RABAEH, K.A. and A.A. BASFAR. New normoxic N-(Hydroxymethyl) acrylamide based polymer gel for 3D dosimetry in radiation therapy. *Physica Medica*. 2017, 33, 121–126.
25. HSIEH, L-L. and J-I. SHIEH. Polymer gel dosimeters for pretreatment radiotherapy verification using the three-dimensional gamma evaluation and pass rate maps. *Physica Medica*. 2017, 37, 75–81.
26. GUSTAVSSON, H., et al. Linear energy transfer dependence of a normoxic polymer gel dosimeter investigated using proton beam absorbed dose measurements. *Physics in Medicine and Biology*. 2004, 49, 3847–3855.
27. YOSHIOKA, M. Examination of fundamental characteristics of a polymer gel detector in a proton beam irradiation. *Radiation Measurements*. 2011, 46, 64–71.
28. ZEIDAN, O.A., et al. Dosimetric evaluation of a novel polymer gel dosimeter for proton therapy. *Medical Physics*. 2010, 37(5), 2145–2152.
29. FURUKAWA, A., et al. Tunnel formation inferred from the I-form structures of the proton-driven protein secretion motor SecDF. *Cell Reports*. 2017, 19(5), 895–901. doi: 10.1016/j.celrep.2017.04.030.
30. HURLEY, C. *The Development of Normoxic Polymer Gel Dosimetry Using High Resolution MRI*. 2006. [accessed on 2017-10-11]. Available from: <https://core.ac.uk/download/pdf/10885141.pdf>.
31. MAITRA, J. and V.K. SHUKLA. Cross-linking in hydrogels — A review. *American Journal of Polymer Science*. 2014, 4(2), 25–31. doi: 10.5923/j.ajps.20140402.01.
32. JIRASEK, A., et al. How does the chemistry of polymer gel dosimeters affect their performance? *Journal of Physics: Conference Series*. 2009, 164, 012003. doi: 10.1088/1742-6596/164/1/012003_c.
33. OKAY, O. General properties of hydrogels. *Hydrogel Sensors and Actuators. Springer Series on Chemical Sensors and Biosensors (Methods and Applications)*. 2009, 6. doi: 10.1007/978-3-540-75645-3_1.
34. JIRASEK, A., et al. Investigation of tetrakis hydroxymethyl phosphonium chloride as an antioxidant for use in X-ray computed tomography polyacrylamide gel

- dosimetry. *Physics in Medicine and Biology*. 2006, 51, 1891–1906. doi: 10.1088/0031-9155/51/7/018.
35. SEIFFERT, S. and J. SPRAKEL. Physical chemistry of supramolecular polymer networks. *Chemical Society Reviews*. 2012, 41, 909–930. doi: 10.1039/c1cs15191f.
 36. AHMED, L.E. Hydrogel: Preparation, characterization, and applications: Natural-based polymers for biomedical applications. *Journal of Advanced Research*. 2015, 6(2), 105–121.
 37. *Collins English Dictionary-Complete & Unabridged*. 10th ed. [accessed on 2018-01-16]. Available from: <http://www.dictionary.com/browse/cross-link>.
 38. RATNER, B.D., HOFFMAN, A.S., SCHOEN, F.J., LEMONS, J.E. *Biomaterials Science. An Introduction to Materials in Medicine*. 3rd ed. Oxford: Elsevier, 2013.
 39. VAICIUNAITĖ, N. and D. ADLIENE. Investigation of diffusion properties in proton irradiated polymer gels. In *12th International Symposium on Systems with Fast Ionic Transport (ISSFIT-12), Program and Abstracts. July 03–07, Kaunas, Lithuania*. Kaunas: Technologija, 2016. p. 69.
 40. SUN, Y. and A.G. CHMIELEWSKI. *Applications of Ionizing Radiation in Materials Processing*. ISBN Institute of nuclear chemistry and technology: Warszawa, 2017.
 41. KIM, B.H. and J.W. KWON. Plasmon-assisted radiolytic energy conversion in aqueous solutions. *Scientific Reports — Nature*. 2014, 4, 52–49.
 42. DE DEENE, Y. Essential characteristics of polymer gel dosimeters. *Journal of Physics: Conference Series* 3. 2004, 34–57. doi: 10.1088/1742-6596/3/1/006.
 43. LEPAGE, M., et al. The relationship between radiation-induced chemical processes and transverse relaxation times in polymer gel dosimeters. *Physics in Medicine and Biology*. 2001, 46, 1061–1074.
 44. KRYVEN, I. and P.D. IEDEMA. Transition into the gel regime for free radical crosslinking polymerisation in a batch reactor. *Polymer*. 2014, 55(16), 3475–3489.
 45. JIRASEK, A.I. and C. DUZENLI. Effects of crosslinker fraction in polymer gel dosimeters using FT Raman spectroscopy. *Physics in Medicine and Biology*. 2001, 46, 1949–1961.
 46. SANO, H. and T. OBATA. *The Influence of Temperature on Polymer Gel Radiation Dosimetry with MRI*. 2014. [accessed on 2017-03-15]. Available from: <http://dev.ismrm.org/2014/3237.html>.
 47. IMATO, K., et al. Network reorganization of dynamic covalent polymer gels with exchangeable diaryl benzofuranone at ambient temperature. *Journal of the American Chemical Society*. 2014, 136(33), 11839–11845. doi: 10.1021/ja5065075.
 48. ZAMMALI, M., et al. A microrheological study of physical gelation of hydrophobically modified associating polymers: Effects of temperature. *Polymer*. 2017, 121, 204.
 49. HAYASHI, S., et al. A study on the role of gelatin in methacrylic-acid-based gel dosimeters. *Radiation Physics and Chemistry*. 2010, 79, 803–808.
 50. ADINEHVAND, K., et al. Verification of dose rate and energy dependence of MAGICA polymer gel dosimeter with electron beams. *Iranian Journal of Radiation Research*. 2008, 6(1), 31–36.
 51. DEENE, Y.D., et al. Three dimensional radiation dosimetry in lung equivalent regions by use of a radiation sensitive gel foam: Proof of principle. *Radiation Measurement Physics*. 2006, 33(7), 2586–97. doi: 10.1118/1.2208939.
 52. JEBASEELAN, S.E.J. Study on energy dependence of PAGAT polymer gel dosimeter evaluated. *Radiation Measurements*. 2010, 45, 92–97.

53. ZEHTABIAN, M., et al. Investigation of the dose rate dependency of the PAGAT gel dosimeter at low dose rates. *Radiation Measurements*. 2012, 47(2), 139–144. doi: 10.1016/j.radmeas.2011.11.002.
54. RUSSO, G., et al. Reproducibility study of normoxic polyacrylamide gel (nPAG) dosimeters. *Journal of Physics: Conference Series*. 2009, 164(1), 012010. doi: 10.1088/1742-6596/164/1/012010.
55. CRUZ, R.S. Oxygen scavengers: An approach on food preservation. *Structure and Function of Food Engineering*. 2012. doi: 10.5772/48453.
56. VANDECASTEELE, J. and Y. DE DEENE. On the validity of 3D polymer gel dosimetry: II. Physico-chemical effects. *Physics in Medicine and Biology*. 2013, 58, 43–61. doi: 10.1088/0031-9155/58/1/43.
57. JIRASEK, A., et al. Experimental properties of THPC based normoxic polyacrylamide gels for use in x-ray computed tomography gel dosimetry. *Journal of Physics Conference Series*. 2007, 56(1), 263. doi: 10.1088/1742-6596/56/1/045.
58. MCAULEY, K.B. and A.T. NASR. Fundamentals of gel dosimeters. *Journal of Physics: Conference Series*. 2013, 444, 012–001. doi: 10.1088/1742-6596/444/1/012001.
59. HURLEY, C., et al. A study of a normoxic polymer gel dosimeter comprising methacrylic acid, gelatin and tetrakis (hydroxymethyl)phosphonium chloride (MAGAT). *Applied Radiation and Isotopes*. 2005, 63, 443–456.
60. CHENG, K-Y., et al. A comprehensive evaluation of NIPAM polymer gel dosimeters on three orthogonal planes and temporal stability analysis. *PLoS ONE*. 2016, 11(5), 0155797. doi: 10.1371/journal.pone.0155797.
61. BASFAR A.A. and B. MOFTAH. Novel composition of polymer gel dosimeters based on N-(Hydroxymethyl) acrylamide for radiation therapy. *Radiation Physics and Chemistry*. 2015, 112, 117–120.
62. OLDHAMA, M., et al. Optical-CT Gel-Dosimetry I: Basic Investigations. *Medical Physics*. 2003, 30(4), 623–634.
63. MOORE, C.S., et al. Quality assurance of registration of CT and MRI data sets for treatment planning of radiotherapy for head and neck cancers. *Applied Clinical Medical Physics*. 2004, 5(1), 25–35.
64. GAMBARINI, G., et al. Optical analysis of gel dosimeters: Comparison of Fricke and normoxic polymer gels. *Nuclear Instruments and Methods in Physics Research B*. 2007, 263, 191–195.
65. KAWAMURA, H., et al. Evaluation of three-dimensional polymer gel dosimetry using X-ray CT and R2 MRI. *Applied Radiation and Isotopes*. 2013, 77, 94–102.
66. SKOOG, A.D., HOLLER, F.J., CROUCH, S.R. *Principles of Instrumental Analysis* 6th ed. Belmont, CA: Thomson Brooks/Cole, 2007. [accessed on 2017-01-09]. Available from: [http://zeus.qui.ufmg.br/~valmir/livros/analitica/Principles%20of%20Instrumental%20Analysis%20\(6ed\)%20%20Skoog,%20Holler%20&%20Crouch.pdf](http://zeus.qui.ufmg.br/~valmir/livros/analitica/Principles%20of%20Instrumental%20Analysis%20(6ed)%20%20Skoog,%20Holler%20&%20Crouch.pdf).
67. TITUS, D., et al. Silver nitrate based gel dosimeter. *Journal of Physics: Conference Series*. 2017, 847, 012066. doi: 10.1088/1742-6596/847/1/012066.
68. ISHAK, S.A. 6 MV photon beam induced UV/VIS absorption of hema polymer gel. *Sains Malaysiana*. 2017, 46(2), 303–308. doi: 10.17576/jsm-2017-4602-15.

69. MOHAMMAD, T.I., et al. The potential of Raman spectroscopy as a process analytical technique during formulations of topical gels and emulsions. *Pharmaceutical Research*. 2004, 21(10), 10–15.
70. BONG, J., et al. Raman spectroscopy of irradiated normoxic polymethacrylic acid gel dosimeter. *Bulletin of the Korean Chemical Society*. 2011, 32(2), 625. doi 10.5012/bkcs.2011.32.2.625.
71. AFIRAH, A.R., et al. A study of normoxic polymer gel dosimeter using Raman spectroscopy analysis. In *2011 International Conference on Biomedical Engineering and Technology*. IPCBEE, 2011. pp. 19–23.
72. MATTEA, F. Molecular structure effects on the post irradiation diffusion in polymer gel dosimeters. *Applied Radiation and Isotopes*. 2015, 100, 101–107.
73. ADENAN, M.Z., et al. Raman study of lower toxicity polymer gel for radiotherapy dosimetry. *Journal of Physics: Conference Series*. 2014, 546, 012011. doi: 10.1088/1742-6596/546/1/012011.
74. RAGHAVENDRA, R., et al. Raman spectroscopy for the characterization of the polymerization rate in an acrylamide-based photopolymer. *Applied Optics*. 2008, 47(2), 206–212. doi.org/10.1364/AO.47.000206.
75. RAMYA, C.S., et al. Proton-conducting membranes: Poly (N-vinyl pyrrolidone) complexes with various ammonium salts. *Journal of Solid State Electrochemistry*. 2008, 12, 807–814. doi 10.1007/s10008-008-0531-5.
76. LEPAGE, M., et al. ¹³C-NMR, ¹H-NMR, and FT-Raman study of radiation-induced modifications in radiation dosimetry polymer gels. *Journal of Applied Polymer Science*. 2001, 79, 1572–1581.
77. BALDOCK, C., et al. Fourier transform Raman spectroscopy of polyacrylamide gels (PAGs) for radiation dosimetry. *Physics in Medicine and Biology*. 1998, 43, 3617–3627.
78. CALÓ, E. and V.V. KHUTORYANSKIY. Biomedical applications of hydrogels: A review of patents and commercial products. *European Polymer Journal*. 2015, 65, 252–267. doi: 10.1016/j.eurpolymj.2014.11.024.
79. CHAI, Q., et al. Hydrogels for biomedical applications: Their characteristics and the mechanisms behind them. *Gels*. 2017, 3(1), 6. doi: 10.3390/gels3010006.
80. PAL, K. Polymeric hydrogels: Characterization and biomedical applications — A mini review. *Designed Monomers and Polymers*. 2009, 21(3), 10–30.
81. GRODZINSKI, J.J. Polymeric gels and hydrogels for biomedical and pharmaceutical applications. *Polymers for Advanced Technologies*. 2009, 21(1), 27–47. doi: 10.1002/pat.1504.
82. KADAJJI, V.G. and G.V. BETAGERI. Water soluble polymers for pharmaceutical applications. *Polymers*. 2011, 1972–200. doi: 10.3390/polym3041972.
83. RAO, M. Preparation and performance of gel polymer electrolyte based on electrospun polymer membrane and ionic liquid for lithium ion battery. *Journal of Membrane Science*. 2012, 399–400, 37–42.
84. HÄGERSTRÖM, H. *Polymer Gels as Pharmaceutical Dosage Forms*. 2003. [accessed on 2017-04-03]. Available from: <http://www.diva-portal.org/smash/get/diva2:163176/FULLTEXT01.pdf>respect.
85. HUO, Z., et al. A supramolecular gel electrolyte formed from amide based co-gelator for quasi-solid-state dye-sensitized solar cell with boosted electron kinetic processes. *Journal of Power Sources*. 2017, 359, 80–87.

86. PARK, S., et al. Sol-gel metal oxide dielectrics for all-solution-processed electronics. *Materials Science and Engineering: R: Reports*. 2017, 114, 1–22.
87. ŁATOSZYNSKA, A.A. Proton conducting gel polymer electrolytes for supercapacitor applications. *Electrochimica Acta*. 2017, 242, 31–37.
88. BOTELHO, M., et al. X-ray transmission through nanostructured and microstructured CuO materials. *Applied Radiation and Isotopes*. 2011, 69(2), 527–530.
89. EL HABER, F. and G. FROYER. Transparent polymers embedding nanoparticles for X-rays attenuation. *J. Uni. Chem. Technol. Metallurgy*. 2008, 43(3), 283–290.
90. SERVA Electrophoresis GmbH. *Gel Preparation, Technical Note and Recommendations*. [accessed on 2017-05-13]. Available from: <https://www.serva.de/en/DE/DownloadDetails/?navSeq=18&categorie=1>.
91. GASTALDO, J., et al. Induction and repair rate of DNA damage: A unified model for describing effects of external and internal irradiation and contamination with heavy metals. *Journal of Theoretical Biology*. 2008, 251, 68–81.
92. PAPADAKIS, A.E., et al. Three-dimensional radiation dosimetry with optical projection tomography. *Journal of Physics: Conference Series*. 2009, 164, 012027. doi: 10.1088/1742-6596/164/1/012027.
93. BARTELINK, H., et al. Recurrence rates after treatment of breast cancer with standard radiotherapy with or without additional radiation. *The New England Journal of Medicine*. 2001, 345, 1378–1387. doi: 10.1056/NEJMoa010874.
94. WU, V.W.C., et al. Inverse planning in three-dimensional conformal and intensity-modulated radiotherapy of mid-thoracic oesophageal cancer. *The British Journal of Radiology*. 2004, 77(919), 568–572. doi: 10.1259/bjr/19972578.
95. KAWAMURA, H., et al. Polymer gel dosimetry for neutron beam in the Neutron Exposure Accelerator System for Biological Effect Experiments (NASBEE). *Journal of Physics: Conference Series*. 2015, 573, 012068. doi: 10.1088/1742-6596/573/1/012068.
96. *Technical Reports Series No. 398 Absorbed Dose Determination in External Beam Radiotherapy: An International Code of Practice for Dosimetry*. Vienna: IAEA, 2000. [accessed on 2017-05-15]. Available from: http://www-naweb.iaea.org/nahu/DMRP/documents/CoP_V12_2006-06-05.pdf.
97. FIESER, L.F and K.L. WILLIAMSON. *Organic Experiments*, 9th ed. Thomson Brooks/Cole, 2003. [accessed on 2017-05-16]. Available from: https://mnh20.files.wordpress.com/2010/07/organic_experiments_fieser_williamson_1.pdf.
98. ADLIENE, D., et al. Evaluation of new transparent tungsten containing nanocomposites for radiation protection screens. *Radiation Protection Dosimetry*. 2015, 165(1–4), 406–409. doi: 10.1093/rpd/ncv072Report.
99. HAIDER, M., et al. Shielding calculation based on NCRP methodologies for some diagnostic X-ray facilities in Bangladesh. *Scientific Research Journal*. 2014, 2(3), 47–53.
100. No. 147 — *Structural Shielding Design for Medical X-Ray Imaging Facilities*. 2004. [accessed on 2018-01-10]. Available from: <https://www.ncrppublications.org/Reports/147>.

101. ADLIENE, D., et al. Evaluation of new transparent tungsten containing nanocomposites for radiation protection screens. *Radiation Protection Dosimetry*. 2015, 165(1–4), 406–409. doi: 10.1093/rpd/ncv072.
102. MAYERHÖFER, T., et al. Employing theories far beyond their limits — The case of the (Boguer-) Beer-Lambert law. *ChemPhysChem*. 2016, 17(13), 1948–1955. doi: 10.1002/cphc.201600114.
103. GUO, H. A simple algorithm for fitting a Gaussian function. *IEEE Signal Processing Magazine*. 2011, 28(9), 134–137.
104. FUJIBUCHI, T., et al. Dose-response measurement in gel dosimeter using various imaging modalities. *Journal of Physics: Conference Series*. 2013, 444, 012089. doi: 10.1088/1742-6596/444/1/012089.
105. ZHAO, L. Characteristics of a new polymer gel for high-dose gradient dosimetry using a micro optical CT scanner. *Carbohydrate Polymers*. 2003, 51, 169–175.
106. SONG, J., et al. Poly(N-vinylpyrrolidone)-grafted poly(N-isopropylacrylamide) copolymers: Synthesis, characterization and rapid deswelling and reswelling behavior of hydrogels. *Polymers*. 2011, 52, 2340–2350.
107. NOVOTNY, JR.J., et al. Three-dimensional polymer gel dosimetry: Basic physical properties of the dosimeter. *Radiation Physics and Chemistry*. 2001, 61, 255–258.
108. ULANSKI, P. Radiation synthesis of polymer nanogels for biomedical applications. *International Conference on Applications of Radiation Science and Technology. Programme and Abstracts*. IAEA–CN–241–422, 2017. p. 82.
109. MUJADIH, A. and F.L. DICKET. *Molecularly Imprinted Catalysts*. 2016. doi: 10.1016/B978-0-12-801301-4.00005-0.
110. THONIYOT, P., et al. Nanoparticle-hydrogel composites: Concept, design, and applications of these promising, multi-functional materials. *Advanced Science*. 2015, 2, 1400010. doi: 10.1002/advs.201400010.
111. VAIČIŪNAITĖ, N. and D. ADLIENĖ. Optical properties of photon irradiated N-vinylpyrrolidone based polymer gel. In *Radiation Interaction with Materials: Fundamentals and Applications 2014: 5th International Conference, May 12–15, 2014, Kaunas, Lithuania. Program and Materials*. Kaunas: Technologija, 2014. pp. 464–467.
112. KARLSSON, A., et al. Dose integration characteristics in normoxic polymer gel dosimetry investigated using sequential beam irradiation. *Physics in Medicine and Biology*. 2007, 52, 4697–4706. doi: 10.1088/0031-9155/52/15/021.
113. HILTS, M., et al. Effects of gel composition on the radiation induced density change in PAG polymer gel dosimeters: A model and experimental investigations. *Physics in Medicine and Biology*. 2004, 49, 2477–2490.
114. DE DEENE, Y., et al. An investigation of the chemical stability of a monomer/polymer gel dosimeter. *Physics in Medicine & Biology*. 2000, 45(4), 859–78.
115. JIRASEK, A.I., et al. Characterization of monomer/crosslinker consumption and polymer formation observed in FT-Raman spectra of irradiated polyacrylamide gels. *Physics in Medicine and Biology*. 2001, 46, 151–165.
116. BONG, J., et al. Raman spectroscopy of irradiated normoxic polymethacrylic acid gel dosimeter. *Bulletin of the Korean Chemical Society*. 2011, 32(2), 625. doi: 10.5012/bkcs.2011.32.2.625.

117. TAI, F.C., et al. Multipeak fitting analysis of Raman spectra on DLCH film. *Journal of Raman Spectroscopy*. 2009, 40, 1055–1059. doi: 10.1002/jrs.2234.
118. MEIER, R.J. On art and science in curve-fitting vibrational spectra. *Vibrational Spectroscopy*. 2005, 39, 266–269.
119. RIEGEL, B. and W. KIEFER. FT-Raman spectroscopic investigations on the organic crosslinking in hybrid polymers part II: Reactions of epoxy silanes. *Journal of Sol-Gel Science and Technology*. 2002, 24, 139–145.
120. BRADLEY, M. *Curve Fitting in Raman and IR Spectroscopy: Basic Theory of Line Shapes and Applications*. 2017. [accessed on 2018-02-18]. Available from: https://www.thermofisher.com/content/dam/tfs/ATG/CAD/CAD%20Documents/Application%20&%20Technical%20Notes/Molecular%20Spectroscopy/Raman/Raman%20Instruments/AN50733_E.pdf
121. GUPTA, S., et al. Unraveling the conundrum of seemingly discordant protein-protein interaction datasets. *Conference Proceeding. Annual International Conference of the IEEE Engineering in Medicine and Biology Society*. 2010, 783–786. doi: 10.1109/IEMBS.2010.5626490.
122. VAIČIŪNAITĖ, N. and R. ŠEPERYS. Raman spectroscopy of polymerization processes in nPAG and nMAG dose gels. In *12th International Conference Medical Physics in the Baltic States, 5–7 October, 2015, Kaunas, Lithuania*. Kaunas: Kaunas University of Technology, 2015. pp. 141–144 .
123. BONG, J., et al. Raman spectroscopy of irradiated normoxic polymethacrylic acid gel dosimeter. *Bulletin of the Korean Chemical Society*. 2011, 32(2). doi: 10.5012/bkcs.2011.32.2.625.
124. HAYASHI, S. and M. YOSHIOKA. A study on the role of gelatin in methacrylic-acid-based gel dosimeters. *Radiation Physics and Chemistry*. 2010, 79, 803–808.
125. TANAKA, F. *Polymer Physics. Applications to Molecular Association and Thermoreversible Gelation*. Cambridge: Cambridge University Press, 2011. [accessed on 2018-03-19]. Available from: https://www.researchgate.net/publication/281894443_Polymer_Physics_Applications_to_Molecular_Association_and_Thermoreversible_Gelation.
126. YAMAGUCHI, H., et al. Estimation of yields of OH radicals in water irradiated by ionizing radiation. *Journal of Radiation Research*. 2005, 46, 333–341.
127. XCOM. [accessed on 2018-02-18]. Available from: <http://www.nist.gov/pml/data/xcom/>.
128. KAUNO TECHNOLOGIJOS UNIVERSITETAS (LT). Radiation protecting material composition, screen for radiation protection and method of making the same. Inventors: Egidijus GRIŠKONIS, Stanislovas ZACHAROVAS, Diana ADLIENĖ, Pranas NARMONTAS, Rimas ŠEPERYS, Ramūnas BAKANAS, Neringa VAIČIŪNAITĖ. LT patent LT 6292. 2016-08-10. Lietuvos Respublikos valstybinis patentų biuras. [accessed on 2018-01-11]. Available from: http://www.vpb.lt/db_patentai/rezult-singl.php?id=X531233.

LIST OF PUBLICATIONS

Articles published in journals belonging to the scientific international databases Clarivate Analytics. Indexed in the Web of Science with Impact Factor

1. ADLIENĖ D., JAKŠTAS K., VAIČIŪNAITĖ N. Application of optical methods for dose evaluation in normoxic polyacrylamide gels irradiated at two different geometries // Nuclear instruments & methods in physics research A: Accelerators, spectrometers, detectors and associated equipment. Amsterdam: Elsevier Science. ISSN 0168-9002. 2014, vol. 741, p. 88–94;
2. ADLIENĖ D., GRIŠKONIS E., VAIČIŪNAITĖ N., PLAIPAITĖ-NALIVAIKO R. Evaluation of new transparent tungsten containing nanocomposites for radiation protection screens // Radiation protection dosimetry. Oxford: Oxford University Press. ISSN 0144-8420. 2015, vol. 165, iss. 14, p. 406–409;
3. ADLIENE, D., JASELSKĖ E., RUDŽIANSKAS V., ŠEPERIENĖ N. First approach to ionizing radiation based 3D printing: Fabrication of free standing dose gels using high energy gamma photons. Nuclear Inst. and Methods in Physics Research B (2018), <https://doi.org/10.1016/j.nimb.2018.01.033>.

Publications in other international databases and WoS Proceeding

1. VAIČIŪNAITĖ N., ADLIENĖ D. Optical properties of photon irradiated N-vinylpyrrolid one based polymer gel // Radiation interaction with materials: Fundamentals and applications 2014 : 5th international conference, Kaunas, Lithuania, May 12–15, 2014 : Program and materials / Kaunas University of Technology, Vytautas Magnus University, Lithuanian Energy Institute, Riga Technical University, Hydrogen Energy Association. Kaunas: Technologija. ISSN 2351-583X. 2014, pp. 464–467;
2. VAIČIŪNAITĖ N., ŠEPERYŠ R. Raman spectroscopy of polymerization processes in nPAG and nMAG dose gels // Medical physics in the Baltic States : Proceedings of the 12th international conference on medical physics, Kaunas, Lithuania, November 5–7, 2015. Kaunas: Kaunas University of Technology. ISSN 1822-5721. 2015, pp. 141–144;
3. ADLIENĖ D., JAKŠTAS K., VAIČIŪNAITĖ N., LAURIKAITIENĖ J., ČERAPAITĖ-TRUŠINSKIENĖ R. Application of dose gels in HDR brachytherapy / IFMBE Proceedings : World congress on medical physics and biomedical engineering, June 7–12, 2015, Toronto, Canada. Berlin: Springer. ISSN 1680-0737. 2015, vol. 51, pp. 724–727.

Other publications

1. ŠEPERYS R., VAIČIŪNAITĖ N., ADLIENĖ D., ZACHAROVAS S., BAKANAS R. Evaluation of digital test holograms embossed in different plastics // Radiation interaction with materials: Fundamentals and applications 2014 : 5th international conference, Kaunas, Lithuania, May 12–15, 2014 : Program and materials / Kaunas University of Technology, Vytautas Magnus University, Lithuanian Energy Institute, Riga Technical University, Hydrogen Energy Association. Kaunas: Technologija. ISSN 2351-583X. 2014, pp. 460–463;
2. GRIŠKONIS E., ADLIENĖ D., PROSYČEVAS I., VAIČIŪNAITĖ N., URBONAVIČIUS B., NARMONTAS P., ŠEPERYS R. Investigation of X-ray attenuating properties of high concentration phosphotungstic acid solutions // Medical Physics in the Baltic States : Proceedings of the 11th international conference on medical physics, Kaunas, Lithuania, October 10–12, 2013 / Kaunas University of Technology. Kaunas: Technologija. ISSN 1822-5721. 2013, pp. 123–126.

International conferences

1. GRIŠKONIS E., ADLIENĖ D., PROSYČEVAS I., VAIČIŪNAITĖ N., URBONAVIČIUS B.G., NARMONTAS P., ŠEPERYS R. Investigation of X-ray attenuating properties of high concentration phosphotungstic acid solutions. 11th international conference on medical physics Medical Physics in the Baltic States. October 10–12, 2013, Kaunas, Lithuania;
2. VAIČIŪNAITĖ N., ADLIENĖ D. Optical properties of photon irradiated N-vinylpyrrolidone based polymer gel. Radiation interaction with materials: Fundamentals and applications 2014. 5th International conference. May 12–15, 2014, Kaunas, Lithuania;
3. ŠEPERYS R., VAIČIŪNAITĖ N., ADLIENĖ D., ZACHAROVAS S., BAKANAS R. Evaluation of digital test holograms embossed in different plastics. Radiation interaction with materials: Fundamentals and applications 2014. 5th International conference. May 12–15, 2014, Kaunas, Lithuania;
4. ADLIENĖ D., GRIŠKONIS E., VAIČIŪNAITĖ N., PLAIPAITĖ-NALIVAICO R., PROSYČEVAS I. Evaluation of new transparent tungsten containing nanocomposites for radiation protection screens. Medical physics international: International conference on radiation protection in medicine. 30 May–2 June, 2014, Varna, Bulgaria;
5. ŠEPERYS R., VAIČIŪNAITĖ N., ADLIENĖ D., ZACHAROVAS S., BAKANAS R. Enhancement of the developed hologram quality using ultrasonic bath. 11th International conference on Nanosciences and Nanotechnologies (NN14). July 8–11, 2014, Thessaloniki, Greece;

6. ADLIENĖ D., VAIČIŪNAITĖ N., ŠEPERYS R. Variations of optical properties of photon irradiated nPAG, nMAG and VIPET polymer dose gels. Optimisation in X-ray and Molecular Imaging 2015. May 28–30, 2015, Gothenburg, Sweden;
7. VAIČIŪNAITĖ N., ŠEPERYS R. Raman spectroscopy of polymerization processes in nPAG and nMAG dose gels. 12th international conference Medical physics in the Baltic States. October 5–7, 2015. Kaunas, Lithuania;
8. VAICIUNAITE N., ADLIENE D. Investigation of diffusion properties in proton irradiated polymer gels. 12th International Symposium on Systems with Fast Ionic Transport, ISSFIT-12. July 3–7, 2016, Kaunas, Lithuania;
9. VAIČIŪNAITĖ N., ADLIENĖ D. Protonais apšvitintų dozimetrinių gelių polimerizacijos analizė. 7-oji Jaunųjų mokslininkų konferencijoje “Fizinių ir technologijos mokslų tarpdalykiniai tyrimai”. February 09, 2017, Vilnius, Lithuania;
10. SEPERIENE N., ADLIENE D., JASELSKE E. Proton irradiation induced radiation effects in dose gels. 19th International conference on radiation effects and insulators, REI-19. July 2–7, 2017, Versailles, France.

Patent

1. KAUNO TECHNOLOGIJOS UNIVERSITETAS (LT). Radiation protecting material composition, screen for radiation protection and method of making the same. Inventors: Egidijus GRIŠKONIS, Stanislovas ZACHAROVAS, Diana ADLIENĖ, Pranas NARMONTAS, Rimas ŠEPERYS, Ramūnas BAKANAS, Neringa VAIČIŪNAITĖ. LT patent LT 6292, 2016-08-10.

Short information about the author of the dissertation

Neringa Šeperienė (Vaičiūnaitė) was born in 1988-04-29 in Marijampolė, Lithuania. In 2006, she graduated from Marijampolės Sūduvos gymnasium.

In 2010, she graduated from Bachelor's studies in Applied physics at Kaunas University of Technology.

In 2012, she graduated from Master studies in Medical physics at Kaunas University of Technology.

In 2010, she was awarded as one of the 100 best graduates of Lithuanian universities.

In 2011, she was awarded with KTU Rector's scholarship for significant study and research results.

During 2013–2017, she was a PhD student of Materials engineering at Kaunas University of Technology.

In 2015, she was awarded with a PhD student scholarship for research by the Lithuanian Science Council.

During 2012–2014, she worked as a project engineer in two projects funded by the Lithuanian Research Council.

During 2013–2014, she worked as a technologist in UAB “NovaTeco”.

From 2014, she is working as a project administrator in small enterprise MB “Šeši partneriai”, which was co-founded by the author of the dissertation.

In 2016, she was elected as a president of the student's fraternity at Kaunas University of Technology “TauTiTo”.

For four years, Neringa was a member of athletics team of KTU and participated in national athletics competitions.

In 2016, she became a member of KTU Radio club and the Lithuanian Radio Sports Federation. During the study period, she was an active participant of national and international scientific festivals: “Tyrėjų naktis”, “Erdvėlaivis Žemė”, and “Piknik Naukowy”.

Contact information:

Neringa Šeperienė

email: neringa.vaiciunaite@ktu.lt

+37061134592

Annex 1



HORIZON 2020

SME Instrument 2015: PHASE 1

Future commercialization plan for dosimetry system (BrachyDOSE) that is based on the polymer gels

Introduction

Since the polymer dose gel is not only an instrument to image the 3D distribution of the absorbed dose, it has a potential to be used as a dosimeter to measure the dose for cancer treatment procedures where high-dose gradients exist. Such procedures include brachytherapy, stereotactic radiosurgery, intensity modulated radiotherapy, and other. The feasibility study reviews the situation of cancer treatment procedure worldwide, the possible position of the polymer gel dosimeter in the medical equipment market. Moreover, this study includes main competitors of polymer gels and unique selling points, which should be developed to become competitive in the market.

Cancer is a key public health concern and a tremendous burden in the European societies and economies. The disease is one of the 3 main reasons of death and disability among the working age people worldwide with approximately 15 million new cases and 8 million cancer related deaths annually. The number of new cases is expected to rise by about 70 % over the next 2 decades, and the need to combat the disease is highlighted in both national and European action strategies. In order to increase the effectiveness of the cancer treatment, the precision medicine trend is rapidly developing.

The worldwide incidence of cancer is estimated to reach 25 million cases by 2030, which is mainly driven by the growth of the aging population and lifestyle impact. Ninety percent of all cancers are projected as solid tumors, i.e., potentially treatable with radiotherapy. It is estimated that 50–60 % of all cancer patients worldwide would benefit from radiotherapy. This is especially the case for prostate cancer, which is expected to increase by 75 % in terms of incidence. Radiotherapy is effective and the most cost-efficient option for solid tumors. A growing preference for non-surgical treatment options has become a recent trend.

The radiotherapy market is large and expected to reach 7.5 billion USD by 2020 from 5.8 billion USD in 2016, at a Compound Annual Growth Rate (CAGR) of 6.2 %

between 2016 and 2020. The technological advancements in radiotherapy products rise in number of geriatric population, increasing incidence of cancer cases across the globe, increasing symposiums that are driving the investments in radiotherapy, and growing adoption of radiotherapy devices and procedures that will majorly drive the radiotherapy market. The predicted growth in radiotherapy market is represented in Fig. 1. It is expected that this market will reach 6.3 billion USA dollars in revenue until 2018. In 2022, the market revenue would seek 8.5 billion in USA dollars. The market value can be represented by the number of new cancer incidents, which is expected to increase by 53 % in 2030.

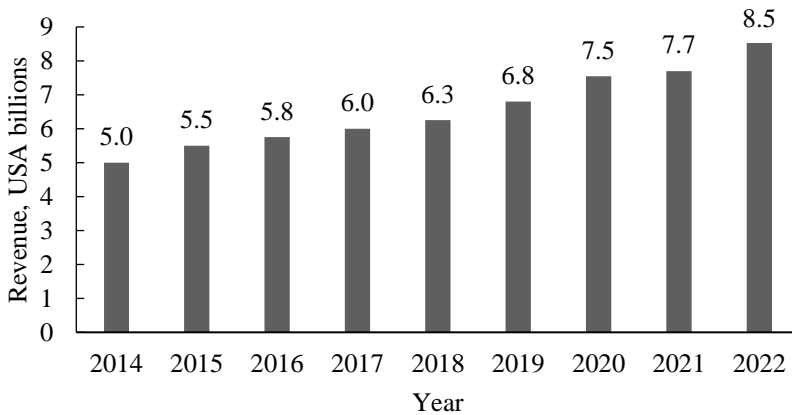


Fig. 1. The analysis of radiotherapy market growth. Global radiotherapy market revenue in USD billion in 2017

The study of the new cancer incidence per year has revealed a great demand for cancer treatment procedures as well as equipment such as dosimeters. According to the investigation, the cancer incidence is more probable for persons older than 65 years and could reach ~12 000 000 new cases up to the year 2030. About 3 00 000 new cancer cases are predicted to appear in 2020 in the European Union. Fig. 1 represents the number of new cancer incidence worldwide. It is predicted to encounter ~ 300 000 new cancer incidents in the European Union in 2020.

Šeši Partneriai Limited (further Šeši Partneriai) is developing a new dosimetry system, which could be used for the evaluation of doses for cancer patients that are delivered during high-dose rate brachytherapy treatment. The main objective for the implementation of the Phase 1 of SME Instrument was to develop an elaborate feasibility study for BrachyDOSE commercialization that would include a thorough analysis of market and user needs, a commercialization plan, and IPR strategy.

Market research

Cancer is a key public health concern and a tremendous burden in European societies and economies. The disease is one of the 3 main mortality and disability causes among the working age people worldwide. The number of cancer incidents is expected to grow rapidly by reaching 25 million cases by 2030. Such speedy growth is mainly driven by the increasing lifespan. In 2015, 8.5 % of people worldwide were 65 and older; in 2050, this percentage is expected to reach 17 %. Lifestyle is one of the key factors for the increase in cancer incidents. For example, smoking remains responsible for nearly one fifth of all cancer cases, while the increased popularity of sunbathing and using sunbeds contributes in increasing the rates of melanoma skin cancer. Due to the number of prevention programs, cancer is detected earlier for a higher number of people. Ninety percent 90% of all cancers are projected as solid tumours and radiation therapy is one of the most effective and cost-efficient treatment option for it. Therefore, it is estimated that 50%-60% of all cancer patients worldwide would benefit from radiation therapy.

Brachytherapy represents the internal and external radiation therapy method, used as an effective treatment for different types of cancer. Brachytherapy primarily uses two different techniques: Low Dose Rate (LDR) and High Dose Rate (HDR).

Brachytherapy market is a niche market accounting for less than 0.01% of the global health expenditure and was valued at 605 million euros in 2015. However, it should grow at 9% CAGR, reaching 1890 million Euros in 2030. The growth of brachytherapy is two times faster than 4 % CAGR growth of the total global healthcare.

Besides ageing population, the main factors that are affecting the demand for brachytherapy are as follows:

1) Technological advancements.

The demand for brachytherapy is growing as biotechnological advancements in dose delivery along with image guided procedures such as 3D treatment planning help physicians to get better treatment results. Physicians are able to deliver a high dose of radiation to the target with minimal impact on the healthy tissues.

2) Efficiency of brachytherapy.

Minimally invasive treatment measures have become the preferred treatment mode of patients, leading to the increase in brachytherapy demand. Patients as well switch to brachytherapy from the other treatment modes due to short treatment time, efficiency, and low cost. The main limitation to the growth of brachytherapy is the lack of equipment and trained staff rather than the small demand. The analysis that was

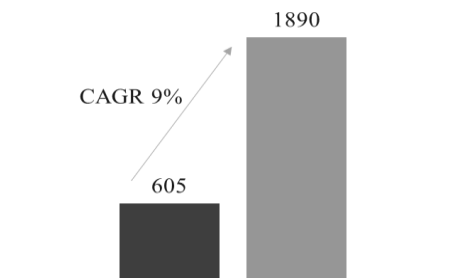


Fig. 2. Global brachytherapy market in mln EUR

published in *Lancet Oncology*, 2013, revealed that only 7 out of 27 European countries has sufficient capacity of radiation therapy equipment, while the remaining 20 do not have the quantities to meet the needs of the patients.

3) Investments and government support.

Increasing government healthcare expenditure and improving medical insurance plans as well as growing symposiums are driving private and public sector investments in radiation therapy, and thus, in brachytherapy.

Market

Šeši Partneriai plans to sell the product in the European Union, the United States of America, Canada, Switzerland, and Norway. According to International Atomic Energy Agency (IAEA), there are 1622 high-dose rate afterloaders in the world, 734 of which are in Europe and North America. The United States and Germany are the absolute leaders with 188 and 168 HDR afterloaders, respectively. Šeši Partneriai will as well target countries in Europe and North America.

As mentioned above, the analysis revealed that the majority of European countries do not have the quantity or quality of radiation therapy facilities, including HDR brachytherapy that is required to provide adequate services. The machines are being over-used. New machines from Western Europe are sold to hospitals in Eastern Europe after 8–10 years, where they are being used for 15–20 years more. This indicates that the need for the HDR brachytherapy procedure is already very strong and will continue to grow in the future.

Target user groups

Three major target groups were distinguished: healthcare centers (including specialized cancer treatment clinics, hospitals, and university clinics), institutes and research centers, and manufacturers of brachytherapy equipment.

Healthcare centers

Hospitals are one of the largest groups with approximately 300 hospitals that have the brachytherapy equipment in the target region. Healthcare centers could use BrachyDOSE in everyday HDR brachytherapy procedures to measure the dose that is delivered to the patient. The biggest markets are the US with 94 hospitals and Germany with 79. There are around 170 university hospitals that conduct cancer treatment, some of which as well have brachytherapy equipment. The United States and Germany are leaders with 53 and 34 university hospitals, respectively, followed by the United Kingdom (12), Italy (10), and the Czech Republic (10). Hospitals could be one of the best accesses into the markets like Switzerland and the United Kingdom, as they have a low number of the other types of organizations that are involved in the cancer treatment and research. The largest number of specialized cancer care clinics is in the United States (82), Germany (38), Canada (17), and France (17). More than half of the clinics are in the United States

Institutes

There are 70 institutes in target regions where Italy is the leader (13 institutes), followed by France (8) and the United States (8). Institutes could use BrachyDOSE in their research projects as well as when treating patients; 35 institutes have hospitals to conduct the clinical trials and treat patients. There are 12 research centers that focus purely on research with limited patent treatment capabilities, 5 of which are in the United States.

Brachytherapy equipment manufacturers

The market of the afterloaders is very concentrated. The top 10 companies control about 80 % of the world brachytherapy market, and other 20 companies control the remaining 20 %. The prime players operating in the market for brachytherapy devices include Eckert and Ziegler BEBIG S.A., C.R. Bard Inc., Elekta AB, Theragenics Corp., GE Healthcare Ltd., Varian Medical Systems Inc., Boston Scientific Corp., etc.

Competitor analysis

During the market research, competitor analysis was conducted. All the competitors were divided into three groups: current competitors, potential competitors, and potential partners (see Fig. 3 below).

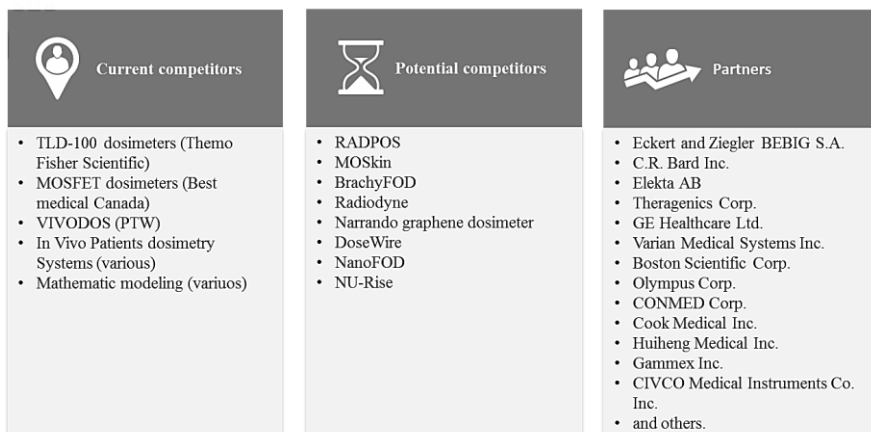


Fig. 3. Competitor analysis

Potential competitors are companies who do not have fully developed dosimetry system yet. There is available only limited information about what technology will be used in their dosimetry systems, what will be the cost per procedure, how compatible it is with HDR afterloaders, or when the product will be ready for commercial use. However, these companies advertise themselves as new players in dosimetry market, and they could become serious competitors in the future. The BrachyDOSE dosimetry system has the highest compatibility with other brachytherapy equipment, high ease

of use, and high speed of procedure in comparison to currently available solutions. It is as well inexpensive in comparison to its competitors.

Summary of the patent landscape and freedom to operate analysis

During the initial analysis of Espacenet data base (database that was developed by the European Patent Office together with the member states of the European Patent Organization), 23 similar patents were found. During the additional research, another 7 similar patents were found, summing up to 30 similar patents. These patents are related to polymer gel dosimeters and similar scanning equipment. However, patented products differ from BrachyDOSE solution. Therefore, the BrachyDOSE dosimetry system can be patented and commercialized without infringing anybody's intellectual property rights. The analysis has as well revealed that the BrachyDOSE dosimetry system is patentable. Patented technology is not self-explanatory.

Conclusions

The tasks that were performed during the SME-instrument Phase 1 project showed that the BrachyDOSE dosimetry system could be commercialized profitably. Šeši Partneriai has conducted market research, which revealed that the demand for brachytherapy services is and will continue to grow due to the increased number of cancer patients and the improvement of brachytherapy treatment. Competitors that currently exist in the market are not able to offer high-accuracy, user-friendly solution for affordable price.

Reference: Technical report of the project BrachyDOSE - H2020-SMEINST-1-2016-2017 - 775025. Future commercialization plan for dosimetry system (BrachyDOSE) that is based on polymer gels.

SL344. 2018-08-22, 18,25 leidyb. apsk. I. Tiražas 12 egz. Užsakymas 250.
Išleido Kauno technologijos universitetas, K. Donelaičio g. 73, 44249 Kaunas
Spausdino leidyklos „Technologija“ spaustuvė, Studentų g. 54, 51424 Kaunas